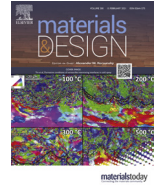




Contents lists available at ScienceDirect

Materials and Design

journal homepage: www.elsevier.com/locate/matdes

Wire and arc additive manufacturing: Opportunities and challenges to control the quality and accuracy of manufactured parts



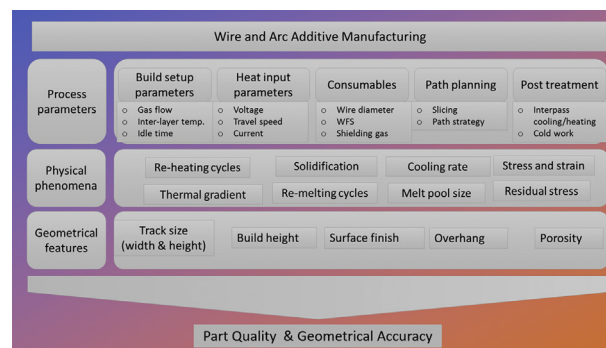
Davoud Jafari*, Tom H.J. Vaneker, Ian Gibson

Faculty of Engineering Technology, University of Twente, P.O. Box 217, 7500 AE Enschede, the Netherlands

HIGHLIGHTS

- We review recent progress in wire and arc additive manufacturing with a focus on the part quality and accuracy.
- We cover heat input and management concept, related to the resulting deformation and part quality.
- We study process planning for different geometrical features, including several case studies.
- We summarize guiding designs and future needs through the numerous WAAM geometrical issues.

GRAPHICAL ABSTRACT



ARTICLE INFO

Article history:

Received 22 June 2020

Received in revised form 29 October 2020

Accepted 9 January 2021

Available online 14 January 2021

Keywords:

Direct metal deposition

Wire and arc additive manufacturing

Geometric features

Heat management

Distortion

Geometrical accuracy

ABSTRACT

Wire and arc additive manufacturing (WAAM) has proven that it can produce medium to large components because of its high-rate deposition and potentially unlimited build size. Like all additive manufacturing (AM) technologies, however, an optimized process planning that provides uniform, defect-free deposition is key for the production of parts. Moreover, AM, particularly WAAM, is no longer just a prototyping technology, and most of today's attention is on its transformation to a viable and cost-effective production. With this transformation, a number of issues need to be addressed, including the accuracy and effectiveness of the manufactured components. Therefore, the emphasis should be on dimensional precision and surface finish in WAAM. This paper covers heat input and management concept, related to the resulting shrinkage, deformation, and residual stresses, which is particularly critical. In addition, we focus on process planning including build orientation, slicing, and path planning, as well as the definition of process parameter selection from a single track to multi-track and multilayer, and finally geometric features from a thin-wall to lattice structures with several case studies. Central to addressing component quality and accuracy, we summarize guiding designs and future needs through numerous WAAM-specific issues, which require for manufacturing of complex components.

© 2021 The Author(s). Published by Elsevier Ltd. This is an open access article under the CC BY license (<http://creativecommons.org/licenses/by/4.0/>).

1. Introduction

Due to its flexibility and process capabilities, additive manufacturing (AM) for the metal components has gained an increasing market share [1–3]. Powder bed fusion (PBF) is the most common metal-based method where a powder bed is deposited in layers between 20 and

100 μm thick and melted with an electron beam or laser locally [2,4]. This method is commonly adopted for small-scale parts, such as highly customized components [5,6]. The recent industrial developments allow the production of parts up to hundreds of mm wide through using a large working envelope of PBF systems[5,7]. However, the most suitable AM process for larger components with medium complexity can be dealt with using methods of direct metal deposition (DMD). This process introduces metal powder or wire to the desired spot, where the feedstock is melted through a nozzle or deposition

* Corresponding author.

E-mail address: davoud.jafari@utwente.nl (D. Jafari).

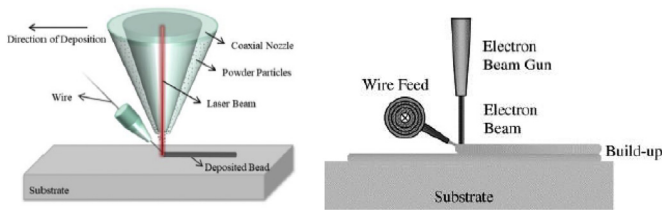


Fig. 1. Schematic view of WLAM (left) [46] and electron beam wire-feed DMD (right) [44]

head [2]. It allows for a relatively fast (compared to PBF) realization of large dimensions, with almost no size limitations.

Powder-based DMD typically performs laser for manufacturing large components, but the scale of the powder and the thickness of the layer is generally greater than PBF. Nevertheless, the feedstock price is often very high compared with conventional subtractive manufacturing, and only a few materials are available [8]. Large components may, therefore, be impractical to fabricate using powder DMD and so a method called wire and arc additive manufacturing (WAAM) has been created to meet this need [9–11]. This method uses wire feedstock and standard arc welding equipment to produce builds layer-by-layer [9]. Many materials are available in the welding community at relatively low cost and allow multi-millimetre thicknesses for individual layers. In particular, WAAM offers special benefits in the manufacture of near-net-shaped pieces including the ability to produce large structural components (1000–3000 mm) [12] efficiently with modest complexity, and a high rate of production (50–130 g/min) [13]. As an emerging AM technology, WAAM has, however, some potential drawbacks that need to be overcome given their many attractive aspects [9,11], including (i) residual stress and heat input distortion – deformations caused by residual stress are a major cause of tolerance loss in WAAM, (ii) poor dimensional accuracy and feature resolution of the component, and (iii) poor surface finish of the components manufactured. The WAAM involves a high periodic heat input due to the process of arc welding [14]. Thereby, in terms of parts quality, microstructures for metal alloy components manufactured by WAAM are complex, often spatially varying in deposition due to their complex thermal history [15,16]. In WAAM, solidification poses significant challenges in processing materials due to the promotion of a large-grain microstructure. Although large grains are beneficial for applications with high temperature creep resistance, they provide less strength, durability, and corrosion resistance compared to a fine microstructure at normal operating temperatures [17]. One of the effects of long periods of high temperatures in WAAM of low alloy steel is, for example, grain growth, which reduces hardness [18]. Concerning dimensional characteristics, the WAAM technologies have specific constraints to the degree of precision that can be achieved in the deposition process. For example, the accuracy of a deposited

component is limited by (i) the wire diameter used, (ii) arc ignition and extinguishment processes leading to significant changes in deposited bead geometries, (iii) improper process parameters that can affect the geometry of the deposited components, and (iv) distortion caused by heat accumulation, among others.

In summary, WAAM is still considered new technology for manufacturing of consistent production of parts according to necessary quality standards. WAAM research has been centered on physics, metallurgy, and applications rather than studying the relationship between processing parameters and geometric characteristics and challenges, including underlying physics, part quality, and accuracy, part distortion, and deformation. Few studies have been carried out on the accuracy of WAAM production and there exists a gap in the available knowledge. In order to achieve the appropriate component dimension and surface finish, the process parameters relating to geometry must be controlled. In this regard, careful attention should be paid to the consistency of the materials, i.e., surface finish and geometric precision. Whilst this review focuses on process-specific parameters for the part quality and accuracy of WAAM parts, it is important to clearly state the boundaries of which specific subjects are covered and which are not as discussed as follows.

- o Section 2 – This section includes a brief overview of wire-feed DMD, particularly WAAM.
- o Section 3 – This section includes a fundamental part quality and accuracy including heat input and heat management related to deposited part quality and accuracy. The precision of the deposition layer is not only related to the positional accuracy of the arc torch and path planning but also depends on the stability of the forming process. The part generates thermal stress and thermal deformation as the temperature changes in manufacturing progress – thermal stress and deformation during WAAM as well as common defects including crack and delamination and porosity are discussed in Section 3.
- o Section 4 – This section includes process planning: build orientation, slicing and path planning, the principle of process parameter selection, the principle of geometric features, and case studies. Each of these criteria needs to be integrated to address the materials and deposition technologies requirements with a range of features. Due to the fast development of 3D slicing and path planning and various newly suggested methods, the literature on slicing and path planning is lacking [19]. On the other hand, the size and morphology of the deposition layer are very important to have a high accuracy geometrical feature. When fabricating the parts by WAAM, the dimension accuracy of each deposition layer itself affects the accuracy of final products. Since the WAAM is a multi-pass deposition when the center of the cross-section of each layer is offset, the structural variation of the WAAM is caused – different control processing parameters affecting the bead profile are discussed. Geometrical behaviour includes single beads, overlapping beads, overlapping multilayer beads, and geometrical features such as thin and thick

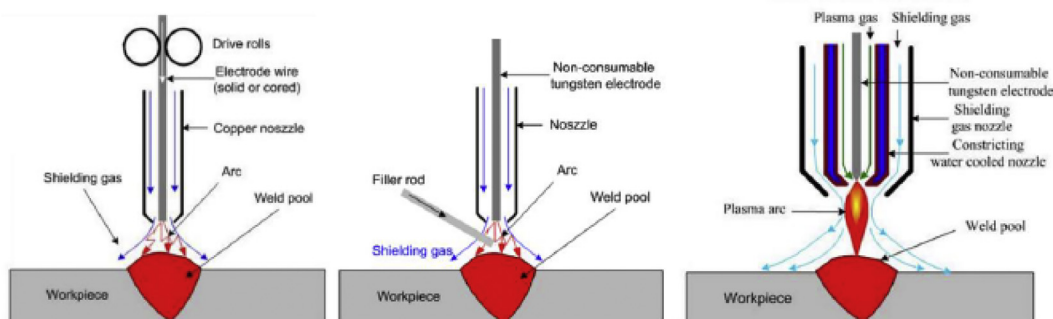


Fig. 2. Schematic diagram of GMAW, GTAW, and PAW [11]

Table 1
Comparison of various WAAM techniques including GMAW [61,62], CMT [61,63], Tandem [64–66], DE-GMAW[67], GTAW [68–71] and Plasma [53,54,72–74]

Energy source	Short description & features
GMAW-based	
GMAW	<ul style="list-style-type: none"> o The electric arc is formed between a consumable wire electrode and the metal workpiece. o Different modes of transfer: globular, short-circuiting, spray, and pulsed-spray; poor stability to the arc. o Consumable wire electrode with an average deposition rate 3–4 kg/hour. o Highly potential in large-scale part production due to its high energy efficiency, and high deposition rate.
CMT	<ul style="list-style-type: none"> o Improved arc stability, high-quality material deposition, controlled transfer of material, less distortion, low thermal input, almost zero spatter and high process tolerance. o Electrode reciprocating consumable wire with an average deposition rate of 2–3 kg/hour. o Used to produce thin-walled components that have relatively low efficiency for medium and large panels.
Tandem	<ul style="list-style-type: none"> o Twin-wire electrodes with an average deposition rate of 6–8 kg/hour – high deposition rate. o Simple mixing to monitor the composition for developing intermetallic materials. o There is a few reporting of the ability to produce intermetallic alloy as well as the gradient materials. o It provides the feasibility to deposit the demanding width once for a single path, which is suitable to fabricate width-walled structures with the merits of high melting efficiency and simple path planning strategy.
DE-GMAW	<ul style="list-style-type: none"> o Double electrode GMAW using GTAW. o Reducing the difference in height between the point of the striking arc and the point of extinguishing the arc in the deposited pieces. o Promising to produce tight thin-wall components. o Increasing the product coefficient by more than 10% using DE-GMAW to deposit thin-wall components.
GTAW-based	
GTAW	<ul style="list-style-type: none"> o Back feeding, side feeding, and front feeding can be used (front feeding for Ti-based and Fe-based WAAM is usually implemented). o Twin-wire to manufacture intermetallic materials with a practical gradation. o Non-consumable electrode; separate process for feeding wire with an average deposition rate of 1–2 kg/hour.
PAW-based	
Plasma	<ul style="list-style-type: none"> o A micro-PAW based framework was introduced o Non-consumable electrode; separate process for feeding wire. o The average deposition rate of 2–4 kg/hour. o Used to produce width-walled structures required applicable wire feed position.

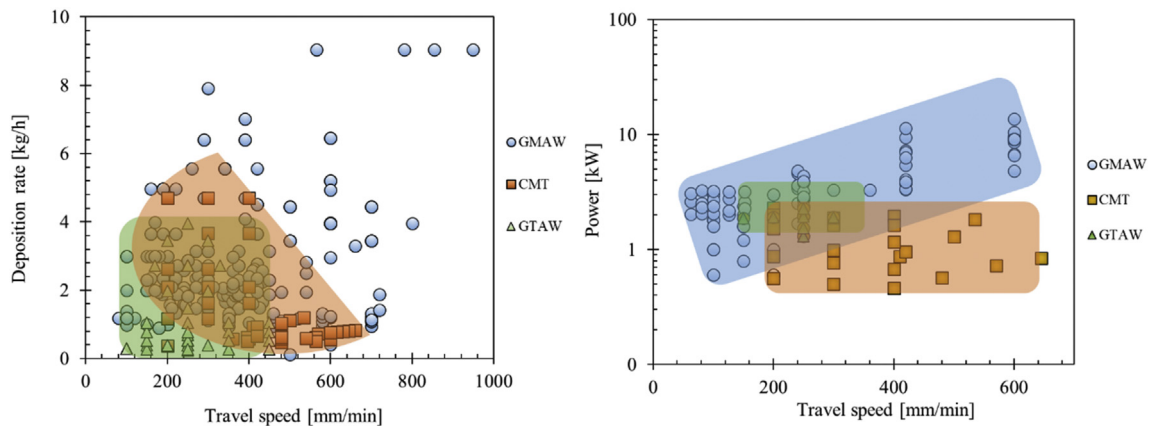


Fig. 3. Relationship between travel speed, arc power and deposition rate of GMAW, CMT and GTAW processes [53,54,61–74].

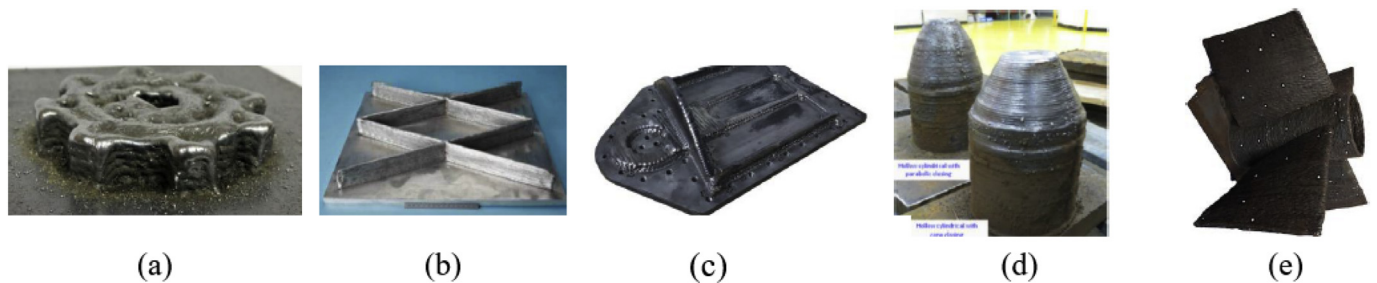


Fig. 4. An example of metal components manufactured via WAAM: (a) deposited 60 mm diameter ER70S-6 steel gear via GMAW [83], (b) aluminium stiffened panel structure via GMAW [84], (c) a deposited Ti-6Al-4V Airbus A320 aft pylon bracket mount via GMAW [85], (d) ER-70S-6 and AWS ER316L stainless-steel closed cone and closed parabolic cylinders forming by GMAW [86], and (e) EH700-1 ship propeller manufactured via CMT [87].

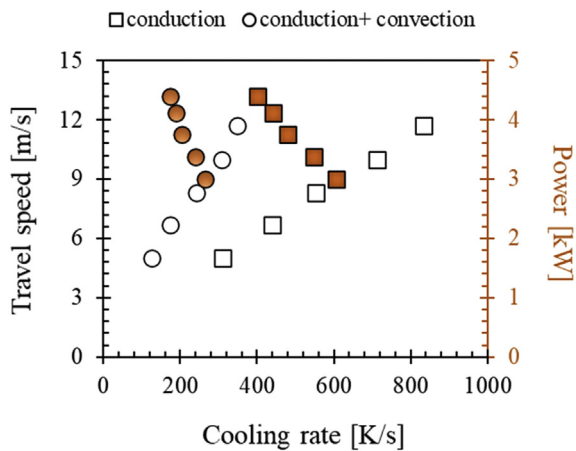


Fig. 5. Variations of cooling rate during solidification concerning arc power and travel speed [88]

walls, crossing features, overhang features, and lattice structures. Understanding geometrical behaviour provides information for the slicing procedure to select a reasonable layer thickness for the path planning procedure to control the offset distance between adjacent beads, and for the deposition process to adopt the optimum welding parameters.

- o **Section 5** – This section includes a summary of WAAM capabilities and limitations with a focus on manufacturing the geometrical features. From the analysis and synthesis of the experimental results in the literature, the part quality and accuracy challenges related to the WAAM process and planning are discussed, and the first draft of design guidelines appropriate for use in design practice is created.

Exclusion topics as reviewed elsewhere include mass transfer phenomena and topology optimization modelling [20], design methodologies and software [21,22], microstructural and materials related WAAM [23–25], in-process monitoring and in-machine surface metrology [26,27], mechanical properties [9,11,28], design for AM and application of WAAM [29–31]. In particular, the main goal of this review is to obtain comprehensive process information and geometry-related reliance on quality objectives and to create geometry-related information for the manufacture of (large) components based on the knowledge gained from a thorough study of the geometric features.

2. A brief overview of wire-feed DMD and applications

This section provides a brief introduction to wire-feed DMD technology, as well as the classification, specifications, and industrial applications of wire-feed DMD. A metal wire is used in wire feed AM, with up to 100% of the wire material deposited into the component. This process is, therefore, more sustainable and does not expose operators to the hazardous powder environment. The rate of deposition is much higher than the powder feed processes up to 2500 cm³/h [32]. In addition, metal wires are cheaper than metal powder with properties appropriate for AM and more readily available, which makes it more cost-competitive for wire feeder technology. This technology also is a promising alternative to the traditional production of subtractive components with a complex geometry that generates large, costly metals. Wire-feed AM can be grouped into three categories depending on the energy source used for metal deposition, namely: (i) arc welding-based, (ii) laser-based, and (iii) electron beam-based [33].

Wire and laser additive manufacturing (WLAM) is an AM process for the manufacturing of components in full density that uses metal wires as the additive and laser as the source of energy. The WLAM device typically involves a laser system, an automated wire-fed supply unit, a

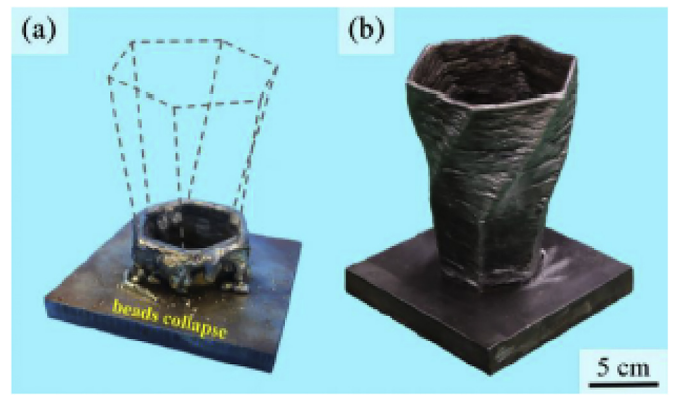


Fig. 6. Thin-wall twist bottles deposited by WAAM: (a) without a compulsory cooling solution, and (b) with a compulsory cooling solution [115].

robot, and various accessory devices (e.g., gas shielding, preheating, or cooling). The laser produces a melting pool on the material in which the metal wires are fed and melted to create a component. The laser-processing head and wire feeder are moved during solidification or the substrate is relocated (see Fig. 1). The relative movement of the welding tool and substratum can be accomplished using a numerically operated robot arm or machine worktable. The major concerns of WLAM are morphology and deposit quality performance including surface finish and size (cross-section morphology), microstructural characteristics (grain size, texture, etc.), and the mechanical properties (strength, hardness, residual stress, etc.) [34–36]. Such issues largely depend on both the wire properties and the processing parameters (e.g., direction and angle of wire feeding, wire feeding rates, laser power, and welding speed) [37–41]. The main specifications of WLM include its high precision and poor energy efficiency [42].

Electron beam wire-feed DMD (Fig. 1) is an AM process designed to produce complex, near-net parts that require substantially less raw material and finish than traditional production methods [43]. The process incorporates metal wire feedstock into a molten pool that is produced with a concentrated electron beam in a high-vacuum environment. The electron beam effectively interacts with all metal materials, including highly reflective alloys such as aluminium and copper [11,44]. Electron beam wire-feed DMD has a high-vacuum working environment, with an efficiency of about 15 to 20%. This makes it ideal for aerospace applications [45].

Another common wire feed AM technology is WAAM. There are usually three types of WAAM processes, depending on the nature of the heat source (see Fig. 2):

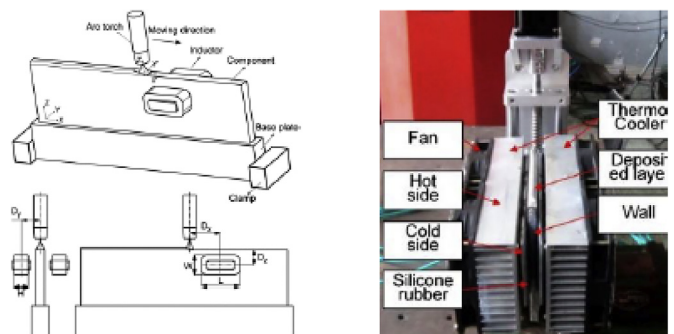


Fig. 7. Experimental setup in situ cooling with symmetrical coils (left) and a thermoelectric (right) [144].

- o Gas metal arc welding (GMAW)-based,
- o Gas tungsten arc welding (GTAW)-based, and
- o Plasma arc welding (PAW)-based

GMAW is a welding method where an electric arc is formed between a consumable wire and the metal workpiece. Four key metal transfer methods in GMAW are known as globular, short-circuit spray and pulsed sprays. Moreover, GMAW is limited to the minimum wall thickness and surface finish by a relatively large melting pool and heat supply [47–50]. Cold metal transfer welding (CMT) can be applied for the purpose of overcoming these constraints by reducing arc burns time and reversing the wire electrode back and forth [51,52]. Like GTAW, PAW produces a weld using a tungsten electrode that is not consumable. Contrary to GMAW, the wire feed orientation is variable in both GTAW and PAW, affecting deposit consistency, making process planning more challenging. In the high-temperature region of the plasma arc, the temperature is narrower than the GTAW [53]. Plasma welding arc energy can exceed three times the amount of GTAW welding, causing lower welding distortions and the heat-affected zone, smaller welds possible, and lower welding speeds [54]. Note that the heat input applied during WAAM affects distortions because of the large volume of melted material and that shrinks during solidification. The reduction of heat input during WAAM is a key factor for the application of this technology.

The reduction of WAAM thermal input is a critical factor in the use of this technology (see Section 3).

Table 1 lists the specifications of WAAM techniques. As evidenced, GMAW based on WAAM's deposition rate is 2–3 times that of GTAW or PAW based methods (see Fig. 3). However, due to the electrical current acting directly on the feedstock, the GMAW-based WAAM is less stable and produces more weld-fume and spatter. The choice of WAAM technique directly affects the processing conditions for a target component and the output rate for it. In particular, as compared to electron beam or laser DMD technologies, the energy efficiency of WAAM processes is as high as 90% at a relatively low cost [55] utilizing a wide range of materials Ti-based [9,56], Al-based [57,58], steel-based [29,59], and Ni-based [60] alloys. WAAM's research focus is on manufacturing complex functional metal components that meet the demanding requirements of the aerospace, automotive, and rapid tool industries with reasonable accuracy, surface finish, and material properties, represented as follows.

In recent years, WAAM has become an increasingly economically viable way in order to manufacture components made of high-value materials of low to medium complexity and medium to large-scale components. For applications that require large near-net-shape parts, with short lead time and millimetre-scales resolution, WAAM provides an efficient process. These near-net-shape parts need post-processing to meet

Table 2
How to mitigate heat accumulation during the WAAM process.

Heat source/material	Highlight
Strategy: inter-pass idle time	
GMAW/H08Mn2Si	FE analysis – the inter-pass idle time is a significant parameter to control residual stresses, decreasing with the increase of inter-pass idle time [131].
GMAW/mild steel	FE analysis – thermal cycling during deposition is the main cause of deformations, in particular, the effect of bolting was also very important [122,130].
GMAW/H08Mn2Si	FE analysis – increasing the idle time is helpful to improve the forming accuracy of each layer [126].
GMAW/ER70S-6	FE analysis – the variation in idle time contributes to a constant inter-layer temperature, ensuring a constant molten pool size, increasing the quality and productivity, and preventing collapses [121,128,129].
GTAW/5A06 Al	Theoretical model – controlling inter-layer idle time for each layer, results in eliminating solidification defects and showed adequate formation and quality [119].
Strategy: active cooling – increasing convection heat flux to the environment	
GMAW/ER70S-6	Water cooling fixtures – its drawback is that the heat of the molten pool is dissipated through conduction, not ensuring a constant cooling rate during the process [33,133].
GMAW/ER70S-6	Water-cooled tank – it is complicated to be applied to existing machine tools [134].
GMAW/ER70S-6	Air-jet cooling – it is a promising approach to prevent the occurrence of heat accumulation by increasing the convective heat transfer between the workpiece and the environment [135].
GMAW/ER70S-6	Air-jet cooling – it has a significant impact on the process; the optimal idle time was 30 s, as a compromise between productivity and reduction of heat accumulation.
GMAW/ER70S-6	Integrated water cooling channels' substrate – the effectiveness of this approach in terms of the changes possible to implement regarding residual stress, and dimensional stability may be limited for components of larger size and lower thermal conductivities [115].
In situ active cooling – cooling localized to the weld pool	
GMAW/2219 Al	Thermoelectric – maintaining stable heat dissipation characteristics without reducing the heat input and WFS; for equivalent welding processing parameters, this changes the weld bead geometry, increasing weld bead height, hence, fewer deposition passes are required [62]; a significant reduction of bead unevenness, grain size, and manufacturing time [112].
GTAW/Ti-6Al-4 V	Forced convective CO ₂ – significantly reduce residual stress in a single pass; the distance from the cooling source to the weld pool was found to be critical to the stress reduction impact on the weld pool shape and thermal field [139].
GTAW/Ti-6Al-4 V	Forced convective CO ₂ – avoid arc disruption; able to reduce the oxidation of the specimens produced as well as refined microstructure, improved hardness, and enhanced strength; improvements to geometric repeatability and accuracy [138].
GTAW/mild steel	Forced convective liquid nitrogen – the extended distance from cooling jet to arc limits the efficacy of the process regarding residual stress [140].
GMAW/mild steel	Forced nitrogen cooling – reducing heat accumulation in the top layers and cyclic reheating of the lower layers, leading to a near-net-shape layer geometry and a fine grain structure. However, due to the possibility of nitrogen adsorption and deleterious effects, the applicability to a wide range of materials is unclear [141].
Strategy – in-suit heating	
GMAW/ER70S-6	Induction coils mounted positioned ahead of and behind the welding torch – reduced residual stresses by causing the distribution of heat input to become more homogeneous in time and space [144].
GTAW/ER70s-6	Wire feeder heating [145] – enables to melt a greater volume of wire compared to the cold wire which subsequently increased deposition rates and productivity [146]; the same welding parameters the droplet detachment occurred at a higher velocity and frequency, and smaller bead width compared to cold wire approach.

dimensional accuracy. This technology is applicable in the aerospace, automobile, military, mould, and dies industries as well as in nuclear energy and naval [75–78]. This includes, for example, manufacturing marine propeller, landing gear assemblies, wing ribs, and engine cases, and excavator arms [9,79–81].

For instance, the aerospace industry focuses on the manufacture of complex titanium and nickel alloy parts, making WAAM a cost-efficient manufacturing process due to the difficulties associated with the subtractive processes used in these components. Titanium makes a contribution of 93% of the Lockheed SR-71 Blackbird structural weight and about 90% of the forging weight has to be removed by machining [82]. As another example, the aerospace and automotive industries use topologically engineered structures increasingly, reducing the weight while maintaining component functionalities and maximizing its performance. WAAM provides the capability to make topologically optimized parts since high material waste and long lead times are costly [21].

Fig. 4 shows examples of metal components manufactured via WAAM including fairly complex geometries, besides previously manufactured simple geometries. These components include combinations of the simple characteristics of thin and thick-walls as well as overhangs. Industrial components also have complex structures optimized topologically and are made from expensive materials, such as titanium and nickel alloys (see case studies in Subsection 4.5). Therefore, to use the maximum capacity of WAAM, we need to:

- o define the geometrical features that are most suitable for industrial applications, for instance, new lightweight structures addressing geometrical accuracy and mechanical constraints. WAAM is an excellent way to manufacture revolutionary designs, as WAAM can eliminate many of the constraints usually encountered in the traditional production.
- o link the processing parameters to part quality and geometrical accuracy. The WAAM process, for example, can offer high deposition levels. However, the massive heat input during WAAM often results in major residual stresses and distortions. These challenges affect the part accuracy and quality.

The following section presents the concept of quality and accuracy of the deposited components through WAAM, with a focus on heat management, to address the aforementioned challenges.

3. Principle of part quality and accuracy

The WAAM process affects the part dimension and accuracy. WAAM comprises melting of wire by the arc, transfer of molten metal to a molten pool, the convective flow of liquid metal into the molten pool driven by surface tension gradient, arc pressure deformation of the surface of the molten pool and solidification of the molten pool [88]. These physical phenomena, among others, influence the distribution of temperature, the shape and size of the deposits and the structure and properties of the components. Transient and spatially non-uniform temperature conditions contribute to residual stress and distortion [50,89]. This section focuses on exploring the concept of quality and accuracy of the deposited parts through WAAM. There should be considerable emphasis on the part quality (mechanical properties and residual stresses) and accuracy (surface finish and geometrical precision). Mechanical and microstructural properties, however, are out of scope in this survey. Hence, first, the concept of heat input is discussed in Subsection 3.1, then the concept of heat management, including heat dissipation, heat accumulation, and different thermal cycling is presented in Subsection 3.2. Next, the methods for quality improvement with a focus on heat management are discussed in Subsection 3.3, followed by common WAAM defects in Subsection 3.4.

3.1. Heat input and heat losses

Manufacturing of structurally sound and defect-free WAAM components, addressing the necessary geometrical accuracy and surface finish, requires an appropriate selection of the process variables. The welding parameters including current (I), voltage (V), and TS are influenced the thermal profile in WAAM and therefore the material properties, dimensional stability, and substrate wettability [16]. The following equation describes the heat input:

$$\text{Heat input} = \eta \frac{VI}{TS} \quad (1)$$

where η is the efficiency of the transferred power, that is, the ratio between the transmitted power and that effectively inserted into the material. A small range of combinations of process parameters results in a defect-free, stable deposition and this area can be represented within a process map. Furthermore, two parameters namely plasma energy per unit traverse length (E_l) and volumetric feed rate of wire per

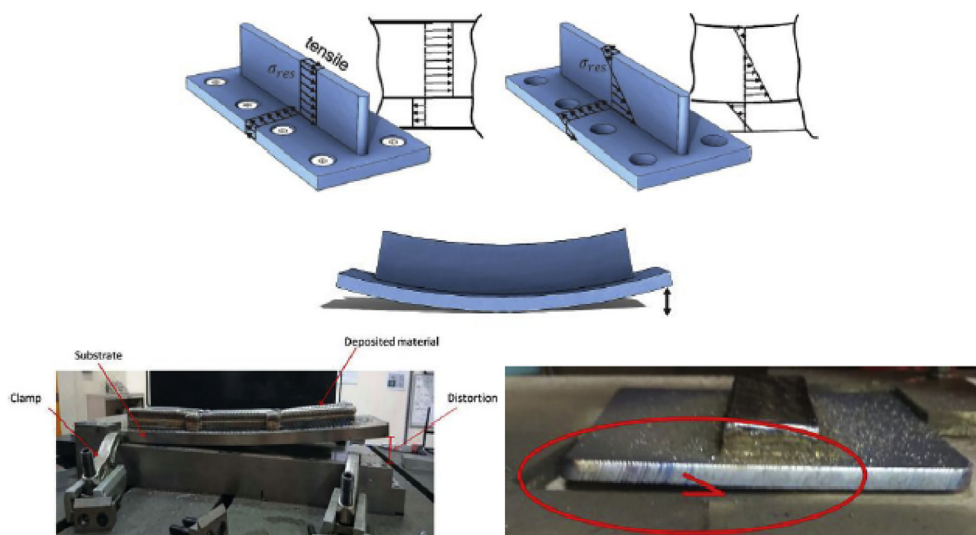


Fig. 8. Residual stress and distortion in WAAM: stress field in a clamped (top-left) and unclamped section (top-right) and out-of-plane distortion of the unclamped section [148,149] unclamping (bottom-left) [27] and thermal induced substrate deformation (bottom-right) [83].

Table 3
Porosity detection in different features.

Feature Heat source/material Control factor	Highlight
Thin-wall [174] GTAW/Ti-6Al-4V CMT mode Single bead [172] CMT/ER 2319 CMT mode, WFS, TS Single bead [175] CMT/ER 2319 CMT mode, WFS, TS	Porosity was visible in the contaminated half, whereas none can be seen under the standard clean conditions. When porosity was avoided, it was possible to achieve good mechanical properties. Porosity did not depend strongly on the ratio of the tested CMT mode, WFS, and WFS to TS. The variation from batch to batch in feedstock wire had a major effect on porosity. A larger weld bead size would limit the ability of hydrogen bubbles to escape to the surface. A high WFS increased the rate of hydrogen absorption to the weld pool, resulted in increasing porosity, while a very high WFS to TS ratio of 25, resulted in decreasing pore count, which was attributed to the high heat input which lowered the cooling rate, allowing more time for the hydrogen bubbles to escape. Reduction in porosity to a combination of lower heat input and more effective removal of the oxide layer from the wire surface.
Thin-wall [176] CMT/ER 2319 CMT mode Single bead [177] CMT/ER4043 Al Wire Properties Block [178] CMT/H13 steel metallurgical bonding	Compared to welding, hydrogen pores were more difficult to control for WAAM as a large amount of wire was continuously fed into the molten pool. A crack-free block with limited porosity and desirable mechanical properties was demonstrated, despite the non-homogeneous microstructures. When the porosity and pore size exceeded a threshold value, the internal defects invariably had the most detrimental influence. Porosity and grain geometries were highly dependent on the location in the build. The largest pores were found in the top-beginning of the pass, far from the base and the smallest in the top-end of the pass, far from the base, but no obvious trend exists with increasing wall height. The pores were not detected by an optical microscope after rolling with a 45 kN load. Pores formed in as-deposited 2319 and 5087 aluminium had different internal morphology because of their distinct microstructures and modes of solidification. Most pores were sub-globular in shape and clustered at the bottom of the beads. The porosity of the bead body zone was 1.56–1.63 times as much as that of the bead overlap zone. Porosity can reach a high level due to wire contamination. The pore distribution was uneven and pores roughly distributed along the fusion boundary.
Thick-wall [179] GMAW/ER308L - Thin-wall [180] CMT/ER 2319 & ER 5087 Inter-layer rolling Block [163] GTAW/Titanium alloy Contaminated wire	

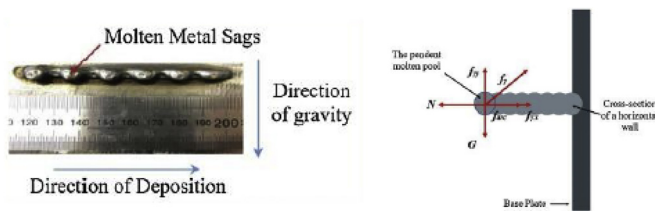


Fig. 9. The sagged bead geometry in the horizontal deposition (left) and a force model for a pendent molten pool in the positional deposition. Normal force, N ; gravitational force (G), arc pressure (f_{arc}), and surface tension force (f_s) (right) [186].

unit traverse length (V_l) control the consumption of plasma energy and feed material for a single track deposition, thus, deciding the material deposition rate (DR) as

$$E_l = \frac{60P}{V}; (J/mm) \quad (2)$$

$$V_l = \frac{A_w WFS}{TS}; (mm^3/mm) \quad (3)$$

$$DR = \frac{60A_w WFS \rho_w}{V}; (J/mm) \quad (4)$$

where A_w is the cross-section area of the wire and ρ_w is the density of the wire. In summary:

- o Heat input is controlled by voltage and current intensity provided by the equipment and coefficient of thermal efficiency (i.e., ranges from 0.52 for GMAW to 0.8 for CMT).

- o Heat input is the most significant parameter that it provides a qualitative estimate of the extension of the fusion zone and cooling rate [90].
- o Heat input affects distortions due to the large volume of melted material and which shrinks during solidification [91].

Typically, WAAM uses heat inputs ranging from tens to hundreds of J/mm and this heat is typically dissipated (i) by conduction through the components and substrates, (ii) by forced convection through the shielding air, and (iii) by radiation to the atmosphere. Therefore, it is critical to adjust the heat input during WAAM. This fundamental variable not only changes the geometry of the materials deposited (i.e., the width and height of a track and a layer) but also affects the microstructure. The thermal inertia increases when a volume is applied during the deposition process. This affects the thermal gradients and cooling rates, which in turn influence residual stress and microstructure [81]. The temperature gradient of the molten pool decreases as the depositing height rises and the amounts of heat loss decrease for the manufacture of large components. This is because the heat conduction toward the substrate is the preferential mode for cooling the molten pool. Increasing the number of deposited layers decreases the magnitude of the heat flow, causing heat accumulation (see Subsection 3.2) [92,93]. Therefore, the amount of heat applied during WAAM, the thermal conductivity, and specific heat of the base material is important for determining the cooling rate, and this is of vital importance for regulating the cooling solid-state transformations that may occur in the affected heat zone.

The heat conduction models have been used to predict the geometry of weld pool geometry, the temperature ranges, the cooling rates of solidified structures. In one of the most used traditional models, Rosenthal introduced the thermal cycle description theory and provided models that still form the basis for analytical and computational mathematical

Table 4
Humping – effect of important factors on the bead geometry.

Heat source Material Control factor	Discussion/suppression mechanism
GMAW [187] Mild steel Magnetic field, current, TS	A good weld bead can be obtained without the humping with suitable magnetic flux density; however, the introduction of the magnetic field causes increases in spatter. The minimum excitation current required to suppress humping bead increased by increasing the TS and correlations were established between them.
GMAW [188] Mild steel Magnetic field	Used an external magnetic field to produce an extra electromagnetic force in front of the welding pond to reduce the momentum of the molten backward flow, improving bead quality considerably and an enhancement of critical TS.
GTAW [189] SS 304 Magnetic field	The upward electromagnetic force was used to lift the molten metal, and it was shown that the shape of the bead was significantly improved.
GTAW [190] SS 304 Magnetic field	Used cusp-type magnetic to change the cross-section of the arc plasma from a circular to an elliptical shape, therefore decreasing the occurrence tendency of humping bead and a good bead appearance.
GMAW [191] ER 70S-6 Laser power	Hybrid heat source improved fluid flow and heat transfer in the molten pool, reducing the momentum of the backward molten metal flow and suppressing the humping bead, however, in addition to adding cost to equipment, hybrid heat source would make equipment more complex.
GMAW [192–194] ER 70S-6, SS 304 WFS, current	The fluid flow and heat transfer within the welding pool can be improved by Tandem, decreasing the momentum of the backward molten metal flow and suppressing the humping. However, two modules contribute to the investment in equipment and complicate the operation of equipment.
GTAW [195] ER 70S-6 Shielding gas	The addition of helium can increase the heat transfer into the work-piece to increase the welding speed without the humping.
GMAW [196–198] ER70S-6 Magnetic field, current, TS	The magnetic field had significant effects on the flow dynamics of the weld, arc column, and the metal transfer, and the optimized excitation currents were determined. Combining a suitable electromagnetic field and the backward inclined welding torch can result in the successful welding bead with neither humping nor spatter.
GMAW [199] ER480S-6 TS, power	The humping was enlarged and formed with the strong backward fluid flow of molten metal, which was mainly induced by the arc plasma force and droplet impact force.
GMAW [184] ER70S-6 Current, TS	Two factors were determined to drive bumping: the effective momentum of backward fluid flow and the capillary instability of the fluid channel.
GMAW [200] ER70S-6 TS, power	They suggested the formation of a thin liquid channel and rapid solidification of the melt associated with the humping phenomenon.
CMT [201] ER70S-6 WFS, TS, welding position	Humping can be avoided through planning an elaborate robot trajectory (vertical-down path is the most recommended direction). They found that it is necessary to use the TS with the most restricted condition (vertical-up) to guarantee a humping free deposition.

analysis of heat transfer in welding [94]. Despite its extensive use, it is worth noting that these equations have some restricting hypotheses, such as heat dissipation simply by conduction under conditions of equilibrium, it considers punctual heat sources, neglecting surface radiation and convection losses in the dynamic molten pool [95]. In addition, it excludes enthalpy of phase transition, including melting, and thermal gradients of the thermal properties. The solutions developed for two-dimensional (2D) and three-dimensional (3D) heat flow makes it possible to measure the peak temperature (T) at any point distant from the heat source as

$$T - T_0 = \frac{Q}{2\pi k} \exp \frac{x}{L_c} K_0 \left(\frac{R}{L_c} \right) \quad (5)$$

$$T - T_0 = \frac{Q}{2\pi k R} \exp \frac{(R-x)}{L_c} \quad (6)$$

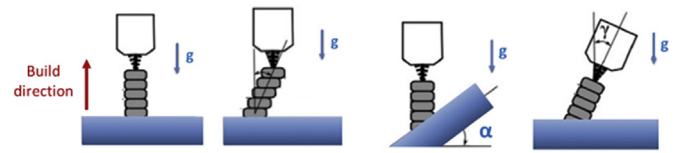


Fig. 10. A schematic view of different build directions. The degree of freedom in WAAM provides different building strategies and the inclination angle can vary in the system restrictions.

$$L_c = \frac{2\alpha}{TS} \quad (7)$$

where T is the temperature at a given position, T_0 is the initial temperature of the base material, Q is the heat input power, k is the thermal conductivity of the material and K_0 is a modified Bessel function of the second kind and zero-order, α is the thermal diffusivity of the material, R is the radial distance from the weld centerline, that is, $R = (x^2 + y^2)^{1/2}$ or $R = (x^2 + y^2 + z^2)^{1/2}$ for 2D and 3D heat flow, respectively, TS is the travel speed and x is the distance from the heat source.

More accurate models which account for convective heat transfer are increasingly being replaced with the heat conduction models [96–98]. For example, Fig. 5 shows the variation of the cooling rate measured for different arc powers and travel speeds during the WAAM process [88]. The convective flow of liquid metal into the molten pool combines hot and cold liquid and decreases the gradient of temperature in the pool. Therefore, heat conduction calculations that neglect the molten metal convection overestimate the temperature gradient and cooling rate [88]. Note that the WAAM processes are extremely complex and extensive calculations are required for a fully-comprehensive model of molten pool heat transmission and fluid flow. The level of simplification that can be accepted for a specific application must therefore be considered. Simulation designs should take into account, including dimensions (2D or 3D), transient versus the steady-state, flat surface of the weld pool versus a deformable surface, and laminar flow in the molten metal versus turbulent flow, etc. [99]. The outcomes of these choices depend on the simulation effort's objectives [100].

As mentioned above, heat can be dissipated by forced convection through the shielding air. Therefore, it is critical to adjust the shielding gas composition and flow rate. WAAM includes a protective environment that primary purpose it protects from the oxidation of the fusion zone and its surroundings. The shielding gas is, therefore, an important parameters because it affects the mode of heat transfer [101], process stability [102], and geometry and appearance of beads, surface waviness and deposition efficiency [103], in addition to the impact on the mechanical properties [104].

During WAAM, shielding gases have also other functions. WAAM deposition, with high energy density, easily generates a large volume of plasma. However, with proper optimization of shielding gas, that is, by careful selection of the type and flow of shielding gas, it is possible to eliminate the plasma plume and adjust the penetration of the weld. The shield gas is often supplied through the welding torch, however, more measures may be needed for materials which are highly susceptible to atmospheric contamination (e.g. Ti-6Al-4V) [104]. By providing laminar shield gas flow as opposed to conventional local shielding devices, during the deposition of WAAM components, the protection zone could be extended to the side walls [103].

Argon is commonly used and it contains elements with greater dissociation and ionization potential than other active gasses such as carbon dioxide (CO₂) or helium, nitrogen and hydrogen, allowing arc temperature to increase [105] or enhancing cooling rate, for example, using argon shielding gas mixture with higher helium content [106] or modify metal transfer [101]. For instance, when only argon was used significant spatter was observed, however, the introduction of O₂ to

Table 5
Various unidirectional slicing and their specifications.

Strategy	Description
Uniform slicing [25]	Each slice has the same top and bottom contours and maintains equivalent slice thickness in the CAD model and restricts the precision of the deposited component due to the staircase effect and the precision can be enhanced by choosing very thin layers.
Adaptive slicing [210,211,216]	This approach uses parallel slices, but parameters like the surface finish and the CAD-geometry curvature in the deposition direction are determined by slice thickness. The surface finish is better than the uniform slicing as the impact of the staircase is reduced.
Region-based adaptive slicing [212]	Depositing critical features with adaptive slicing and non-critical features with the maximum layer thickness to minimize build time. This strategy requires explicit control of surface properties and user versatility to establish different surface tolerance values for various regions.
Feature-based inclined slicing [213,214]	The thickness varies depending on the curvature of the feature, unlike uniform and adaptive slicing techniques. It can be used without the support to deposit overhang structures.

the gas mixture greatly decrease spatter generation, and the introduction of CO₂ in the shielding gas mixture was seen to increase the width and penetration of the fusion zone [101].

As another example, if a chosen shielding gas promotes an increase in both the width and the weld metal penetration, low heat inputs can be used, potentially reducing the risk of distortion. Pires et al. [107] highlighted that during metal active gas welding of low carbon steel using an argon-CO₂ mixture as shielding gas, an increase in CO₂ required an increase in the heat input to obtain a stable arc. As such, the increase in CO₂ content needed an increase in the heat input, which can influence the microstructure and mechanical properties.

The shielding gas flow exerts a mechanical force on the arc, making it more scattered at a low-level heat input, and gas ionizes at a high-level heat input, making the arc plumper and improving arc stability [108]. Too high flow rate can cause poor penetration and porosity can be introduced to the gas column due to turbulence drawing in atmospheric gases [109]. Hence, it is important to select the correct shielding gas flow rate. In Section 4 further discussion on the impact of gas shielding on geometrical features is discussed. The concept of heat dissipation and heat accumulation is discussed in the next Subsection.

3.2. Heat dissipation and heat accumulation

Two major problems limiting the application of WAAM are heat accumulation and the complex thermal conditions (e.g., inter-layer temperature and cooling rate) and therefore difficulties in controlling dimensional accuracy, particularly for large parts [11,104,110]. On the one hand, WAAM induces complex thermal profiles throughout the material as the deposition of component experiences being heated repeatedly. The transfer of heat to the already deposited layers is of great concern as it affects the cooling rate and thermal cycles of both the previous and currently deposited layers, which can lead to microstructural and geometrical changes along the part [111]. Except for the first pass

that only goes through post-heating and the last pass that only goes through preheating, all the others go through both preheating and post-heating, including preheating process. Furthermore, the deposition pattern strongly affects the heat dissipation and impact of thermal cycles, however, it is unclear if trajectory planning alone can overcome the issue of heterogeneity in WAAM parts (see Subsection 4.2 for more details).

On the other hand, during the metal deposition, the high amount of energy transmitted to the workpiece causes a progressive increase in the workpiece temperature. Depending on the balance between applied and extracted heat, thermal energy can accumulate, which can significantly influence the solidification rate and therefore the deposition geometry. The heat is mainly transmitted from the molten pool to the substrate by conduction, the heat dissipation conditions become poor as the number of layers increases, which would cause the layer dimensions to vary [92,112,113]. For example, a lower temperature of inter-layer accelerates the solidification of the molten pool, so the layer would appear narrow and tall. Conversely, a higher temperature in the inter-layer makes the layer wide and short. It has been reported that excessive heat accumulation can lead to deteriorating layer forming quality [114], which can lead to collapsing layers due to insufficient solidification [115]. Zhao et al. [92] showed that the temperature gradient of the molten pool decreases as the height of the wall increases as a result of the heat accumulated which prolongs the time required to solidify the molten pool. They proved that increasing the temperature gradient helps to decrease the molten pool flow behaviour. Wu et al. [16] indicated that the dimensions of the layer differ in the first few layers and then appear to be steady when an equilibrium achieved by heat input and dissipation. This problem affects the dimensional accuracy of the deposited component considerably. More importantly, this dimensional deviation would occur in the direction of deposition and then shift the gap between the torch and the workpiece, which prevents the process of deposition at the upper layers. Additionally, the varying layer width makes the process of machining more complex. This will increase the cost and time needed to post the part process [16,116].

In summary, the aforementioned thermal cycling results in multi-peak thermal cycling, with complex temperature gradient distribution, leading to a significant effect on the stress distribution, deformation, microstructure, and mechanical performance of components (see Subsection 3.4.1). Heat accumulation has detrimental effects, including (i) increase in the molten pool size and widening the deposited layer [116], (ii) non-homogeneous material along the building direction, (iii) increase in inter-pass temperature [68,92,117], (iv) possible workpiece structural collapse [118], (v) surface waviness, and (vi) modification of the metal transfer mechanism [16]. Hence, WAAM is still being matured. Well-established knowledge from heat management can be transferred to better understand and improve additive manufacturing part quality and accuracy. In fact, not only the heat input but also heat dissipation affects the molten pool shape during WAAM. Though the heat input is high, the shape of the molten pool can still be well controlled by improving heat dissipation by additional cooling to compensate for excessive heat input. For example, if the cooling systems or/and introducing interlayer dwell period are specified such that the deposition is conducted on a surface of low enough temperature, steady-state deposition is possible, identifiable by a constant weld pool size

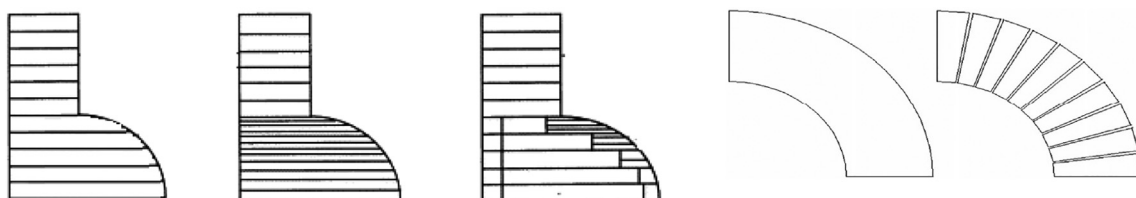


Fig. 11. Various unidirectional slicing according to Table 5: left-to-right: uniform slicing, adaptive slicing, region-based adaptive slicing, and feature-based inclined slicing.

Table 6
Various multidirectional slicing and their specifications.

Strategy	Description
Silhouette edges projection [219]	This approach includes (i) identification of the unbuildable surface features by projecting silhouette edges, (ii) decomposition of a component into buildable and unbuildable sub-volumes, (iii) for the unbuildable sub-volume, determination of a new suitable building path, (iv) for the building path, further decomposition of the unbuildable sub-volume by repeating the same projection procedures. The implementation of the strategy for complex components is complicated and computationally costly.
Projection-based decomposition, transition wall [219]	This approach progressively decomposes the part into sub-volumes, each of which can be entirely constructed in a certain direction. This strategy includes a transition where surface accuracy is considered.
A feature-based volume decomposition technique [220–222]	This approach involves defining the feature in many individual pieces from the CAD model and decomposition from the CAD model. Features may be assessed independently using a module for local process planning, combined into a whole component.
Transition wall [223]	This method involves defining overhang layers by measuring the difference between the current and the previous layers and building an overhang feature as well as depositing a transition feature. A simple technique, but suitable only for a subset of component geometries.
Adaptive slicing [224]	This method is based on two techniques: surface tension and transition wall. This method includes a variety of layer thicknesses and slicing direction, generating optimal slices. In some cases, the centroid axis does not necessarily indicate the geometry of the component, which means this method is not robust.
Centroid axis extraction [225]	This strategy includes (i) extracting the centroid axis of the model, (ii) identifying the splitting surface and conducting subsequent decomposition, and (iii) performing multi-axis slicing and finally generating the collision-free slicing sequence for each subcomponent. In some cases, components cannot efficiently decompose as required because the centroid axes do not always indicate geometry changes.
Offset slicing [226]	This strategy identifies sub-volumes of the component that can be built using non-planar slices for an angle of overhang depending on the operation.
Modular boundary models [227]	This strategy includes three major modules: spatial decomposition, part slicing, and generation of tool paths for each slicing layer.
Decomposition – re-grouping [228]	This strategy includes (i) a model simplification step prior to CAD decomposition, (ii) the decomposition of the CAD model into sub-volumes, and (iii) the introduction of a depth tree structure based on topological data for combining in ordered slicing groups. It's proven to be simple and successful in different features.
Curved slicing [217]	This method involves creating tool paths for a five-axis welding device to deal with building overhanging structures by adjusting the slicing direction according to the geometry of the component, by using a cross-section function of the CAD model.
Curved slicing [218]	This strategy involves creating tool paths by intersecting the curved surface with vertical planes, followed by the algorithm for point offset. Invalid for complicated situations.
Curved slicing [229]	This strategy involves (i) slicing of the

[112]. This may give the possibility to overcome the conflict between consistency forming and performance during WAAM. However, the determination of a suitable surface temperature tends to be by resource-intensive trial and error, with limited systematic approaches proposed [119,120]. The following section discusses the concept of heat management to improve deposition quality during WAAM.

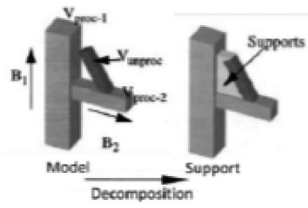
3.3. Heat management

In WAAM, inter-layer temperature (i) reflects the temperature of the previous layer, which is deposited shortly before the new layers [121], and (ii) affects the cooling rate, and therefore the mechanical and microstructural characteristics. Continuous deposition without inter-pass cooling can produce excessive heat input in a local region, resulting in high temperatures and wide re-melting, resulting in poor dimensional accuracy and surface finish [49,122]. On the one hand, if an inter-pass temperature is high, the wettability of the molten pool can be improved, and also causes an additional temperature rise in small areas and overhang features. This results in the melting of the previously deposited layers and may end in the catastrophic failure and can even cause the wall to collapse [119]. On the other hand, a low inter-layer temperature affects mechanical properties and may result in brittleness, poor bead-to-bead re-melting, and void creation. Note that in addition to the interfacial tension and gravitational force, wetting plays an important role in controlling the spread of the deposited metal. The choice of interlayer temperature depends on the material metallurgy [17,123]. For example, the wettability of a molten aluminium alloy to a cold build plate is poor because of the high thermal conductivity and the large temperature difference between the molten metal and the build plate. The contact angle of the molten metal aluminium alloy on a cold build plate is distinctly larger than 80° [124]. Results showed that the wettability of the deposited layers was effectively improved by preheating the substrate at 118 °C [124]. In another example, Alberti et al. [125] showed that when preheating was used, the precipitation-hardened alloy had similar deposition behaviour to that observed without preheating, with improved wettability, but no major changes. The solid-solution-hardened alloy showed a greater increase in wettability. Hence, it is important to keep the inter-layer temperature at a suitable range depending on the alloy used. The following is a description of heat transfer-based processes that can be applied in situ of deposition or inter/intralayer to adjust the total heat flux to the component during the WAAM process, which directly affects distortion and deformation. This includes the effect of idle time, environmental cooling, inter-pass active cooling, localized heating, and preheating on part quality of WAAM parts.

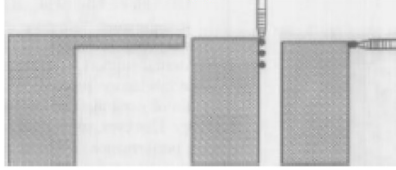
A typical practice for avoiding heat accumulation is to introduce idle times between subsequent layer deposition, i.e., allowing the workpiece to cool down to a secure temperature until the deposition of the subsequent layer [50,121,126]. This parameter is crucial for the WAAM

Table 6 (continued)

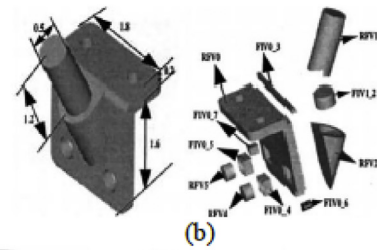
Strategy	Description
	revolving body from part volume decomposition with traditional planar slicing, (ii) spatially tracing the cylindrical coordinates and splitting the offset surfaces by the boundary of the core volume, and then (iii) mapping to the Cartesian coordinate system to generate commands for AM equipment.
Hybrid decomposition-based curved surface slicing [206]	This strategy proposes two non-planar slicing approaches: a decomposition-based curved surface slicing technique and a process-based cylinder surface slicing strategy to minimize the need for support structures and decrease the number of layers.



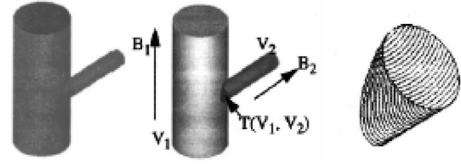
(a)



(c)



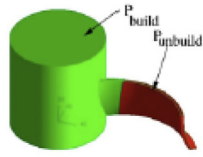
(b)



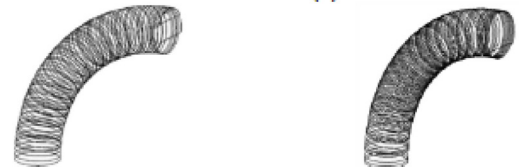
(d)



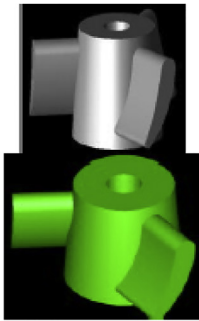
(e)



(e)



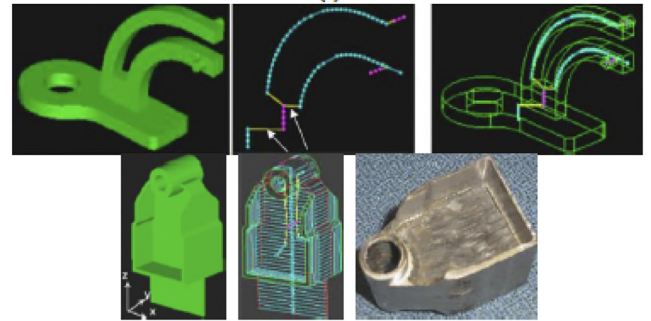
(f)



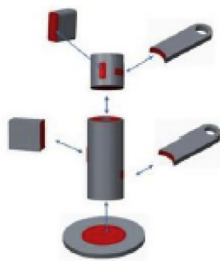
(g)



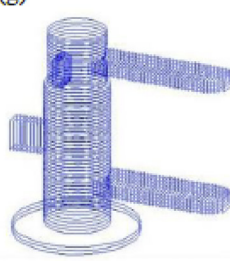
(g)



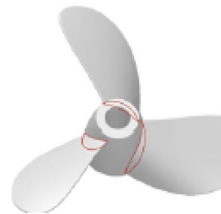
(h)



(i)



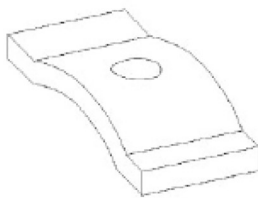
(i)



(j)



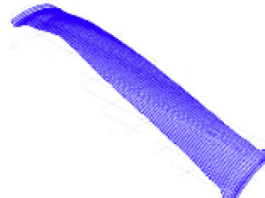
(j)



(k)



(k)



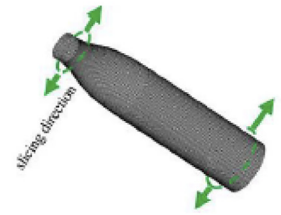
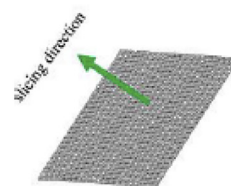
(l)



(l)



(m)



process and two main techniques are used to program idle times in WAAM processes: (i) fixed idle time selection and (ii) substrate temperature monitoring. In the first scenario, the deposition component system implements a fixed idle time at the end of the deposition of each layer [122]. This technique helps the workpiece to cool down; however, setting the right idle time requires a series of pre-tests. In addition, fixed idle times may not allow a constant inter-pass temperature to be preserved. This is due to the process of heat transfer from the molten pool to the workpiece. The most important heat flux is the conduction in the direction of the building, which is greatly determined by the height of the workpiece, i.e., by the number of layers previously deposited [92]. Therefore, the idle time should be increased as the deposition progresses, in order to have the same inter-pass temperature. This is accomplished through the second technique, i.e., monitoring the temperature of the substrate using a sensor, usually a thermocouple. The process is kept idle after the deposition of a layer until the thermocouple signal exceeds the specified value. Although this technique keeps the substrate temperature constant at the end of each layer's deposition it does not allow a constant molten pool size to be achieved. In fact, as the distance between the current layer location and the substratum increases, the volume of the molten pool increases [127]. This is similar to that in fixed idle, due to the increase in the workpiece height during the deposition process, the decrease in the conductive heat flux is associated with that. This is a major drawback of the substrate temperature monitoring technique, since restricting the increase in the volume of the molten pool is crucial for achieving adequate process performance [127] and avoiding the local structural collapse of the workpiece that results in poor dimensional accuracy [49].

As mentioned above, an appropriate inter-layer temperature can be achieved by implementing an inter-layer idle time that can be optimized by simulating the thermal behaviour during the WAAM process [119,121,122,126,128–131]. For example, Lei et al. [126] investigated the effect of inter-layer idle time on GMAW thermal behaviour using finite element analysis and showed improving the forming accuracy of each layer by increasing the idle time. Geng et al. [119] established a theoretical model to optimize the temperature of the inter-layer and heat input during GTAW and stated (i) an adequate formation and quality for each layer by adjusting an appropriate inter-layer idle time and (ii) controlling the inter-pass temperature is essential to prevent component collapse. Montevecchi et al. [121,128,129] proposed an approach to scheduling inter-layer idle times for GMAW using a finite element analysis concluding that the variable idle time leads to a constant inter-layer temperature and ensures a constant molten pool size which then improves the efficiency and productivity of the process. Zhao et al. [131] showed that by increasing the idle times (i.e., by decreasing the inter-pass temperature), the magnitude of the residual stresses can be reduced. Shen et al. [70,132] concluded that the inter-pass temperature has a significant influence on the yield stress and the occurrence of cracking. Ma et al. [117] found a significant influence of inter-pass temperature on the quality of layer deposition.

In summary, idle time can effectively control the temperature field to ensure dimensional accuracy. The downside, however, is that this approach impedes the efficiency of production. It is because due to poor heat dissipation, the needed idle time gets longer as the workpiece height increases. Excessive idle times are unacceptable when large-

scale parts are needed. Therefore, an approach to decrease the inter-layer idle times is to use active cooling systems to increase convection heat flux to the environment using water cooling [33,133–135] and air-jet cooling [135]. Reddy et al. [136] proposed a technique based on controlled cooling of the heated substrate, intending to obtain homogeneous properties along the vertical direction. Active cooling can be performed by increasing the heat sink effect of the substrate by using water-cooled fixtures [33,133]. However, the drawback of this approach is that the heat of the molten pool is still dissipated through conduction, not ensuring a constant cooling rate during the process. Immersing the workpiece in a water-cooled tank can also be used to increase the convective heat flux to the environment [134,135], however, this approach is complicated to be applied on existing machine tools.

Another solution to heat management is in situ cooling with a thermoelectric. In this method to regulate the thermal cycles in WAAM, heat sinks to the side walls by conduction (see Fig. 7), allowing for similar conditions of heat dissipation during the entire deposition. Thermoelectric technology can be very near the molten pool. Shi et al. showed that this technology is more effective than traditional convection and radiation, with the help of strong heat conduction, enhancing the heat dissipation of upper layers [62]. It thus has a major effect on the molten pool both before and after it is solidified, resulting in increased WFS and reduced inter-layer dwelling time [62] – This ensures efficient heat dissipation without reducing heat input and WFS. This modified the weld bead geometry for equivalent welding processing parameters, that weld bead height meant the need for fewer deposition passes. It can also provide a similar thermal boundary condition at the multilayer and substrate, compensates for the poor multilayer heat dissipation [112]. However, it is not straightforward to apply this approach to complex curved geometries and overhangs. An alternative solution, which is simple to implement and ideal for manufacturing complex parts, is to use a gas jet to increase the coefficient of convective heat transfer.

Increasing the convective heat transfer using air-jet impingement cooling to prevent heat accumulation by increasing convective heat transfer between the workpiece and environment performed by [135]. Air-jet impingement has a significant impact on the process, limiting the progressive increase in the inter-layer temperature as compared to free convection cooling [137]. Integrated water cooling channels' substrate was tested by [115] through continuous deposition while maintaining geometric consistency (see Fig. 6). This approach relies on conduction, the efficacy of this approach may be limited in terms of potential changes in residual stress, microstructure, and dimensional stability for larger components and lower thermal conductivity.

In such in situ forced convective cooling, compressed CO₂ [138,139] and liquid nitrogen [140] can be used to control thermal cycles (see also Subsection 3.1). For example, this promises improvement in deposited titanium alloy parts including improved surface finishing, mechanical properties, and production efficiency [138]. In addition, the use of additional gas, such as argon, nitrogen, and hydrogen, decreases heat accumulation in the top layers and cyclically reheats the lower layers, resulting in a near-net-shape layer geometry and a fine grain structure for mild steel [141]. The distance between the cooling source and the weld pool was found to be crucial to the stress reduction effect on the shape of the weld pool and the thermal field [139]. Wu et al. [138] used a CO₂ jet which was directed by a nozzle attached to the welding

Fig. 12. Various multidirectional slicing strategies according to Table 6: (a) silhouette edges projection [219], (b) a feature-based volume decomposition technique [220–222], (c) transition wall [223], (d) projection based decomposition, solid model (left), decomposition (center), and slices of the transition zone (right) [219], (e) offset slicing; the points at which the overhang angle condition was violated (left) and the decomposition of the part into P_{build} and $P_{unbuild}$ for offset slice deposition (right) [226], (f) adaptive slicing; variable direction slicing for a single-branched part – large cusp height (left) and small cusp height (right) [224], (g) modular boundary models; turbine blades CAD model and concave loops found in the body (up), decomposition and deposition and surface grinding (bottom) [227], (h) centroid axis extraction; solid model, centroid axis and centroid axis with solid model (up) and hinge example – solid model, slicing result and deposition results (bottom) [225], (i) grouped sub-volumes (right), feature regions (coloured in red) and slicing in multiple directions decomposition–regrouping (left) [228], (j) hybrid decomposition-based curved surface slicing; CAD model, concave loops (left) and generated tool-paths (right) [206], (k) curved slicing; CAD model with a hole (left) and slicing curved layers (right) [218], (l) curved slicing; tool path pattern for hard facing (left) and buffer layer on the surface of oil drilling tool (right) [217], and (m) multiple-directional slicing of the propeller: CAD model, triangulated approximation, core-volume, overhanging structures, base surface of slices for core-volume, and for overhanging structures [229].

Table 7
A summary of methods for path planning.

Strategy	Description/specification
Raster path [230]	This strategy is based on planar ray casting in one direction to automatically generate a raster fill path. Poor layer accuracy on any edge is not parallel to the tool motion direction. It is simple, efficient, and robust, however, an arc-extinguishing stage is required in each part of the raster path, so it's inappropriate for WAAM.
Zigzag path [231,232]	This strategy connects separate parallel lines into one continuous pass, with fewer transition motions resulting in less build time, hence, commonly used in commercial AM. Due to discretization errors on any borders, which do not correspond to the direction of movement, its contour is not precise. The number of arc-extinguishing points can be reduced, but with the complexity of geometric contours, the number of arc-extinguishing points increases, resulting in increased idles and reduced deposition efficiency.
Continuous path [237]	Hilbert curve-based tool-paths are an example of this approach and are especially useful in reducing shrinkage. Due to large numbers of path direction turning motions, it is not ideal for the WAAM.
Contour path [233,234]	This strategy uses offsetting geometry contours and can overcome poor outline accuracy issues by following the geometric pattern of boundary contours and improving the manufacturing offset path generation algorithm. It produces multiple closed curves and particularly suited for thin-walled structures.
Medial axis transformation (MAT)[240–242]	This method (i) generates the offset curves by beginning from the inside and working toward the outside, rather than beginning from the boundary and filling toward the inside for machining, and (ii) prevents the creation of gaps by depositing extra material outside the boundary; however, more machining is needed after the process. Step-over distance is constant, and it is ideal for WAAM. Suitable only for objects with unique shapes, thin-walled, and solid structures.
Adaptive MAT [243]	This strategy can continuously produce path patterns with varying step-over distances by analysing geometry and changing process parameters. The implementation process is rather complicated and suitable for uniform thin-wall deposition.
Spiral path [235,236]	This method is suited only in certain geometric designs to solve problems with the zigzag tool path. It is often used in milling path planning and the same path spacing is critical to guarantee and therefore does not work for WAAM.
Hybrid path – zigzag & continuous [72,238]	This strategy proposes a continuous path planning for complex polygons, which can be subdivided into a sequence of monotonous polygons. A simple zigzag path is then formed for each monotonous polygon, followed by interacting multiple single paths to create a closed continuous path. This method is capable of producing filling patterns for any arbitrarily formed region, reducing the number of welding passes, however, increasing sharp turns.
Hybrid path – zigzag & continuous [239]	This strategy leverages the advantages of the above-mentioned pattern of zigzag, contour, and continuous paths that offer a continuous path to reduce the number of welding passes per layer and remove the arc start/stop side effects that ignore the residual stress and distortion side effects. This method is suitable for WAAM of bulk

torch on the top surface of the weld bead. The system was tested by depositing a Ti6Al4V thin-wall, which showed improved surface quality, material strength, hardness, and manufacturing performance, as well as improved geometric repeatability and accuracy. A similar approach was also proposed by Montevecchi et al. [135], having two key variations compared to [138]: i) usage of standard compressed air instead of CO₂, which can reduce operating costs for materials less sensitive to the welding atmosphere than Ti6Al4V and ii) the jet's target is not the top layer but the bottom. This method helps the impinging jet to have a wider surface and results in a higher heat transfer [142]. A positive consequence of successful air cooling during the subsequent layer deposition, in which the electrical arc is not extinguished at the beginning and ending stages, is to minimize higher values and residual stress variability in the deposition of circular layers using WAAM [143].

As an in situ heating module, a method to reduce the residual stress was developed, which consists of an inductor with symmetrical coils mounted on both sides of the deposited part (see Fig. 7) [144]. Depending on its position in relation to the arc, this technique can be preheated and post-heated. It can allow a constant inter-layer temperature to be maintained during the entire deposition as well as reducing the residual stresses and distortion of as-built parts.

In addition, preheating the substrate is an efficient way to mitigate residual stress and cracking, reducing thermal gradients, and homogenizing the distribution of the temperature. The width of the early layers of the WAAM is known to be significantly less than that of the rest due to a fast cooling rate due to the large area of the substrate and its initial temperature. Preheating of the substrates minimizes thermal conduction and heat losses, leading to smaller temperature gradients [144].

Table 7 (continued)

Strategy	Description/specification
Hybrid – zigzag and contour offset paths [248] [249]	features. This strategy uses zigzag paths to fill the interior and remove pores, the offset path contour is employed to improve the geometrical accuracy. This method can be used for sharp corner features.
Modular path planning (MPP) [85]	This strategy divides the complex structural component surface contour and then produces the optimum filling path on the basis of geometrical characteristics for each partition. It was observed a much more consistent deposition than the adaptive path planning.
Multi-node trajectory [66]	This method uses Euler theory to develop a continuous path plan with less arc and extinguishing points for the multi-node and trajectory function, thereby reducing interruptions and waiting time. Suitable for depositing stiffened grid panels, particularly more than 10 mm beads.
Sequential path-planning [244]	This method can (i) transfer all intersections to the outer contour, ensuring a consistent and compact internal zone, (ii) enhance dynamic nature of path planning, and (iii) the path direction of the adjacent layer can be adjusted by only one arc extinguished in the process. Compared to the conventional zigzag path planning process, better densification and deposition efficiency can be achieved.
Path planning - curved surfaces [206]	This strategy is based on a cylindrical surface slicing and path planning process. A raster, zigzag, or contour can be used.
Feature-based strategy [12,245–247]	This strategy can build complex parts by designing a path strategy that satisfies the basic targeted type requirements. For every new component such as enclosed features, cross features, T-crossing features, and multi-directional pipe joints, this solution needs long-term path design work that is incompatible with AM.

Table 2 summarizes the above methods to mitigate the accumulation of heat during WAAM. In summary, WAAM-processed materials undergo complex thermal processing cycles varying from point to point, resulting in high residual stresses and distortions due to excessive heat input, and low precision and surface finish – restricting WAAM technology applications. Additionally, this complex thermal history produces location-dependent material properties for large-scale components, which translate into variations of surface properties at various locations of the manufactured parts. Furthermore, significant residual stress levels may result in defects such as cracking and distortion. The following section addresses common defects in materials manufactured through WAAM.

3.4. WAAM common defects

This section aims to identify the most common defects of the WAAM. In general, defects in WAAM can occur for numerous reasons, such as poor programming strategy, unstable weld pool dynamics due to poor parameter setup, heat accumulation-related thermal deformation, environmental impact (such as gas contamination), and other machine malfunctions [16]. Basically, WAAM defects are very close to welding, such as porosity, cracking, delamination, and spatter. Some WAAM processing impacts on the part quality and geometrical accuracy. In particular, porosity, high levels of residual stress, cracking, and humping should be avoided where they lead to modes of failure, as discussed below.

3.4.1. Residual stress and distortions or deformation

Like other AM processes, the residual stress is a major cause of distortions, the loss of geometrical accuracy in WAAM components [147], due to large thermal gradients during repeated melting and cooling processes, besides its influence on mechanical properties and grain structures [148]. Residual stress is the stress that remains in the material after the removal of all external loading forces. Thermal induced stresses arise from thermal-induced strains during the non-uniform expansion during WAAM. The induced strain can distort a material being deposited. If a structure cannot react by macroscopically distorting it, it will either cause microscopic deformation (e.g. yield or crack) or result in residual stresses. The residual stresses that result in component distortion are released when the fabricated component is unclamped (see Fig. 8) [50]. While post-processing technologies may reduce residual stress, residual distortions caused by stress are a major cause of loss in geometric tolerances. Therefore, control and minimization of deformation and residual stress is a key area of research and the best way to minimize distortions is to regulate the accumulation of residual stresses during deposition.

As stated in Subsection 3.1 and 3.2, a high WAAM heat input leads to an increasing internal energy content of the workpiece, known as the heat accumulation [16]. These effects modify the geometry of the layers [147] and the material microstructure [127], especially along with the deposited height [150]. During WAAM, shrinkage of large pools of liquids during solidification and repeated heating and cooling can result in high residual stresses and defects such as delamination, warping and dimensional inaccuracy [151,152]. Similar to residual stress and deformation, cracking and delamination not only includes the production process thermal signature but also refers to the deposit's material characteristics. The crack within the WAAM component can be categorized as

- o Solidification crack depends primarily on the material's solidification quality and is generally caused by obstruction of solidified grain flow or high strain in the melting pool [153].
- o Grain boundary crack generates along the grain boundaries because of variations between boundary morphology and potential precipitate formation or dissolution [153].
- o Delamination or separation of adjacent layers generates between layers because the underlying material is not completely melted.

Inconel alloy, for example, easily generates solidification–cracking problems due to the presence of the liquid film at terminal solidification [154]. Post-process treatment cannot repair this problem; pre-process treatment such as preheating of the substrate must be considered.

In summary, several physical processes simultaneously influence the evolution of residual stresses in the WAAM-produced parts. The complexity of the method prevents a straightforward determination of variables that can be tailored for stress reduction and defect mitigation. In some studies, the effects of individual variables on residual stress accumulation were explored for the mitigation of residual stress and distortions. It includes (i) preheating of the substrates to reduce residual stresses and distortions [123], (ii) decreasing the input power to reduce residual stresses in components fabricated by DMD [155], and (iii) increasing travel speed to mitigate residual stresses along the scanning direction [156], among others. The above findings, however, do not describe the main variables influencing the evolution of residual stress. Defining the essential variables is therefore difficult to uncover. The emergence of big data and the use of data-driven techniques may be useful when the relationships between different types of variables are unavailable [157,158]. For example, Wu et al. [158] showed that the substrate preheat temperature is the most influential variable among the process variables. Both experiments and simulations are required to identify the optimal strategy for residual stresses and distortions. The impacts of processing parameters, deposition patterns, and sequences, heating, cooling, and preheating on stress evolution should be investigated. Good quality and accuracy components can only be achieved if residual stresses and defects are eliminated or reduced.

3.4.2. Porosity

Porosity is another common defect that needs to be minimized in WAAM processing for specific alloys such as aluminium and titanium [159,160]. Porosity results in a component with low mechanical strength due to micro-crack damage and brings low fatigue properties to deposition through different size and shape distribution. In general, this type of defect is categorized mainly as either raw material induced or process-induced [77]. Material-induced porosity: the WAAM raw material, including the as-received wire and substrate, frequently has some degree of surface contamination, such as moisture, grease, and other hydrocarbon compounds that may be difficult to completely extract. Such contaminants can be quickly absorbed into the molten pool and after solidification produces porosity. Process-induced porosity: porosity produced by the process is typically non-spherical and is often caused by poor path planning or unstable deposition. If the deposition path is complex or the manufacturing process is variable, it easily creates insufficient fusion or spatters ejection, creating holes or voids in these affected regions.

Note that the deep penetration and keyhole formation are avoided in the WAAM process as it causes excessive fluidity harmful for forming keyhole induced defects [161]. However, one of the challenges faced by the commercialization of WAAM for the production of aluminium and titanium components is high porosity levels, as summarized in Table 3. Porosity can be formed as [162–168]

- o Spherical pores due to trapped gas – spherical pores resulting from a very significant difference (for example, a factor of 20 for aluminium), in liquid and solid hydrogen solubility. When the weld pool solidifies, hydrogen gas forms and is then trapped in solid metal like bubbles [169]. In addition, the fluid flow in the molten pool driven by the Marangoni convection is radially outward, for example, for titanium alloy, and the pores in the molten pool move along the direction of the fluid flow [170]. Locations near the fusion boundary then solidify first, and the dissolved hydrogen is rejected during solidification [171], hence, pores near to the fusion boundary, therefore, has not enough time to escape from the molten pool and trapped like pores.

o Irregularly shaped – irregularly formed pores (shrinking porosity) resulting from the migration of hydrogen into the voids caused by volumetric differences between the liquid and solid solution. If the

arc length is long and a droplet adheres to the wire before the corresponding peak current period during the last peak current period, the droplet can easily be blown to the outside of the weld track.

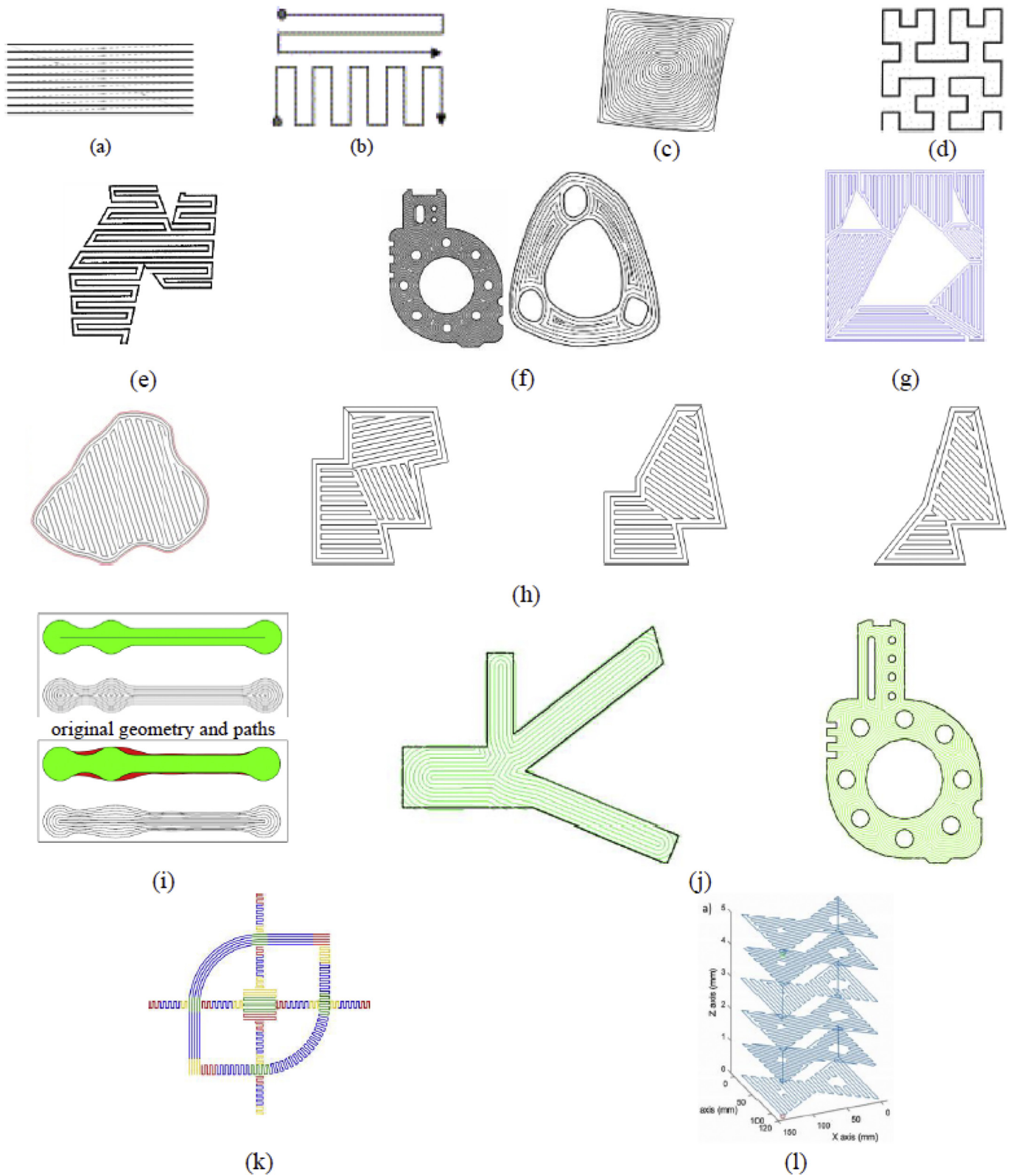


Fig. 13. A summary of path planning methods according to Table 7: (a) raster [230], (b) zigzag [231,232,250,251], (c) spiral [235,236], (d) continuous path planning [237], (e) hybrid path – zigzag and continuous [238], (f) contour path [233,234], (g) hybrid path – zigzag, contour, and continuous [239], (h) hybrid – zigzag and contour offset paths [248,249], (i) MAT; the red region is deposition of excessive materials [240], (j) MAT [241,242] and adaptive MAT [243], (k) modular path planning (MPP) [85], (l) sequential path-planning [244].

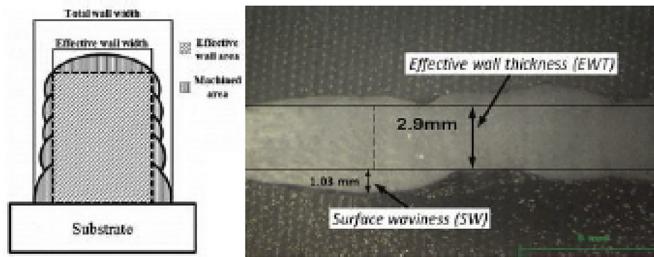


Fig. 14. Description of effective wall width and wall width and surface waviness [125,255]

Table 8
Correlations for estimating the wall specifications.

Parameter	Correlation
Deposition efficiency (DE)	$DE = \frac{EWW}{EWW + \text{Machined area}} (8)$
Surface waviness (SW)	$SW = \frac{TWW - EWW}{2} (9)$
Effective Wall width (EWW)	$EWW = TWW - \text{Machined area} (10)$

This droplet deviation resulted in the creation of spatters, molten pool collapse, and bead voids. If the molten pool from the adjacent bead cannot fill the voids, then due to the poor fluidity of the molten pool and the gas trapped in the voids, the molten pool from the subsequent layer can hardly fill the voids; therefore, irregularly shaped pores can be created. This may explain why such pores usually lie in a plane at an angle to the direction of construction rather than parallel to the layers of deposition.

- o Considerable pore size due to wire contamination because contaminants of raw materials can be easily absorbed into the molten pool and thus generates porosity [172,173].

In summary, high levels of porosity can result in lower values for key material properties. Even more problematic is the lack of reproducibility of the performance of materials. This issue complicates the qualification of both processes and components, which will limit the commercial application of WAAM. In order for WAAM to be commercially viable, porosity needs to be understood, monitored, and reproducibly reduced to an acceptable level.

Table 9
Influencing bead and layer morphology parameters with an emphasis on geometry and surface quality

Refs.	Heat source Material	Feature Control factor	Highlight
[256]	GTAW 5356 Al	Single bead WFS, TS, Current, V	They proposed a mathematical model for a suitable selection of WFS required to achieve various thickness adaptive layers. The effect of WFS on bead width was found to be insignificant.
[88]	GMAW H13 steel	Single bead Heat input, TS	They showed that (i) the deposition dimensions and the area of the fusion were reduced as TS increased and arc power increased; (ii) the peak temperature increased with decreasing TS.
[257]	GMAW HASTELLOY X alloy	Multilayer TS, WFS, current, gas flow rate	The greatest effect on the responses was observed by TS and current; increased TS or decreasing current contributed to a decrease in depth and robustness of the melt. Deposition strategies were tested using multi-layer experiments, and no substantial difference between depositing layers in the same way and depositing layers in different directions was noticed.
[258]	GMAW ER70S-6	Multilayer Current, WFS	The effects of the process variables were measured by a passive vision sensor; the key factor was the deposition current. The optimum current was found to range from 100 to 180 A.
[259]	CMT ER70S-6	Single bead & overlap TS, WFS	A parabola can be taken as the cross-section of the weld bead with an ideal step-over value of 66.66% of the width of the weld bead.
[260]	GTAW 5A06 Al	Single bead & overlap WFS, TS, peak current	SW with peak current did not change uniformly; SW decreased (190 to 160 μm) with an increase in TS (0.15 m/min to 0.30 m/min), and then increased monotonously to 234 μm at 0.19 m/min TS.

Table 10
Bead models and associated heights, width, and area of beads [134,261]

Model	Model function	Bead height, h	Bead width, w	Bead area
Parabola model	$y = ax^2 + c$	c	$2\sqrt{-\frac{c}{a}}$	$A_p = \frac{4c}{3} \sqrt{-\frac{c}{a}}$
Cosine model	$y = a \cos(bx)$	a	$\frac{\pi}{b}$	$A_c = \frac{2a}{b}$
Arc model				$y = \sqrt{a^2 - x^2} + b$
a-b	$2\sqrt{a^2 - b}$			

$$A_a = \arccos\left(-\frac{b}{a}\right) - b\sqrt{a^2 - b}$$



Fig. 15. An irregular appearance of the deposited bead [74,263] (left), single weld bead (right-up), and thin-walled part with 16 layers single-pass [265] (right-bottom).

3.4.3. Humping

Humping is a common defect in overhang features manufactured via WAAM. As shown in Fig. 9, during a horizontal deposition, the sagged bead, or the downward flow of metal, refers to the phenomenon of humping and dripping phenomenon, respectively [181,182]. The molten pool may drop before solidifying, resulting in a poor bead profile. The molten droplet remains equilibrated on the base metal in a vertical position according to the theory of static force balance unless the static forces exceed the holding force [183]. Fig. 9 indicates that the surface tension force can be decomposed along with vertical and horizontal directions. The element of the surface tension force in the vertical direction acts as the holding force during horizontal or vertical welding, while the gravitational force tends to

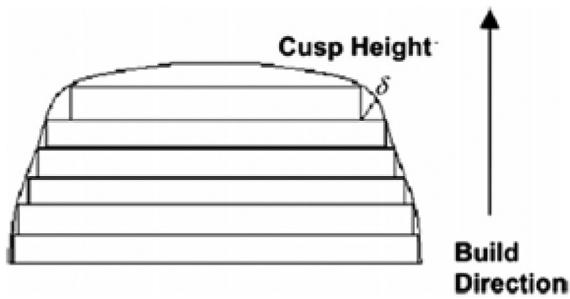


Fig. 16. The staircase effect

Table 11
Multi-bead overlapping models to improve surface conditions (artificial neural network, ANN; Regression analysis, RA)

References	Description/Highlight
RA [261]	The geometrical model was suggested based on an asymmetrical parabola. The overlap criterion suggested in this study was not ideal and results in a wavy surface. 66.66% of the single bead width was considered the step-over distance.
RA [267]	They compared the weld bead boundary with arc model, parabola, and cosine function. The optimal bead profile model was found to be largely dependent on the WFS to TS relation.
RA [268]	They compared the weld bead boundary with arc model, parabola, and cosine function. The sine function can fit the measured data with the highest accuracy. 63.66% of the single bead width was considered the step-over distance.
RA [53]	They suggested a model of two weld beads deposited by assuming circular arc intersection of the weld bead. They noticed that the optimum step-over rate is related to a single bead's width to thickness ratio. The overlap criterion suggested in this study was not ideal and results in a wavy surface.
RA [263]	They developed links between process parameters and bead geometry in weaving deposition.
Tangent model [134]	The bead cross-section was comparable with parabola, cosine, and arc functions. There was a stable overlapping process with excellent flatness for mild steel. 73.8% of the single bead width was considered the step-over distance.
Tangent model [270]	They enhanced the model presented by [134], taking the spreading effect into consideration in path planning. They showed that an ideally smooth, overlapped surface between adjacent beads cannot be achieved.
RA & ANN [110]	They suggested the correlation of GMAW parameters with weld bead geometry for ER 70S-6.
Taguchi method and ANN [242]	They showed that the standard flat-top overlapping model [267] appears to underestimate the optimum step-over distance while Tangent's overlapping multi-bead model produces a more stable deposition [134].
Feature-based model [61] [259]	A geometric model was proposed for an estimation of the height of the bead in the nth layer. The model, developed for achieving accurate layers with the desired layer thickness, can also be used for thin-walled overhang features, and curved surfaces.
Theoretical model [260]	In order to ensure that the molten metal spreads evenly through all unmelting regions to minimize SW, a theoretical model was developed. They proposed two forms of mechanisms called wetting and re-melting, which were calculated according to the width of the re-melting of each deposition.

Table 12
Approaches to improve surface conditions of WAAM deposited parts

Strategy	Control factor Feature Heat source/Material	Highlight
Trajectory control [285]	Arc igniting & extinguishing Thick-wall GMAW/ ER70S-6	Reducing the errors of the height at the arc start.
Structured-light vision sensors – closed-loop [286]	TS, WFS Single bead GMAW/ stainless steel	The one-step multi-variable adaptive geometry control system was developed through an active vision sensor; the thermally operated scan welding was used to monitor the temperature of the joint and to guarantee the desired deposition.
A passive vision sensor system - closed-loop [274]	Nozzle to the top surface Single bead GMAW/ mild steel	They implemented the adaptive controller to track the nozzle up to the top of the surface and to adjust the deposition rate; improving the stability of the weld path layer height between the arc start and end.
Closed-loop control [287]	TS Thin-wall GMAW/ H08Mn2Si	The optimum given layer width varies between 6 and 9 mm when the TS was used as the control variable to minimize the overlap. Layer width differences were approximately limited to 0.5 mm.
In situ monitoring, charge-coupled camera [288]	TS Single bead, multi-layer GMAW/H08Mn2Si	The proposed control system can keep the deposited bead width consistent with a thin-wall and allow efficient use of materials and energies. At a constant TS, the bead width decreased throughout the deposited layers.
Deposition strategy [275–277]	TS, idle time Thin-wall GMAW/ aluminium alloy	Deposition weaving strategy led to lower SW, few spatters, and decreased porosity and contact angle. Incomplete fusion and slag inclusion were not observed
Hybrid - trajectory control, local measuring & inter-layer milling [263]	TS/WFS Large thin-wall GMAW/ER4043 Al	The combination of techniques can improve layer surface flatness and reduce the differences in the layer height. Able to produce large metal parts.
Inter-layer milling [259,273]	TS/WFS Overhanging GMAW/ER70S-6	Higher-order kinematics (5-axis) create complex metal structures without the use of supports in both deposition and inter-layer milling.
Inter-layer milling [271]	Voltage, current, TS Layer surface GMAW/mild steel	Combined traditional milling and GMAW, operating after each layer to ensure z accuracy.
Inter-layer rolling [278]	50, 75 & 160 kN Thin-wall CMT/ER70S-6	Results showed that the SW was decreased by 160 kN rolling from 0.18 to 0.08 mm.
Inter-layer rolling [289]	Deformation temperature Single bead GMAW/steel	Improving geometric repeatability.
Inter-layer rolling [148]	Rolling load Thin-wall CMT/low carbon steel	Distortion and surface roughness decreased by vertical profiles and slotted rollers, although the slotted roller proved more effective – eliminating distortions.

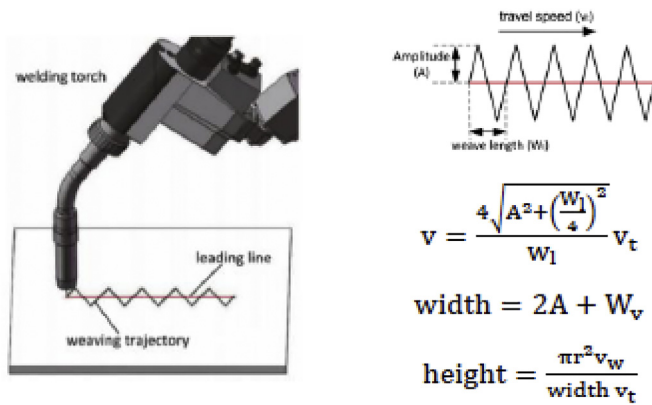


Fig. 17. The schematic diagram of weaving deposition (left) and weaving parameters and formulation to predict bead geometry: amplitude, A ; weave length, W ; travel speed along the leading line, v_t ; the radius of the wire, r ; wire feed rate, v_w ; speed along the weaving trajectory, v ; the width of the bead generated with calculated speed, W_v [263].

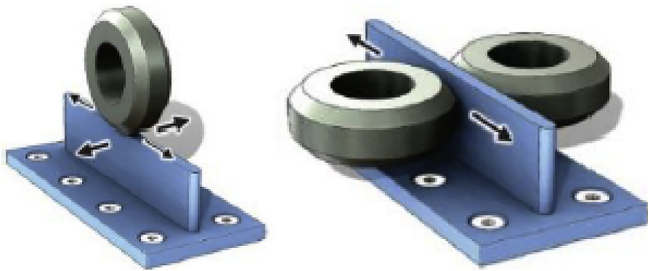


Fig. 18. The concept of vertical rolling (left) and side rolling (right) [149]

cause a detachment from the molten pool. In summary, the formation mechanism of humping includes:

- o A high momentum of the backward fluid flow causes the initiation and growth of swelling [184].
- o The capillary instability makes the weld pool unstable and susceptible to collapse.
- o Humping can occur when the width/length ratio of the weld pool was less than about 0.1 [185] (the width/length ratio in normal speed GMAW process is 0.31, and 0.085 at the neck of the liquid channel in high-speed GMAW process).

In order to gain a better understanding of humping formation in WAAM, Table 4 summarizes previous studies that were made on humping. The next section addresses process planning with the intention of minimizing defects in WAAM processes as well as creating geometric features of high quality and accuracy.

4. Process planning for WAAM

Process planning in WAAM has a significant impact on the performance of deposited parts such as geometric accuracy and mechanical properties [202]. Due to its layer-based nature, WAAM processes can be regulated at multiple scales from the bead/track scale to the overlapping beads and multi-layers and geometrical features and the partial scale level. However, low-resolution beads, layers, and overhang limits do not allow complex geometry by deposition alone. To address these challenges, designing a part for WAAM consists of determining

- o which part orientation will retain the most features while minimizing thermal distortion and post-process machining usage – Subsection 4.1.
- o which slicing and path planning to be chosen – Subsection 4.2.
- o which process parameters should be selected to deposit uniform beads and layers – Subsection 4.3.
- o which geometric characteristics can be deposited because this technique does not give absolute freedom – Subsection 4.4.
- o In Subsection 4.5, available case studies are discussed.

4.1. Build orientation

The selection of the build orientation is a crucial characteristic of the WAAM and refers to the part orientation relative to the deposition table (see Fig. 10). The challenge in this process planning phase is a trade-off between reducing build time, optimizing surface quality, and cost of manufacturing [203]. Based on substrate waste material mass, number of build operations, complicated design, and symmetries, the best orientation should be chosen [204]. Besides avoiding extra material and the costs associated with appropriate orientation, the thermal conditions change with the direction of deposition. For instance, a component's long axis can be vertical or horizontal, with both advantages and disadvantages. The horizontal orientation reduces the number of layers dramatically and allows the bead to get longer. This results in shorter deposition time, which reduces the z-direction error accumulation. The resulting larger thermal gradients from a cooler substrate induce thermal stresses that can exceed the material's yield strength, resulting in residual stress in the component. The other issue is the warping of the build plate, which causes the first layers of the part to deform.

On the other hand, choosing a deposition path to use smaller cross-sections, the vertical orientation increases the time of deposition, but the thermal conditions are closer to ideal. It results in lower thermal gradients as the temperatures of the inter-pass are higher due to the less time required to complete a layer, which decreases residual stress and warp. The deformation resulting from the base warping, however, is the key factor in selecting the vertical orientation. The z-error accumulation can be mitigated by introducing a closed-loop control system and designing extra volume in the part [205]. This is further discussed in the following sections.

In summary, build orientation selection is a complex task in the WAAM context. This is mainly because the selection of building orientation depends on several parameters including substrate and filler wire alloy compositions, heat input and thermal mass, etc. This knowledge needs to be used in combination with thermal modelling to choose the path of the building, which keeps the temperatures of the inter-pass within the appropriate range. The setting of metrics, such as improved part quality or reduced building time, should be taken into account.

4.2. Slicing and path panning for WAAM

WAAM's path strategy is a phase that slices the 3D model into 2D layers and generates process building motions. Slicing and track preparation are crucial steps in obtaining desired deposited components in terms of geometry, material, and function design, specifically deciding process variables and performance of deposited components. This Subsection presents the current status and challenges of slicing and path panning and the guidance for future slicing and path planning improvements.

4.2.1. Slicing strategies

In general, unidirectional slicing based on tessellated model (STL) is the most commonly utilized slicing technique, slicing the STL model into a set of 2.5D layers parallel to the direction of the building, intersecting each triangle from the bottom to the top of the STL model with each z plane, and then rearranging the resulting line segments to

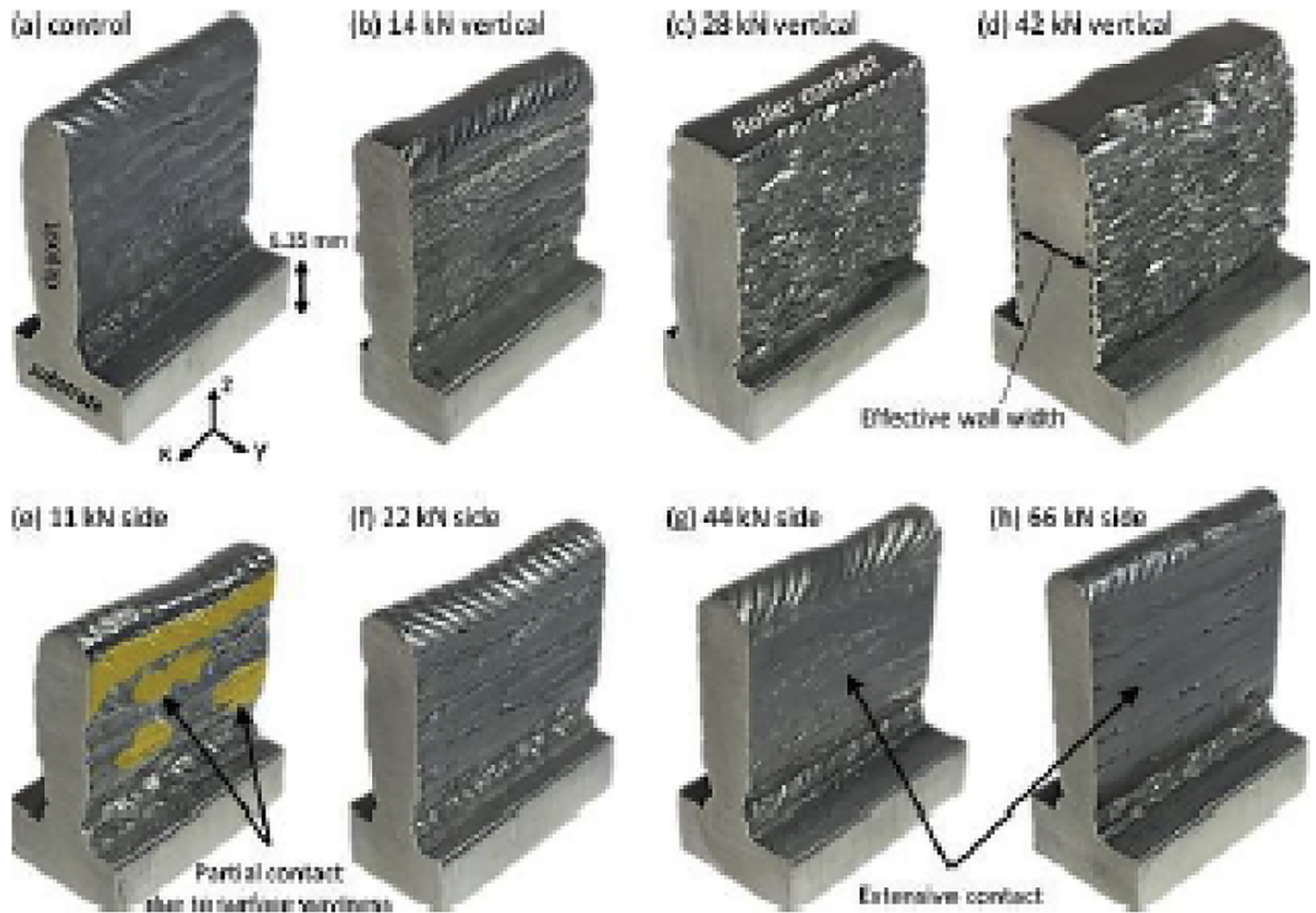


Fig. 19. (a) Wall shape of the control specimen, (b-d) the vertical inter-pass rolled specimen, and (e-h) the side rolled specimen [280].

form layer contours [206,207]. Several algorithms classify and regroup the input triangles before the intersection to improve computational efficiency [208,209]. In general, unidirectional 3D slicing is categorized as uniform layer thickness [25], adaptive layer thickness [210,211], region-based adaptive slicing [212], and feature-based inclined slicing [213,214]. While uniform layer thickness slicing produces non-uniform surface roughness of the building part [215], adaptive slicing adjusts the layer heights to enhance the surface quality [210,213], depending on the circumstances of the situation. Table 5 and Fig. 11 summarize different techniques for unidirectional slicing and their specifications.

The unidirectional slicing strategies are typically restricted to manufacturing parts with overhang features, as support structures are needed in most cases. The multidirectional slicing approach can be proposed as a possible solution for WAAM to these problems, where the slicing directions change according to the geometric shape (Singh and Dutta 2001). These strategies, in general, decompose the model into sub-volumes, and each sub-volume to be deposited has a unique direction of slicing. The main difference between the approaches proposed is the method for decomposing the model. Curved slicing techniques are also proposed for slicing components with curved surfaces. The curved surface used for curved slicing can be divided into elementary features, such as a cylinder surface and spherical surface, and freeform surface. These methods are categorized based on [19,206,217,218] (i) parametric surface and offset reference slicing surface to model adjacent deposits, (ii) offset mesh layer boundary, (iii) planar slicing restricted to cylinder surface sections, and (iv) decomposition volume and offsetting of the concave loop. Table 6 and Fig. 12 summarize various strategies for

multidirectional slicing, with an emphasis on minimizing dependency on WAAM support structures.

In summary, due to its robustness and usability, the unidirectional slicing approach is commonly used on existing commercial AM machines. Supports are however necessary in most cases for overhang features. Hence, a multidirectional slicing strategy increases WAAM capability. Its use, however, is still constrained, as the WAAM machine requires that it is capable of depositing in several directions, and more importantly, multidirectional slicing algorithms are complex and inflexible. In addition, the curved layer slicing needs to break further with infinite directions through the WAAM and further mitigate the problems, resulting in enhanced geometry accuracy due to no stair-step error along the tangential path. However, it is worth noting that the time and energy cost of the slicing algorithm is high, and this method is less effective if complex structures are tackled. Further work needs to be dedicated to finding a balance between the precision of the deposition and building time.

4.2.2. Path planning strategies

The other critical stage of WAAM is path planning, which determines the surface roughness and dimensional precision of the deposited components. Paths primarily include external boundaries, internal boundaries, and filling paths. As shown in Table 7 and Fig. 13, a number of path planning methods have been proposed. These mainly include the raster [230], zigzag [231,232], contour [233,234], spiral [235,236], continuous [237] and hybrid [72,238,239] methods. In the past few years, new WAAM path planning methods have also been developed, including the medial axis transformation (MAT) [240–242], adaptive medial

Table 13

List of thin-wall studies, including EWT and SW (ER70S-6, copper coated steel wire feed; aluminium, Al;)

Refs.	Heat source/Material Control factor Aspect	Highlight
[74]	Plasma arc/Ti-6Al-4V Material dependence	They showed that the wall thickness depends on the composition of the alloy and makes walls of 16 mm thickness, which indicates that it can be used for components with a wide variety of geometries.
[126]	GMAW/H08Mn2Si Inter-layer idle time Forming quality	As the deposition height increased the average temperature gradient in the molten pool along the flow path was consistent.
[125]	Plasma arc/Ni Alloys Material dependence, preheating EWT	The preheated deposition resulted in increasing the wettability of each layer, which can lead to a wall that is more uniformly. The effect of preheating on the geometry of walls made from solid-solution hardened alloy was found to be more significant.
[290]	GTAW/ER70S-6 TS, WFS, current, torch angle Forming quality	They showed the influence of a higher torch angle (90°) on the surface quality due to oxidation marks on the top surface. The torch angle primarily affected the deposition width and deposition height; the deposition width increased, and the deposition height decreased with an increase in the inclination angle. The current impact was found to be insignificant.
[291]	GMAW/H08Mn2Si Torch angle (45° to 135°), WFS Molten pool stability	Enhancing the stability of a formed pool by the inclination angle; depositing with front position (< 90°) was able to increase the deposition rates without decreasing the formation quality compared to vertical (= 90°) position and backward (> 90°).
[292]	GMAW/H08Mn2Si TS, WFS Surface roughness	The increased inclination angle increased the width and height of the bead. Higher WFS decreased the molten pool stability and higher TS decreased the arc stability; both can result in increased surface roughness.
[293]	GMAW/ER5356 Al Power; WFS, current Surface and forming quality	Surface ruggedness may be improved by a lower inter-layer temperature. With the increase in laser power, the width decreased, and the height increased proportionally at equal deposition levels.
[14]	CMT/ER5356 Al WFS, TS forming quality, EWW	They demonstrated that the laser-based GMAW can produce a narrower and thinner wall with better surface quality and greater stability. The EWW increased with the WFS from 26.6 mm to 31.7 mm and was decreased to 28.4 mm from 27.2 mm.
[294]	CMT/Al-Mg alloy TS, WFS Forming quality, SW	The inter-layer boundary was observed with pores and cracks. Pores were typically less than 33.5 µm in size, and crack lengths were up to 696 µm. The correct TS range prevented SW from being too rough below the lower limit and surface undulation above the higher limit.
[295]	MIG/316L SS TS, WFS, current, inter-layer temperature Forming quality	Increasing the WFS and TS (5000–6500 mm/min) resulted in lower height, increased width, and a slightly higher SW. A gradual decrease in current enhanced the formation of the bottom. The height of the layers was uniform and there were no major defects.
[296]	GTAW /Cr-Ni SS TS, feeding deposition Forming quality	An increase in TS lowered the height of the layer, thus increasing the surface quality, decreasing SW. The SW of samples for a single-wire feed was slightly better than that of samples for a double-wire feed at the same process parameters.
[114]	GMAW/H08Mn2Si Inter-layer cooling time Forming quality	The temperature gradient increased with the extended inter-layer cooling time during the deposition process and the cooling rate of the deposited components increases with the prolonged cooling time. The final forming quality of the thin-wall was improved as the time of cooling between the laying was increased in a certain range, but excess cooling led to a sharp increase in the deposition time despite the improved forming quality.
[297]	GTAW/unalloyed tantalum Material & deposited layers Forming quality	The absence of distortion following unclamping attributed to (i) the high geometrical stiffness of the wall-plus-substrate component, and (ii) localized plastic deformation of both the substrate and the lower part of the wall. A larger oxygen content resulted in a micron-sized porosity, the biggest pores were 200 µm on average, and the average porosity had an 80 µm diameter on the scattered porosity.
[174]	GTAW/Ti-6Al-4V - Forming quality	They matched heat input to material input by process optimization. The wall surface showed an uniform fluctuation resulted in a layer-by-layer deposition.

axis transformation [243], modular path planning (MPP) [85], multi-node trajectory [66], sequential path-planning [244], path planning for curved surfaces [206], feature-based strategy for enclosed feature [245], cross features [246], T-crossing features [12] and multi-directional pipe joints [247].

The following observations and suggestions are driven according to Table 7 and Fig. 13:

o Fewer arc-extinguishing points – The reason for reducing arc-extinguishing point numbers is that arc-extinguishing areas can easily cause deflections and WAAM's deposition efficiency is reduced by

idle stroke between arc-extinguishing points. In order to avoid effects on the internal structure, the arc-extinguishing points need to eventually be located on the outer contour.

- o Avoid complicated intersections of the path – The more complicated intersection, the more likely the issue of excessive filling of the materials leads to shrinking, affecting the subsequent accumulation of layers. If a complex path intersection is unavoidable, the junction must be positioned outside the exterior contour in order to prevent affecting the internal structure.
- o WAAM path planning is very robust. Since it is difficult to control the precision of the WAAM external contours and the roughness of the

surface generally is high, further machining is usually necessary. Therefore, in some local zones, maximizing forming direction is reasonable to ensure the stability of the internal structure by sacrificing the forming and machining time.

- o Fast path-planning response. In the WAAM process, the top surface is inevitably undulating, and layer height differences can exceed several millimetres [252–254]. The path designs must therefore be layer-by-layer dynamically modified according to the calculated layer height. An ideal solution is to generate the next path of layers dynamically and adjust it based on real-time layer height measurement without extinguishing the arc.
- o Commercial tools are available for creating zigzag or contour paths for the AM process, but geometries are not typically fully accomplished by such paths, leaving geometry with voids. Advanced design and various tool-path patterns are expected, depending on the characteristics of the geometric features. Major research and more learning are essential.
- o Real industrial components typically have complex geometries; thus, an improved deposition system is required that enhances the WAAM's capability. Yet, most current path panning techniques only refer to a subset of potential component geometries. More focus should be given to designing reliable algorithms capable of satisfying layered deposition that is free of support and free of collisions.

4.3. Process parameters selection for a layer deposition

Usually, a part formed by WAAM has various layers of a bead or several beads with constant or differentiated thicknesses according to a

predetermined overlap strategy [72]. WAAM allows bead-to-bead and layer-to-layer re-melting to create structures that are mechanically stable without voids or cracks. The choice of the appropriate bead dimension, the overlap of the bead, and the height of the layer is an important aspect discussed in this Subsection. A bead geometry refers to geometric parameters, such as the width and height of the material deposited along a single deposition track, a thin-wall deposition is a multi-layer one-bead deposition, and a thick-wall deposition is a multi-layer, multi-track deposition.

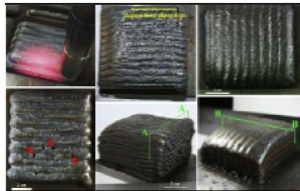
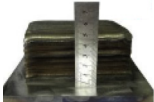
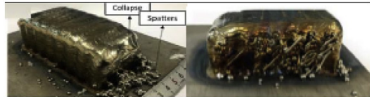
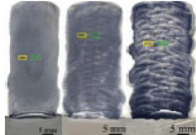

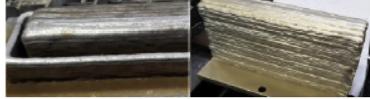

The quality of a multi-layer, multi-bead deposition can be assessed in terms of [74,125,245,255] (see Fig. 14 and Table 8):

- o The total wall width (TWW), which is the thickness of the wall directly after deposition (i.e., without post-processing) that is achievable with a certain set of welding parameters.
- o Effective wall width (EWW), which is the maximum wall width reached after finishing operations of the as-deposited walls.
- o Surface waviness (SW), which is the overall maximum peak-to-valley distances measured from a specific region within a wall.

In general, the findings of thin-wall manufacturing can be used to analyse the manufacturing process for features required for real-world components. These values depend on the set of parameters for the deposition and must be established via experiments, as stated below. The most desirable condition is to achieve a TWW close to the EWW to optimize the deposition efficiency (DE). The factors affecting surface properties are discussed in detail.

The bead morphology regulation is a process control issue that must be addressed in WAAM. In order to conduct and select the WAAM

Table 14
A summary of thick-walls and blocks.

Refs.	Heat source/material/control factor Highlight	Showcase
[277]	CMT/steel alloy/oscillation, parallel, weaving strategy (left to right) Due to the huge local accumulation of heat resulting in small shrinkage holes, the oscillation technique was not applicable to maraging steels. The parallel strategy avoided the small hole problem as the accumulation of heat reduces, the bead form was however wide and narrow, leading to significant lack-of-fusion defects. Weaving was an effective technique.	
[178]	The arc deposition pattern/the opposite deposition direction between any two adjacent tracks There were no obvious defects, overflow and melting pools collapse that indicate a solid metallurgical connection between any adjacent tracks.	
[298]	GTAW/TC4 titanium/ heat input; paths Side collapse, unmelted wire, side spatters, poor flatness. The size and number of spatters were reduced from 261 to 173 J/mm, and a decrease in the degree of collapse can be observed. Nevertheless, unmelted wire occurs with reduced heat input.	
[299]	Thick-wall/deposition path The 1 pass deposition with oscillation at a deposition rate of 3 kg/h (left) was observed as a finer resolution, compared with the multi-pass deposition with a zigzag deposition rate of 3 kg/h (center) and 6 kg/h (left), while the multi-pass zigzag layering significantly modifies the microstructure (isotropic properties).	
[75]	Pulse CMT vs. CMT CMT mode allowed a more regular deposit without major macrostructure alteration, as opposed to pulsed mode.	
[75]	CMT/Cu-Al & AISI 316L/pulsed heat input Without major defects, such as internal oxides or cracks, large components may be deposited. However, the continuous deposition of the filler metal in the case of Cu-Al alloy deposits can reduce slightly its mechanical characteristics.	
[300]	GMAW/copper-coated steel/path strategy The updated overlap-layer model permitted the deposited components to exceed the predicted width and remove the impact of accumulation on the first perforation of material shortage areas, increasing surface flatness.	

slicing and path planning, the relationship between process variables and bead geometry should be studied for the optimum welding parameters of the designed beads. The understanding of bead geometry and its connection to process parameters is an important part of determining the smoothness, the thickness of the layer, and dimensional precision of the deposited components (see Table 9). The morphology of the WAAM deposited bead is based on the WFS, TS, arc current, wire offset, preheat, and inter-pass temperatures [110,119]. Optimizing process parameters to enhance the surface quality is repetitive task-based on trial-and-error methods. As shown in

Table 10, the cross-sectional profile of a welded bead is based on three common math functions, the parabolic, cosine, and arc. Bead width (w), height (h), and area (A) are described for specific model parameters and a , b , and c model parameters that must be defined by experimental data for these functions.

WAAM also requires overlapping beads if the width of a feature is greater than that of a single pass welding bead. In general, single-path welding beads with a stable geometry can be used to set overlapping weld parameters. In addition, the height of the layer depends on the height of the weld bead, related to the welding parameter. For the

geometry specified in a part scale, it is therefore essential to select the correct sets of a track (bead) and multi-track welds. In fact, thermal inertia increases if a volume is added in the process of deposition. This initializes thermal gradient and cooling rate, which in turn influence residual strain, microstructure, and morphology of beads or layers. [81]. Thus, beads with no process control vary in height and width, with additional layers [262]. The key problems are discussed as follows.

The layer geometry relates to the conditions of heat emission from various layers. The bead geometry in one welding pass is not uniform, especially at the beginning and ends, because of the inherent characteristics [263]. At the start of the bead, the profile is wide and high (the arc-igniting portion), while the end of the bead is small and sloping where the arc ends (the arc-extinguishing portion) [263,264]. To address such challenges, CFD simulation was developed to simulate molten metal flow and solidification in the weld bead [265]. The irregular bead geometry can be explained by the backward fluid flow and the metal swelling in the molten pool and the length of the initial area is positively associated with the sloped form at its end and the length of the melt pool. The irregularity of the weld bead accumulates and deteriorates as the deposited layers increase with multi-layer WAAM. It

Table 15
Overhang features (90° refers to torch position and wall angle perpendicular to the substrate)

Refs.	Feature Heat source/material Positional deposition	Control strategy Deposition torch angle Aspect	Highlight
[269]	Thin-wall CMT/steel Planner	Deposition direction 90° Forming quality	The manufacturing of a 70° longitudinal angle demonstrated that the arc's beginning was likely to miss the previous weld bead. If possible, it is useful to set the working angle of the torch to the transversal angle (transverse direction) [246].
[245]	Thin-wall CMT/ER70S-6 Planner	Inclination angle, TS Positional welding Forming quality	They suggested deposition in the shape of a pyramid to prevent hump form. The torch head orientation of 15 to 90° was examined. TS selection was claimed to be critical for the process.
[245]	Thick-wall CMT/ER70S-6 & ER4043 Planner	WFS, TS, overhang, material Positional welding Forming quality, EWW	The successful deposition was shown by increasing WFS and current while maintaining the low TS (0.2 m/min). EWT was reduced with angle reduction from vertical to 0°. Due to the impact of density, the effect of gravity force was more pronounced in carbon steel compared to aluminium, decreasing the EWW more significantly.
[254]	Thin-wall GMAW/H08Mn2Si Planner	Offset distance, WFS, TS, overhang 90° Forming quality	The average inclination angle increased with the TS and decreases with the WFS. The average inclination angle with the TS increased while keeping the WFS constant. The average inclination angle reached over 45°.
[259]	Thin- & thick-wall CMT/ER70S-6 Rotary table	Inclination angle, TS, WFS Positional welding Forming quality	The thick wall angles of up to 30° were possible (overhang angle of 0 to 35° was tested). The thin-wall with maximum overhang was also adjusted. The application of different TSs was more effective than the application of different WFSs.
[61]	Thin-wall CMT/ER70S-6 Rotating table	WFS, TS Positional welding EWW; SW	Tilting the substrate at an angle equal to the thin-wall growth direction showed better geometry and a more stable deposition process.
[308]	Thin-wall GMAW/mild steel Planner	TS, current 90° Forming quality	The average inclination angle of WAAM with flat location deposition was estimated to be less than 45°.
[309]	Thin-wall GTAW/Ti-6Al-4V Planner	Pulsed laser 90° Forming quality	Horizontal overhang without support structure assistance or rotation was accomplished by low heat input WAAM.
[285]	Thick-wall GMAW/mild steel Planner	TS, WFS 90° Forming quality	A contact angle hysteresis model may show the deposition mechanism. A mathematical model of multi-layer inclined bead components was developed. Material failure areas were found at the edges of the inclined sections and additional material should be stored for improvement on local geometry in those areas.
[80]	Overhang hole GMAW/mild steel Planner	- 90° Overhang constraint	The overhang constraint was 75°, so the hole geometry can appear as a teardrop shape.
[245]	Enclosed features CMT/ER70S-6 Planner	WFS, TS Positional welding Forming quality	They examined overhang features including closed shape with 50 mm bridge overhang, closed shape with 200 mm bridge, and closed half-circle. A smooth radius was created at the start of the horizontal wall of squared features to fuse between the two walls. In the end, however, a sharp angle was made. The joining was produced in the middle of the 200 mm horizontal wall and the closed half-circle; misalignment of approximately 1 mm was observed between two sections.

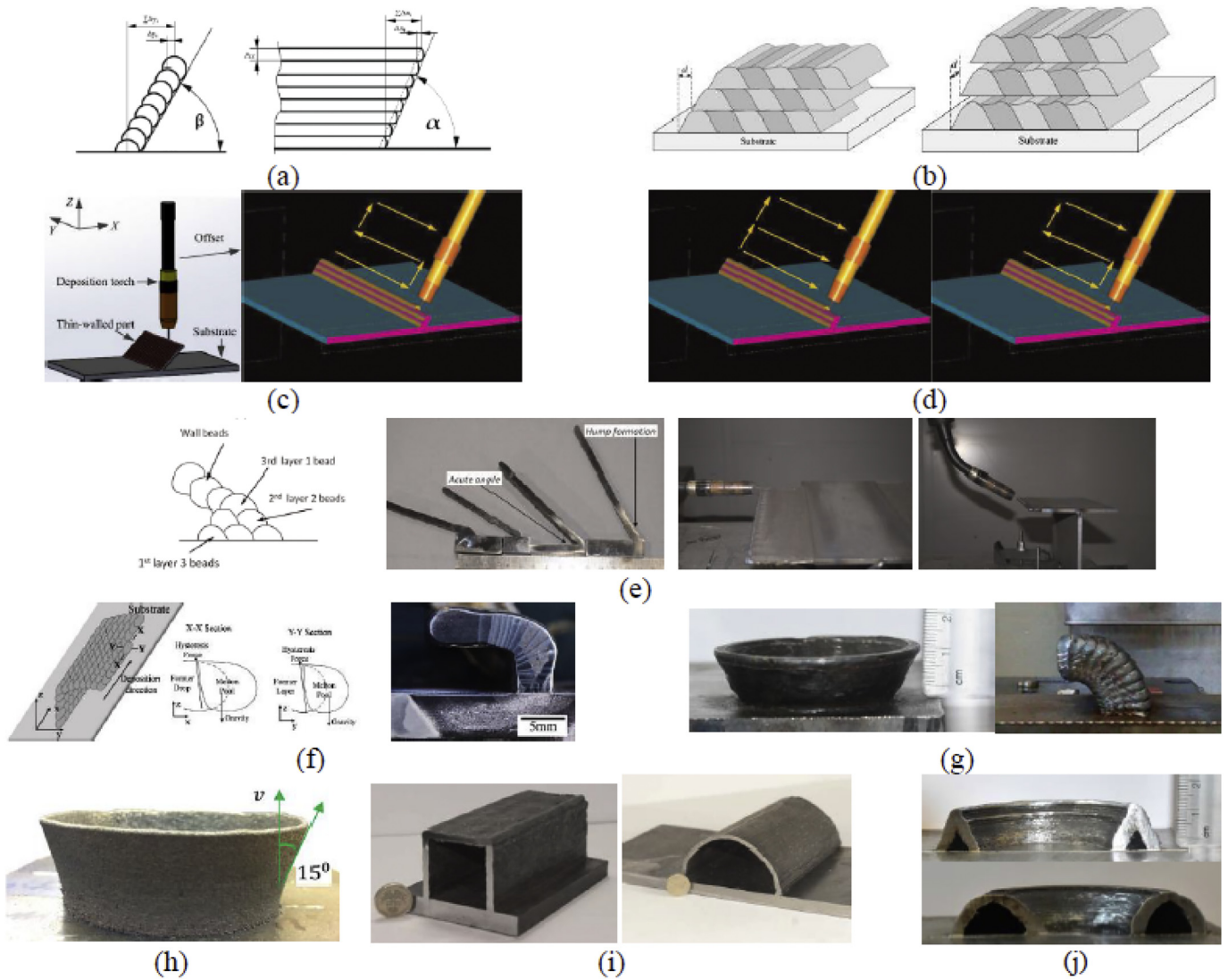


Fig. 20. Schematic diagram and examples of overhang features according to Table 15: (a) inclined thin-wall in transversal direction, $0 < \beta < 180$ (left) and longitudinal direction, $0 < \alpha < 180$; an angle $\alpha < 90^\circ$ resulted in an overhang (right) [269], (b) inclined thick-wall layer-by-layers that overlap with different horizontal layer positions (left) and by overlapping layers with different start and end locations (right) [285], (c) inclined wall with a flat position deposition: deposition torch at inclination angle of 0° (left) and positional welding technique (right) [246], (d) one direction torch welding (left) and the torch welding travel direction reversing after each layer deposited (right), (e) deposition of four inclined walls with angles to the substrate plate of 60, 45, 30 and 15° , demonstrating a hump formation in the second or third bead (up), horizontal wall (0° overhang) (bottom) [245], (f) overhangs fabricated by pulse current (right) and schematic of the molten pool sticking to the former layer and former droplet due to contact angle hysteresis (left) [309], (g) 30° thin-wall, single overhang (truncated cone) [259], (h) overhang wall [229], (i) closed-shape with 50 mm bridge overhang, closed-shape with 200 mm bridge overhang, and closed-half-circle [245], (j) triangular and semi-circular duct [259].

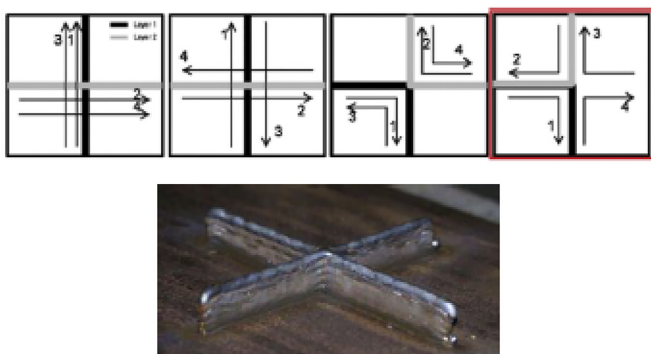


Fig. 21. Example of crossing feature and its path strategy achieving a good appearance; left to right: (a) direct crossing using a perpendicular layer pattern, (b) direct crossing in which each layer reverses the direction of travel, (c) opposite angles generated in two L-shapes "back to back", (d) opposite angles deposited as L-forms, beginning in turn from each of the four cross members (the lowest peak values at less than 0.4 mm) [246].

would affect the stability of the additional layer production, lead to uneven bead geometry, poor surface finish, and precision of component [72]. Fig. 15 provides an example of thin welded walls with major variations in bead geometry at the beginning and end of the paths of welding [74,263]. The staircase effect is applicable also to approximate the deposition of surfaces not aligned in the direction of deposition and determined by cusp height (see Fig. 16 [266]).

Another challenge is the irregular overlapping of multiple beads, where the overlapped surface between adjacent beads is not smooth. The unevenness can accumulate during the depositing cycle with multiple layers and eventually prevents it from continuing to deposit multiple layers of material in large structures. Considering the above issues, surface waviness (SW) (i.e., $500 \mu\text{m}$) presented in WAAM is a serious challenge. In addition to high levels of geometric stress, it restricts the use of WAAM as-deposited structures [9], especially where a component is loaded in a dynamic manner [147]. We should be aware of the two main mechanisms for SW regulation in WAAM components that are wetting, spreading, and re-melting. The re-melting mode allows a

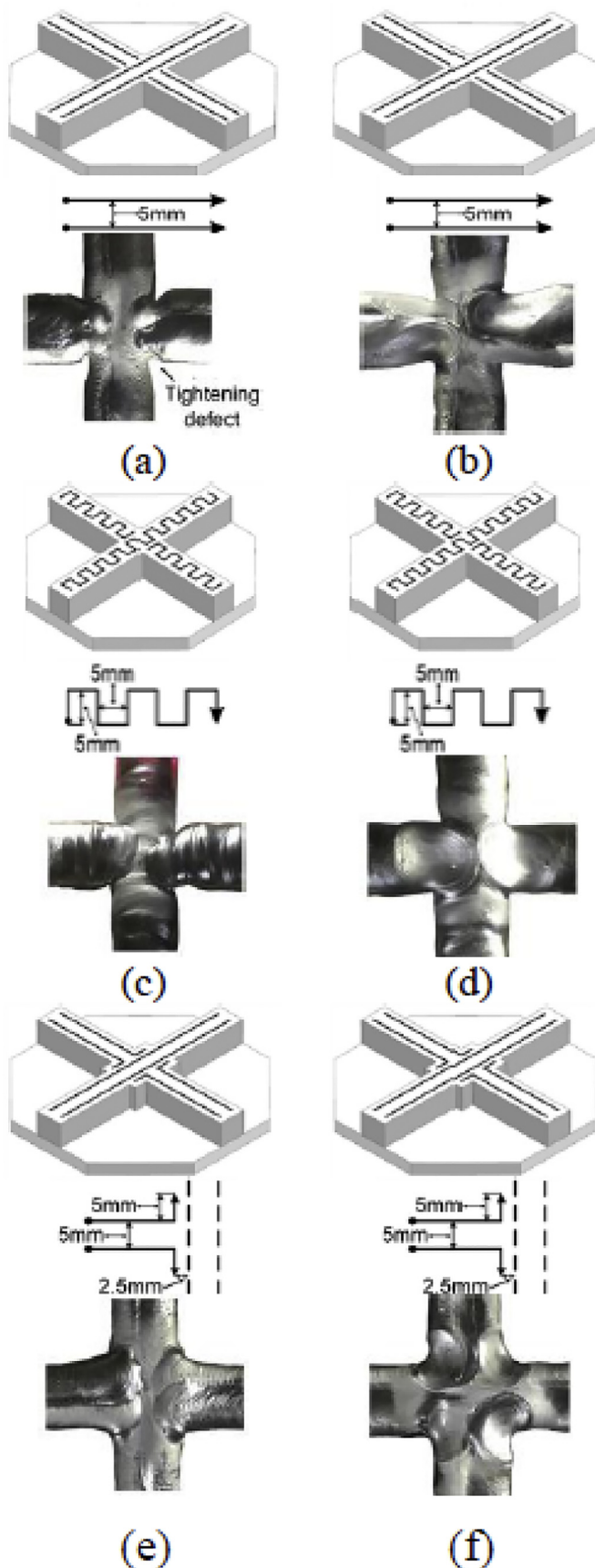


Fig. 22. An overview of direct crossing features applying arc striking and arc-extinguishing points at the intersection reported by [250]: (a) the parallel path-arc striking point at the intersection: at the intersection, tightened defects occurred and the top surface was prone to an incomplete fusion defect, (b) parallel path – arc-extinguishing point was at the

broader and deeper deposition of the formed pool due to low layer height; higher WFS contributes to a higher SW. The wetting and spreading mode ensure the smooth, narrow deposition of the formed pool in the un-melted region induced by high layer height; higher WFS contributes to a high SW [260].

The estimation and controlling step-over distance or overlapping beads is an important task where defines as the distance between the next deposition track and the previous one. For WAAM, the overlapping of weld beads guarantees a smooth surface. Gaps resulting from poorly planned paths in WAAM can be a severe problem as well. The unavoidable gaps can lead to structural failure of highly loaded components. Various models have been proposed to identify suitable step-over distance values for optimizing the material usage ratio. The determination of the finishing surfaces of the manufactured products is determined by detailed models for the single bead and multi-bead overlap. In this light, different models were proposed as presented in Table 11. These approaches include regression analysis, artificial neural networks, and the Taguchi method.

The artificial neural network has demonstrated a dynamic relationship between multiple inputs (WFS, TS, etc.) and responses (bead height and width), which is extremely nonlinear. The network has an input layer, a hidden layer, and an output layer. In the hidden layer, neurons are computational elements that perform non-linear mapping between process variables and responses. A multidimensional dependency between process parameters can be established by learning in artificial neural networks. Nonetheless, the artificial neural network data for training must be chosen carefully [110].

The Taguchi method, one of the factorial fractions, shows a successful experiment with only the major effects of the parameters in the design. Consequently, in the statistical design of experiments, if the training data for the artificial neural network are chosen to use the orthogonal array table and the process properties as output data are transformed by Taguchi, this approach generates more reliable results with a smaller training set than others [134,242,267].

The overlap between the individual beads can be measured as a function of a single bead's width. The optimal overlapping distance includes 39% [178], 55% [75], 63.7% [268], 66% [269], or 73.8% [134]. Although the prediction of weld bead geometry has been extensively investigated, WAAM needs the introduction of certain models and relates the morphological properties of beads to thermophysical properties. All the strategies suggested for improving WAAM components surface flatness in Table 11 are only capable of reducing and not eliminating all surface roughness or SW impact. It should be remembered that the overlapping models for multi-bead applications cannot be applied to thin-wall components (i.e., with features with a single deposition pass).

To avoid cumulative deviations, addressing the aforementioned challenges, improving surface conditions at the start and end of the weld bead, and controlling the layer thickness, the following approaches have been proposed (see Table 12).

Hybrid deposition can control deposition parameters and facial milling to achieve the appropriate layer height [33,261]. Conventional milling processes combined with GMAW used to produce injection mould

intersection: proof of a long narrow shape and deep depression under the parallel pattern appeared on the top surface, (c) the zigzag-arc striking point at the intersection: the ripple occurred on the weld surface; at the beginning, there was not enough metal deposition since the arc striking point was at the joint, (d) zigzag – arc-extinguishing point at the intersection: unilateral tightened defect at the cross-region was similar to that of the arc striking; the height fluctuation area caused by arc-extinguishing became shorter, and the depression was shallow, (e) ELE path – arc striking point at the intersection: the striking point was filled with additional material at the intersection with the side due to the path extension, addressing both sides of the weld shrinking problem and generated internal fillets, reduces stress, and ensures accessibility during subsequent milling, and (f) ELE path – arc-extinguishing point at the intersection: the crossover core area switched from a linear to almost a square zone; the superposition effect avoided the dispersion of the extinguishing arc, resulting in a flat crossing area profile.

Table 16
A summary of crossing features reported in the literature investigation geometrical formation

Refs. & Figure	Feature Thickness Heat source/Material	Highlight
[246] Fig. 21	Direct crossing 4 mm thick CMT/Mild steel	Four cross features with different build patterns were investigated; the lowest peak values of 0.4 mm were observed.
[250] Fig. 22	T-crossing 10 mm thick CMT-P/ER 2319	They solved the problem of peak development, and deposition failure with a reverse angle strategy. The proposed end lateral extension method (ELE) eliminated tightened defects at the crossing and achieved a deviation to the fitting plane of 0.7 – 1 mm was observed.
[85] Fig. 23	Direct crossing 25 mm thick GMAW/Ti-6Al-4V	They built the MPP strategy to ensure consistent deposition, implementing a single path strategy independent of geometry type, such as adaptive path design.
[311] Fig. 24	Direct crossing n.a. GMAW/n.a.	A feature recognition module for critical part features, such as free end walls, T-crossings, and direct crossings was proposed to reduce geometric deviations and to ensure appropriate machining afterwards.
[312] Fig. 25	Direct crossing n.a. GTAW/ER308LSi	The overlap pattern with continuous ignition arc was found to be the most suitable strategy, as it can (i) reduce the total deposition time, (ii) produce one arc ignition for each layer and (iii) continue for the sequential layer, make the deposition process more stable, and (iv) remove the peak existing in the overlapped pattern.
[12] Fig. 26	Thin T-Crossing n.a. GMAW/ER70S-6	They compared six deposition patterns for the manufacture of T-crossing and selected the optimal strategy to improve surface smoothness and arc stability. They concluded that the introduction of a fillet in the internal corners results in a very fluent tool path and, consequently, in a stable deposition process.
[263] Fig. 27	Thick T-Crossing 11-19 mm thick CMT/ER4043	Three strategies were proposed to obtain flat layers and showed that these strategies can combine to improve the layer flatness on the surface and reduce differences in layer heights.
[313] Fig. 28	Thick T-crossing 22 mm thick GTAW/Ti-6Al-4V	They used adaptive path planning [243] and observed well-built crossing characteristics with a uniform layer height.

inserts [271,272]. For example, 5-Axis robot for both material deposition using GMAW and inter-layer milling processes to produce complex metallic structures was used by [61,259,273]. Higher-order kinematics (6-axis) robot with GMAW was used for depositing large aerospace components by [9,246]. The height of the layer is ensured by such a hybrid operation. This, however, comes at the increased cost in the overall time, lowering the use of materials (because of the removal operations), increasing process complexity, and decreasing productivity [239]. This method is no longer appropriate because the management of welding parameters can be used to maintain a stable deposition process by means of an open-loop and a closed-loop control [274] of processing parameters or an inter-pass dwell [16].

A passive vision sensor can be used to monitor the nozzle at the top surface distance and to adjust the deposition rate with an adaptive controller [274]. This can increase the stability of the layer-height of the

welding path from the start to the end of the arc, but the height variation remains between the start point and stop points of the arc.

Additional techniques include speed and trajectory control to address the problem of uneven surface conditions due to the starting and ending of the arc [72,264]. For example, at the beginning and end of weld paths, the deposition parameters can be adjusted, and for two adjacent layers, the deposition can be formed in the opposite direction. In the beginning, the current and TS should be higher and slowly lowered at the end of the deposition, to maintain stable rates of deposition during arc extinguishment [72,264]. A continuous tool path generation strategy to avoid the frequent starting-stopping sequences was developed by [239]. However, when the width of the thin-walled structures is greater than that of a weld run, it does not remove unevenness. Moreover, in addition to inter-layer cooling adjustment, this strategy requires precise monitoring of the frequency. Although the weld pass can

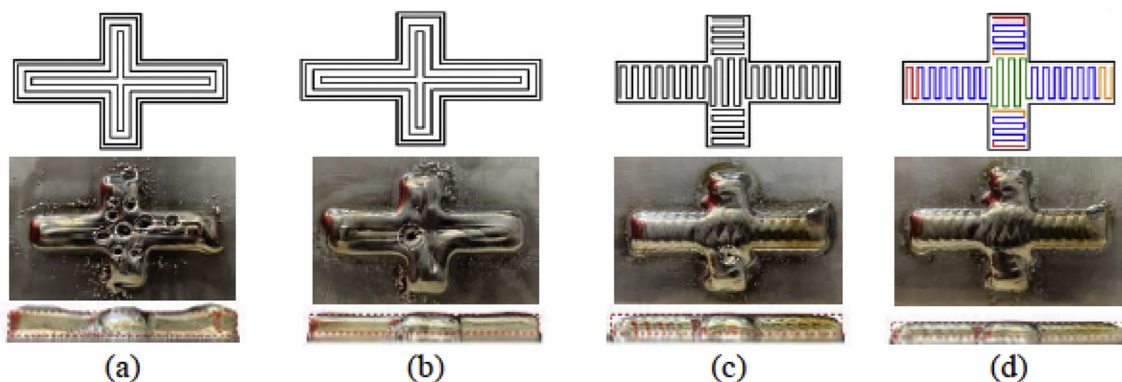


Fig. 23. An overview of direct crossing features reported by [85]: (a) adaptive path planning, contour path with constant process parameters: the extensive presence of keyhole defects and the irregular height of the deposit, (b) adaptive path planning, contour path with varied process parameters: the presence of a small keyhole defect, a stable deposited height, (c) modular path planning, segmentation; zigzag with constant process parameters: a stable deposited height, the lower height at the ends of the part, (d) modular path planning, segmentation; zigzag with varied process parameters: no defects, a stable deposited height, the part ends are less steep compared to that of constant process parameters.

Table 17

A summary of the corner junction (L-shaped), sharp corner and squared junction features reported in the literature investigation geometrical formation

Refs. Figure	Feature thickness	Heat source/Material	Control strategy	Highlight
[314] Fig. 29	Thin-walled square	5.5-8.5 mm thick GTAW/Titanium	Control strategy	With the hot-wire current increasing, the morphology of the samples had great changes. The surface of samples with lower layer thickness was much smoother and with the rising layer thickness, the periodic bulges became obvious.
[71,315] Fig. 30	Sharp corner	n.a. GTAW/5A06 Al	Wire feeding manner	An optimizing of the wire-feeding manner was developed by considering both the layer size precision and layer surface appearance. The geometrical limit for WAAM was a plane angle of 20 degrees when the layer width was 7.2 mm.
[269] Fig. 31	L-shape	15, 8 & 4 mm thick CMT/Steel	WFS, TS	The accumulation of material at the corner point can increase for angles less than 90° in corners and compensation could be required by the adjustment of local TS. An overlap distance of 0.66 to 0.75 was tested.
[316] Fig. 32	Rectangular	n.a. CMT/Al alloy	Deposition strategy	In optimized conditions, the testing direction was remarkably independent of its superior mechanical characteristics (parallel or perpendicular to the deposit beads), and only small dispersed porosities were observed.
[317] Fig. 33	Sharp corners	N.a. CMT/Al alloy	WFS, TS	They adopted an adaptive process control system for the testing of a tool-path based on rational non-uniform B-Spline and control points. These strategies ensured the uniform bead morphology respecting the dynamic constraint in complex features.
[241] Fig. 34	T-crossing and corner	n.a. GMAW/Copper coated steel	Deposition strategy	The MAT-based path patterns proposed can create gap-free walls for varied wall thicknesses. Thin-walled structures were shown to be sensitive to the step-over distance.
[66] Fig. 35	Sharp corner	12 mm thick GMAW- Tandem/2219 Al	Path strategy	The theory of trajectory planning was described and validated. They showed that the defects caused by heat accumulation and dissipation can be avoided through increasing substrate geometry and change the angle of twin wires along the welding direction.
[249] Fig. 36	Sharp corner	Varied thickness GMAW/304 SS	Path planning	Pores formed in the sharp angle corner, where the angle is less than 59°. They observed that the optimal bead overlap of 0.738, however, eliminated pores at an angle of less than 59°. The filling path in the sharp corner should be changed to 0.262.

be regulated flexibly using this process, empirical and time-consuming adjustment procedures need to be applied.

The welding with weaving technology offers an alternative technique in order to increase the surface flatness of wide welding beads (see Fig. 17) [275]. The weaving of the arc is advantageous to diffusion and can thus achieve better quality [276]. Some researchers have found that weaving would enhance the surface finishing in the production of bulk materials [277]. The consistency of the bead geometry can be enhanced by weaving deposition, except at the beginning and end of the bead [263].

Inter-pass rolling has also shown that it can affect SW reduction [278], besides compressive stress induction and effect on static and fatigue properties [148,149,279–283], as well as improving microstructural properties and reducing porosity [57,284]. Two methods for enhancing surface quality and geometrical accuracy are typically used: (i) vertical rolling over the wall and (ii) side rolling on the wall's side surface (see Fig. 18). Although vertical rolling can increase the surface waviness, it was reported to be smoothed by side rolling (see Fig. 19) [149,280].

In brief, the surface properties improvement methods are restricted in some way at a low deposition rate and limit the overall purpose of the low-cost WAAM. A balance should be achieved between the surface properties and productivity in order to completely harmonize and leverage the full benefits of the WAAM process. The following Subsection covers various geometrical features in the literature.

4.4. Geometric features

The identification of features is essential to design a manufacturing process and is restricting factors whether a specific design's geometry can be produced. Features may be classified as geometric areas with properties that differ from the rest of the object, such as the faces of a cube. The benefit of WAAM is to manufacture parts with geometrical features, with substantially reduced waste material, which cannot be manufactured with traditional machining processes. This subsection covers the features generated by WAAM, taking their limitations into consideration.

4.4.1. Thin- and thick-walls

WAAM is widely used to produce (large) thin- and thick-walls, thus, the issue of manufacturing such a component with WAAM is one of the topics of recent research, which has been widely documented in the literature. This involves researching the effects of process parameters and process planning to enhance their surface finish and precision, as summarized in Table 13. This includes discussion and highlighted results and reports from EWT and SW, where appropriate. Table 14 also summarizes a summary of thick and bulk materials deposited via WAAM.

4.4.2. Overhang features

The manufacturing of overhang structures is a major challenge in WAAM, as components are typically deposited vertically layer-by-layer. Hence, parts with overhanging features that have an angle above a limited

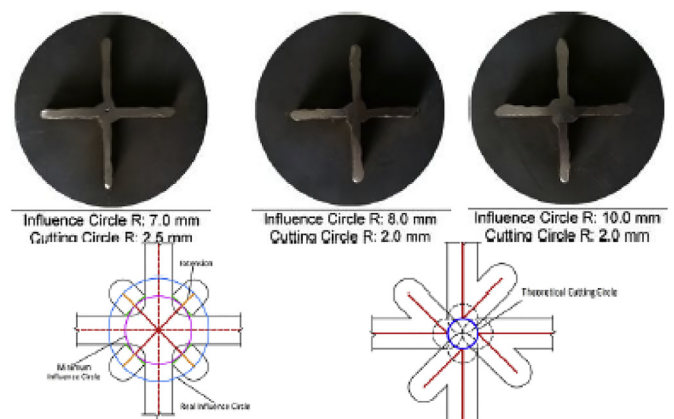


Fig. 24. Direct crossings deposited to show the impact of the values of the influence and cutting radii reported by [85]: the crossing showed both a central void and a failure of material on the fillet areas using the theoretical radii (left), reducing the cutting circle radius and increasing the influence circle – eliminating a central void but not producing enough material for fillets (center), and further increasing the circle radius, producing the best results.

Table 18

A summary of cylindrical junction features reported in the literature investigation geometrical formation (dia refers to diameter)

Refs. Figure	Feature Dimension Heat source/Material Control strategy	Highlight
[124] Fig. 37	Thin cylinder 4.3/101 mm thick/dia GTAW/5356 Al TS, WFS, current	A machine vision sensor was used to monitor and control the arc length, and the height of the deposited layer is regulated by optimizing TS in order to match the heat input to pre-set WFS. The wettability of the deposited layers was effectively increased at a substrate temperature of 118 °C, resulting in acceptable surface quality.
[311] Fig. 38	Thin cylinder n.a. GMAW/steel Deposition strategy	They used a layer-by-layer approach and a continuous (helical) to avoid inter-layer arc ignition and extinguishing. The aligned start-stop strategy aimed at compensating for the defect by introducing a self-overlap of the layer in the stop region, compensating for the lack of material in the extinguishing region, observing the best results.
[265] Fig. 39	Cylinder 11/80 mm thick/dia GMAW/ER70S-6 TS, WFS	They showed that different path patterns result in different surface geometries due to bead abnormality at the beginning and end of the bead. The proposed approach led to thermal accumulation areas, which promoted higher residual stress at the wall boundaries.
[86] Fig. 40	Cylinder 15/110 mm thick/dia GMAW/ER-70S-6 Deposition strategy	A thick asymmetric cylinder was achieved by weld tool oscillation, 84% thickness reduction was observed.
[318] Fig. 41	Cylinder n.a. CMT/steel WFS, welding direction	Welding direction had a critical influence on the temperature field as well as on the component geometry.
[319] Fig. 42	Cylinder 3.4-6.4/40 mm thick/dia GMAW/H13 steel Arc power, TS, WFS	They developed a 3D heat transfer and fluid flow model and showed that the deposit shape and size could be improved by controlling TS and WFS. The experiments and model provided a calculation method to find the control points during the complex build.
[320] Fig. 43	Cylinder 3/110 mm thick/dia GTAW/4043 Al-alloy Current, TS, WFS	They showed that the width of the layer deposited increases as the heat input increases. With the increased WFS, the height of the deposited layers increases, while WFS has a reversed effect on the layer width. TS was found to be an important factor, decreasing TS increased penetration and flattening the contour.
[252] Fig. 44	Cylinder & square 6.1/40 mm thick/dia VP-GTAW/Ti6Al4V Wire feeding manner	They showed a consistent deposition in an optimal wire-feeding angle of 60° and discussed the reasons based on arc/molten pool temperature distribution characteristics.
[321] Fig. 45	Cylinder 50 mm dia CMT/mild steel Deposition strategy	Three kinds of welding procedures were studied and showed that the height of the deposition is uniform when each layer is reversed toward a torch motion.
[322] Fig. 46	Cylinder n.a. GMAW/410 SS	They showed an approximately linear tube diameter relationship as $D_{\text{print}} = 1.2894 \times D_{\text{designed}} - 13.419$.
[315] Fig. 47	Curve sharp n.a. GTAW/Al 5A06 Curvature angle	They demonstrated that the geometric constraints are related to the width of the layer and if it is wider, the deposition of sharp turns would be worse. They showed a 10 mm plane curvature radius as a geometric limit when the layer width is 7.2 mm GTAW is not ideal for the sharp turning of plane shapes.
[61] Fig. 48	Cylinder, squared, triangular pipe joint CMT/ER70S-6 TS, WFS	It was found that the range of 0.35–0.9 m/min as TS and 5–8 m/min as WFS were a suitable range of process parameters for stable and continuous single bead weld-deposition for thin-walled structures.

threshold are difficult to deposit. For depositing parts with overhanging features, the addition of support is usually required, which raises expenses due to the reduced rate of materials and further post-machining requirements [301,302]. For WAAM in particular, because of its low precision, it is difficult to shape suitable support structures. Therefore, the construction of unsupported overhangs is an urgent necessity. WAAM's main challenges for overhang deposition include:

- o High heat input – Owing to the intense heat supply, WAAM's angled inclined walls hang down. As the heat input is decreasing and the cooling rate is increasing, the molten pool is easily solidified, which can help to create the overhang structure. For example, the CMT variant of GMAW was found to be an ideal process for multi-directional layer deposition due to its relatively low heat input [245]. Nevertheless, the humped weld bead-shaped in an unsupported horizontal position when deposited (see Subsection 3.4.3).
- o High-temperature substrate – The molten weld pool tends to overflow with a thin-wall at a high substrate temperature. At welding

temperatures, the viscosity of molten metals and alloys is small, hence, the weld metal flows over the thin, molten wall side if the substrate temperature is too high [72]. In this case, the selection of filler wire is a factor in the overflow capacity.

- o Gravity distortion – The downward formed metal, caused by the force of gravity, has difficulty in properly regulating the deposition; causing inherent defects, such as the irregular shape of the bead, lack of penetration, porosity, undercutting and forming of the humped bead [303]. However, as described in Table 15, WAAM can be performed with proper control in any direction/orientation,



Fig. 25. A direct crossing feature reported by [312], overlap with two start-ends of the arc.

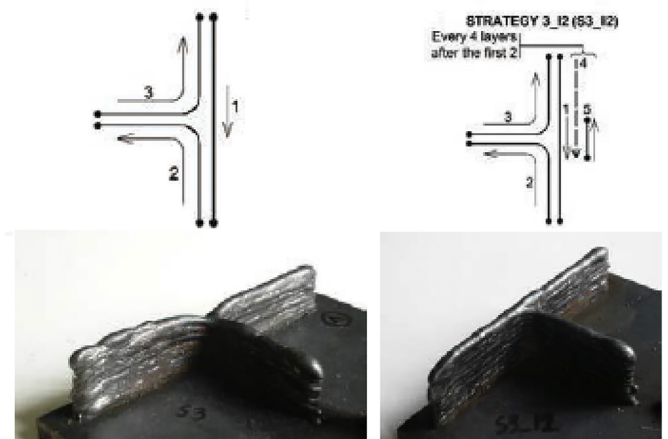


Fig. 26. T-crossing built with failure in the central zone (left) and good appearance (right) [12].

because the molten pool surface tension force may sustain the weight of the deposited material.

- o The offset distance – When each layer is deposited, a part of the distance must be shifted by the torch: the offset distance along the X-axis. The deposition material is melted and moved to the molten pool, which then solidifies the liquid metal. If the offset distance is too large, the overflow of the molten pool may occur, causing the deposited parts to be poor quality. The combination of process parameters is therefore compatible with a maximum offset distance and a maximum tilt angle, preventing the apparent molten pool overflow [254].
- o Torch orientation – While welding in many directions is possible, it is difficult to design the torch direction in a CAM package automatically [304,305]. Automatic path design is time-consuming and complex programming and the amount of use of the path justifies development time. Medium, low run jobs are usually performed using manual welding like welding ship panels. However, WAAM's performance depends on the custom design on demand, so the future deposition techniques need a reliable, automated path planning technique. The torch is now directed toward the workpiece in order to simplify the programming for large-scale WAAM.

A variety of WAAM techniques have been developed for reducing reliance on supporting structures, including (i) articulated tool path manipulation (see Subsection 4.2), (ii) modifying the deposition direction on a flat position, (iii) positioning of the deposition torch angle, (iv) additional degree of robot freedom to adjust the orientation of the workpiece, as discussed in Table 15 and Fig. 20. Flowing discussion is accordingly driven.

- o For a large overhang, inclined and horizontal wall features can be created by a tilted torch position [245]. 15° has been stated to be a reasonable angle of overhang to be used without altering the torch orientation. Steeper overhang angles are possible, but for the deposition time required in large components, they were not effective.
- o While there has been a number of developments in inclination wall deposition, still small areas of the possible inclination angle using a flat deposition method and inherent technical challenges remain. For multidirectional WAAM, the forming process of a welding bead in various directions is not fully explored. A set of practical guidelines for multi-directional WAAM must, therefore, be provided.
- o The use of rotary positioners in multidirectional WAAM has been explored to reduce or eliminate the use of support structures [61,229]. A rotating table gives additional flexibility to make the components with complex geometries more flexible [224]. Tilting the substrate in an angle equal to the direction of growth in the material can produce better geometry of the deposited material and a more stable process of deposition [61,259]. The horizontal structures can be deposited with WAAM when the torch is rotated [245], but not all the forming equipment is able to rotate the torch. WAAM is used, for instance, to manufacture medium to large parts, so rotating such a large part is difficult and expensive in operation. WAAM has also been used to repair large components locally, which cannot be installed on a rotary table. Hence, the design phase becomes less complex and the subsequent manufacturing process is more cost-efficient if the layers can be deposited in multi-directions [306,307].
- o While many strategies have been established in the literature for producing thin-walls with overhang features, i.e., inclined walls, there is no reliable common strategy to produce overhang large scale components with near-net shape. A mathematical description of inclined parts has not sufficiently addressed, relating input parameters and underlying physics. The surface quality of the produced layers can necessity be improved by applying a face milling process, but the process efficiency can be greatly reduced. Therefore, future studies should be an emphasis on providing the layer-overlapping process of overhanging features for large scale

production.

- o WAAM parts may have included characteristics as a kind of overhang feature, like passages that cannot be manufactured with traditional subtractive manufacturing. Enclosed features can be created with multi-axis deposition techniques without supporting structures. When designing parts with enclosed features, care should be taken because they cannot be machined easily afterward.

4.4.3. Corners, crossing, thin-wall squared and cylindrical

Crossing features are the most critical features as an incorrect depositing strategy can lead to non-uniform layer thickness. The literature studied the possibility of using WAAM to produce different designs for the thin- and thick-wall crossing, as discussed in Table 16, Table 17 and Table 18. Because the parts of WAAM must be post-machined to match the required surface finish, it is important to evaluate the machinability of the material produced by the WAAM [310]. Regarding direct crossings, T-crossings, and corners, the internal sharp corners may be the most important issues for post-machining, as these are not accessible using end-mill. The creation of tool paths to redesign these areas by adding fillets could boost the corners' usability for processing on the final part and make the route more fluent. The existence of fillets can also enhance mechanical properties, in particular the fatigue-resistance. Additionally, adding more material in the corners prevents voids and porosity. Of course, if a sharp corner is needed, this excess material must be machined away.

Apart from avoiding the resultant distortions/residual stresses of the final crossing part during the generation of deposition patterns for WAAM, the deposition efficiency needs to be taken into account. In this context, the deposition efficiency means both the avoidance of deposition failures (such as depressions) and the generation of the best tool path able to manufacture a part that dimensions are as close as possible to the final desired geometry [310]. For example, the accumulation

Table 19
A summary of lattice and struts structures reported in the literature

References	Feature	Highlight
[324] Fig. 49	Heat source Material Control strategy Deposition torch angle	
[327] Fig. 50	Struts-lattice Pulse GMAW/Mild steel Process parameters Positional torch	They showed that the fabrication of strut shapes depends on the heat input condition and the arc discharge time had the highest influence on the layer height and diameter. The inclination angle of an overhanging shape had little influence on the dimensional accuracy of the built object. The maximum deviation was approximately ± 2.3 mm.
[306] Fig. 51	Struts-lattice Pulse GTAW/Titanium alloy WF direction, heat input Positional rod Struts-Skeleton CMT/G3Si Processing parameters Positional torch	The use of pulse WAAM greatly improved the material usage rate. The wire-feeding direction and the force of the droplet affected the shape of the forming surface and the actual inclination. The cell formation was best when the angle is between 45° and 90°. They proposed an image-based closed-loop control strategy to monitor the bead shape, computer-aided manufacturing (CAM) software to correct the geometry of the bead deposition, resulting in automatically manufacturing complex truss structures without any support.
[326] Fig. 52	Struts-lattice CMT/ER 2319 Current, voltage Positional torch	The struts' diameter was no less than 2.5 mm with a relative deviation of less than 2.0%. The strut angle was from 15° to 90° with a relative deviation of 4.0%. A 3-layer pyramid lattice structure demonstration composed of struts with a diameter of 3 mm and an angle of 45° was fabricated.

Table 20
Case studies reported in the literature

Case	Geometrical elements	Reported details/ Requirements	Challenges/ Highlight/design rules
Fig. 53 Case 1 [328]	Irregularly curved Thin-wall	GMAW/Steel TS/WFS of 0.2/4.6 (m/min) V/I of 18V/80A Mass (kg) = 0.595	A significant energy saving was recorded, not including recycling, compared to conventional machining at 34%.
Fig. 54 Case 2 [329]	(open) T-crossing Sharp corner Enclosed features Thin-wall	GMAW/316 L TS/WFS of 0.224/3 (m/min) I of 180 A	In the longer features, the achieved temperature was higher than in the shorter ones.
Fig. 55 Case 3 [80]	Thick-wall (12 mm) Plates Overhang holes Pinhole Curved features	GMAW/Steel Overlap beads of 12 mm 2.1×0.4×0.2 m and 133 kg	Pinholes considered as an omitted feature; Adjusting the deposition direction to (i) conform to the overhang constraint, and (ii) have a smaller cross-section area; The overhang limit of 15° was implemented.
Fig. 56 Case 4 [330]	Thick-wall (20 mm) Joint interface	GMAW/AISI12 40 mm height extension 190 °C preheating Layer: WFS(m/min)/I (A)/V(V) 1 st : 7.1/140/15 2 nd : 6.3/105/14 3 rd : 6.1/96/13.7 ≥4 th : 6/91/13.6	A maximum recorded temperature of 460 °C in the first layers and 270 - 325 °C for the subsequent layers were recorded. The maximum porosity of 1.2% directly in the interface zone and below 1% for the subsequent layers were observed.
Fig. 57 Case 5 [263]	(Open, closed & straight) T-crossing Corner junction Closed junction Thick-wall (13 mm)	CMT/ ER4043 Al TS/WFS of 0.3/7 m/min I of 140A 2.8 m × 0.86 m × 1 m	Weaving methodology was employed. A 3 mm fluctuation of the layer height was observed.
Fig. 58 Case 6 [201]	Thin-wall Overhang squared feature Squared junction Cylindrical junction T crossing	CMT/ER70S-6 TS/WFS of 0.2/200	Demonstrated a humping free surface of the overhang sub-volume through (i) planning an elaborate robot trajectory (vertical-down path is the most recommended direction), (ii) using TS with the most restricted condition (vertical-up).
Fig. 59 Case 7 [331]	Thick-wall (22 mm) Cylinder Concave radii Angular overhang	CMT/ ZG230-450 steel I/V of 185 A/24.4 V Bead width/height 7.4/2 mm 400 mm cylinder radius 660 mm thick-wall height	A 3D scanner was used for geometric qualifying. A cylinder with a cross-section center error of 1.6 mm was deposited successfully. The error of 1.2 mm for thick-wall was observed.
Fig. 60 Case 8 [247]	Thick-wall (10-20 mm) Cylinder Overhang	GMAW/ IYHJ507M TS/WFS of 0.42-0.48/ I/V of 120-150 A/20-22 V 95-265 mm outer diameter 220-700 mm length	The dimensional deviations of 2 mm, the angular error of 1°, and intersecting curved surface deviation of 3 mm were observed. The forming accuracy was mainly influenced by the process parameters and the forming path.
Fig. 61 Case 9 [269]	Corner junction Thick-wall Transition wall Inclined wall	CMT/Steel	For the stable build-up of multi-track walls, overlap distance (0.66 to 0.77 bead width) and track sequence were found to be crucial.
Fig. 62 Case 10 [149]	Corner junction Direct crossing T- crossing Thick-wall	GMAW/Ti-6Al-4V 0.7 m height and 20 kg	A significant time, material, and cost savings.
Fig. 63 Case 11 [254]	Open surface Overhang Thin-wall (6-8 mm) Inclined wall	GMAW/ H08Mn2Si TS/WFS of 0.288/3.73 for 8 mm width TS/WFS of 0.348/3.09 for 6 mm width	No large pores or inclusions were observed. The positioning error of 1.4 mm was observed. The deposited inclination angle of thin-walled parts can be greater than 45°.
Fig. 64 Case 12 [285]	Solid bulk Angular overhang	GMAW/ ER70S-6 2.5/2.7 mm thickness/height	They deposited 1 layer more for compensation of height reduction. Overlapping beads of 0.73 were applied. The maximum and absolute error of 4.4 and 1.8 mm, respectively, were recorded.
Fig. 67 Case 15 [333]	Thick-wall Inclined overhang wall Corner junction	GMAW/ ER70S-6 TS/WFS of 0.41/5.08 m/min 30 cm width, 30 cm length, and 8 cm thickness	Compression moulds should be able to withstand pressure up to 13.79 MPa and operate within 170-180 °C. The mould was manufactured with a hollow design and the results have demonstrated that the mould meets deflection needs.

of peaks, in which the weld bead is overlapped at crossing points, has been demonstrated to make this feature difficult to produce. In order to limit the volume of the material to machine away during final machining operations and optimize the deposition capacity, the crossing point must remain as near as possible to average wall height far from the central region. In this light, different assessment parameters can be taken into account, including:

- o The appearance or absence of fillets in the intersection;
- o The difference in height between the central point height (crossing) and the average value of the other sections; the deposition efficiency is directly linked to this parameter: if the height in the central point is close to the other distant points, less material needs to be removed.
- o It is also necessary to achieve a (back) surface of T-crossing as flat as possible in order to optimize deposition performance.

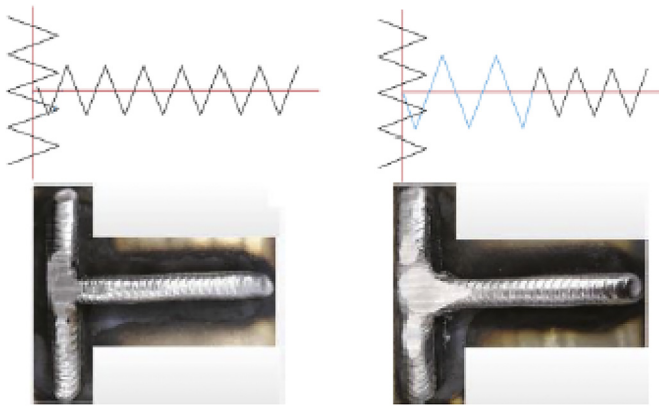


Fig. 27. T-crossing features reported by [263]: local milling was conducted when the sample was deposited; the flatness of the layer was maintained by milling the crossing, the contour profile, however, was not good at the corner of the crossing (left); amplitude adjustment at the crossing when a track began or ended at the crossing, the connection of the corner was found to be smoother, resulting in good mechanical properties (right).

- o Because the arc ignition and stop stage frequently cause large spreads, the number of arc start/stop phases should be limited as much as possible. As an assessment parameter, the number of start/stop phases can, therefore, be considered.

The cylindrical feature deposition is a challenging task in addition to the crossing and corner junction features. One of the key objectives of cylindrical deposition strategies is to prevent arc ignition and extinguishing defects, which affect the surface flatness [264]. In fact, due to the heat sink effect of the base metal, the region of the layer near the arc ignition shows excessive thickness in its central part. On the contrary, because of the arc pressure on the molten pool in the arc-extinguishing area, the layer shows less thickness. Therefore, a deposition defect is present on the surface if a cylindrical shape is deposited by igniting and extinguishing arc at the same point for each layer. To overcome these issues, several strategies have been proposed as summarized in Table 18.

4.4.4. Lattice structure

With the rapid development of aerospace technology, the requirements for lightweight and high performance of aircraft and its engines

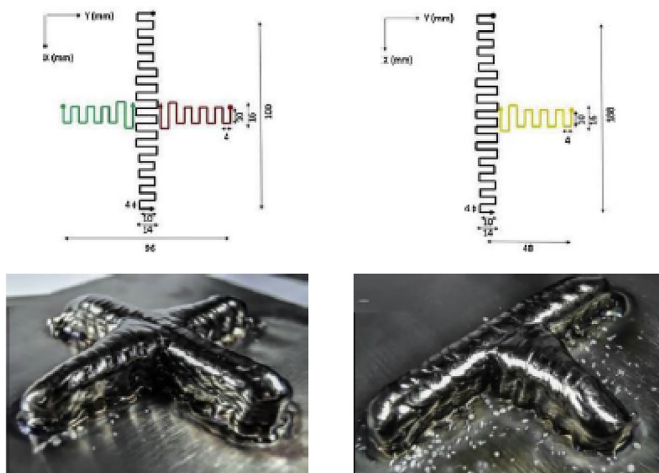


Fig. 28. Direct-crossing and T-crossing including deposition paths [313]

are becoming higher. Building lattice structures inside components enable weight reduction while maintaining high strength. In this regard, AM can be used to fabricate lattice structures of any complex form by depositing the material layer-by-layer, and it has become a new method of manufacturing lattice structure developed in recent years. At present, the main methods for AM of lattice structures are powder bed fusion technologies [1,4]. WAAM enables the fabrication of not only thin-walled and solid shapes (discussed above) but also complex shapes such as lattice structures. In addition, it also has the advantages of unlimited size in an open forming environment, high efficiency, and low cost. However, few studies have investigated the lattice structure fabrication using WAAM.

For a specific lattice structure, the diameter and angle of the inside inclined struts are important structural parameters [323]. The struts with different angles and diameter form lattice structures with different relative-density and construction, which form different mechanical properties of elastic modulus, compressive strength, heat insulation, and shock absorption, etc. Therefore, how to control the diameter and angle of the struts in the lattice structure by WAAM is a challenge. For fabricating strut shapes with high accuracy, the process parameters should be optimized. However, the relationship between layer geometry and process parameters is not clear.

In the literature (see Table 19), different strategies have been used for the deposition of lattice structures:

- o Pulsed GMAW [324] – In this approach, the struts form via repeated spot-welding processes when WAAM was used. In other words, a small amount of molten metal is deposited in a short time and the molten metal solidified and cooled. Then, additional molten metal is deposited. In such processes, the molten pool forms an almost hemispherical shape under the influence of factors such as surface tension, gravity, and arc pressure [321].
- o Pulsed GTAW [325] – In this method, the WAAM uses the droplets, solidified layer-by-layer by pulse, and the metal is continuously formed along the fixed direction as the welding gun moves. They controlled heat input by adjusting the process parameters to prevent the molten pool from collapsing. Therefore, the fabrication of the unsupported inclined structure can be realized by finding suitable process parameters. Obviously, since the formation of unsupported rods is the key to the formation of pyramidal lattice cells, the most important question is how to achieve the expected shape through process control and theoretical analysis, and finally, use this method to obtain pyramidal lattice cells. They showed that it is feasible to use

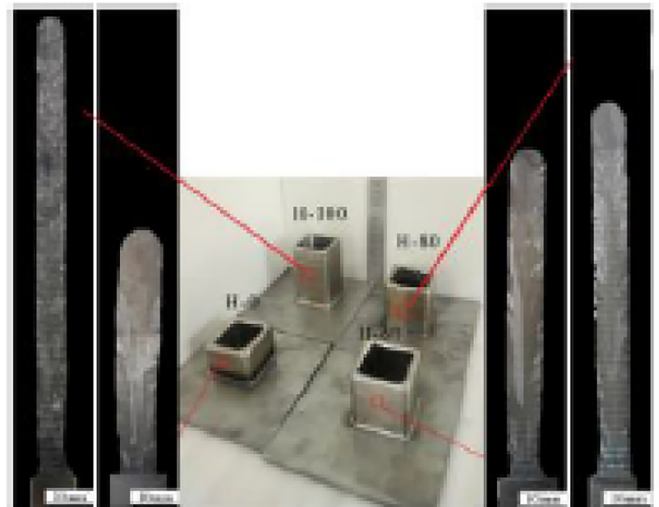


Fig. 29. Thin-walled square components manufactured by hot-wire GTAW (H-0 to 100 indicates hot-wire currents from 0 to 100 A) [314].

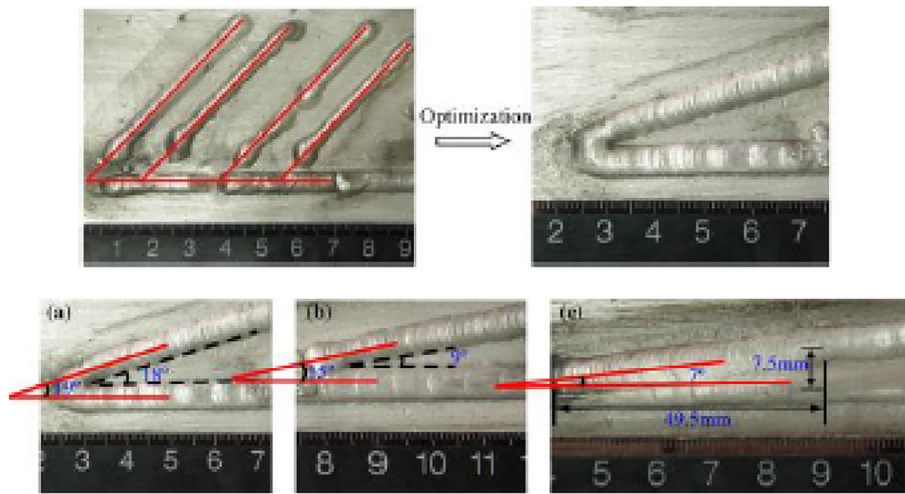


Fig. 30. Comparing the as-deposited cross structure without dimension correction (up-left) and layer size correction by optimizing of wire feed manner (up-right), plain shapes with a sharp angle of 10, 15, and 20° (bottom) [71,315]

this method to fabricate large-scale metal lattice structure.

- o CMT [326] – Metal skeleton manufacturing creates similar structures to continuous lattice fabrication. In this methodology, the building of the different branches is done by increment and is similar to the layer-by-layer additive manufacturing. The only difference is that the branches are not sliced by a cutting plane but are sliced independently. The slicer detects the first points to build near a starting plane. Then, the algorithm has to propagate points along each

branch with an increment δ corresponding to the height of the deposit. The main control parameters include (i) a geometry and (ii) the welding parameters. The CMT process has the advantage (i) to minimize the weld pool temperature and (ii) to reduce spatter formation during the transfer. Different process parameters can be controlled, such as the WFS, the welding time, as well as pre and post gas time to protect the weld bead during solidification. All depositions were done with the synergy implemented in the power source. Process settings are often kept constant during the whole process except for the welding time. This time determines the mass of deposited material and the quantity of energy transferred to the part and is controlled by the supervision software and an external trigger relay. One important parameter to ensure good deposit is the contact tip distance to the working part (approximately 10 mm ensures good shielding and better control of the CMT process).



Fig. 31. The top view of the L-shaped path strategy with various wall thicknesses; set i: WFS= 5 m/min and TS=10 mm/s, two tracks (12 mm); set ii: WFS= 2.5 m/min and TS=10 mm/s, two tracks (8 mm), and set #iii: WFS= 1.5 m/min and TS=4 mm/s, single track (4 mm) [269].



Fig. 32. Rectangular-shaped specimen: 170 mm long, 30 mm width and 120 mm height, and 5 mm radius for the corners [316].

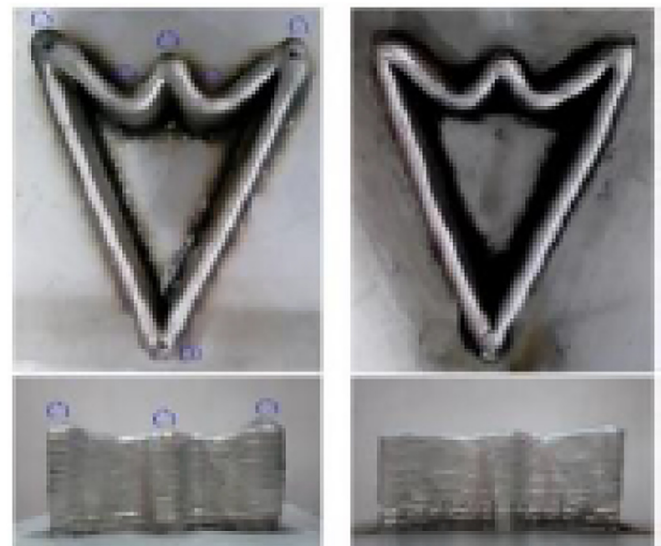


Fig. 33. Near-net-shape comparison between the conventional process control scheme (left) and the adaptive process control scheme (right) [317].

4.5. Case studies

WAAM has been developed to produce near-net-shape parts with larger dimensions. Even if these components are not directly usable in a mechanical system, less machining is required to produce the final part, which then reduces the cost compared to a traditional manufacturing sequence. Geometries however with complex areas remain difficult to produce with WAAM. Case studies reported in the literature are summarized as follows and their details reported in Table 20.

Fig. 53 Case 1: a blade designed according to the NACA 9403 standard [328]. It was identified as an appropriate candidate for a WAAM process. An energy comparison was presented between a WAAM process and a traditional bulk processing solution for the production of a steel blade. In order to calculate the primary energy demand at each stage of the life cycle, experimental measurements and environmental base data were used. The results showed that an integrated WAAM subtractive production route makes substantial savings in material and primary energy compared with traditional approaches.

Fig. 54 Case 2: a complex geometry consists of a vertical T-crossing feature that is difficult to achieve with material removal [329]. This study showed WAAM integration and an in situ monitoring and control system. A complex component (SS 316 L) was developed and generated for the validation of the proposed systems, appropriate phases were used, including the design of a CAD, selection of process parameters, the specification of tool-paths and part deposition. They showed the feasibility of WAAM for the manufacturing of complex shapes.

Fig. 55 Case 3: an excavator arm [80]. They revealed how WAAM interacted in the context of a topological optimization of excavator arm case study, including overhang constraints, deposition direction, and large weld bead thickness. The flowchart was introduced with part orientation, part functionality, and deposition physics necessary for deposition. They found that topology optimization needs development in order to become an effective method for large-scale WAAM procedures because the results are too complicated to produce. Consequently, design rules and processing parameters should be incorporated into topology optimization as further optimization constraints.

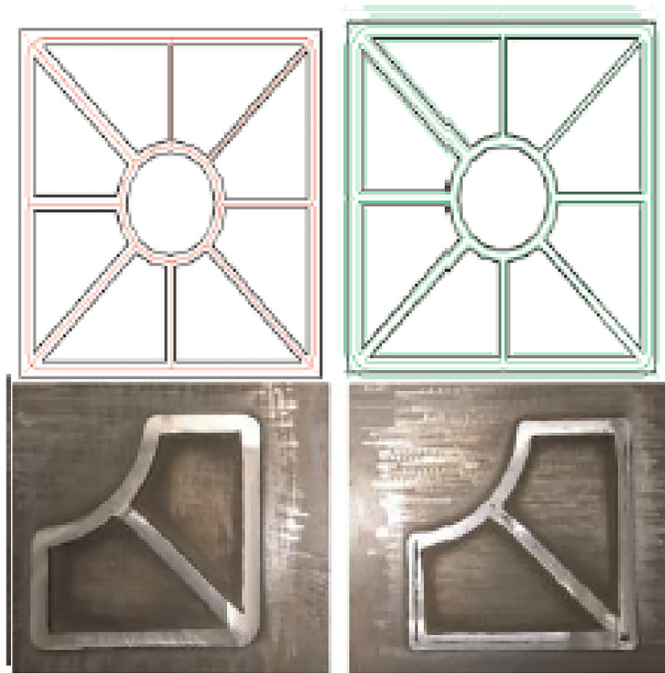


Fig. 34. Corners and T-crossing features reported by [241]. Geometry is shown by black lines (up), MATs are represented by red dotted lines and branches by red solid lines. Generated trimmed path (right-up), finished surface (left-bottom), and traditional contour path patterns (right-bottom).

Fig. 56 Case 4: an extension of a T-section rib [330]. As a reference, T6-heat treated EN-AW 6082 bulk material was used, which was milled to a T-section geometry with a cross-section of 120 mm × 50 mm × 20 mm. On the rib of this section, AlSi12 was added using WAAM. The porosity 1.2% was observed at the intersection area.

Fig. 57 Case 5: a complex large crossing features [263]. The goal was to explore strategies to optimize the production of large and high-thin wall metal structures. The combination of these strategies showed that they could improve layer surface flatness, and differences in layer heights. The wall flatness was measured by moving a laser displacement sensor at a fixed height along the thin wall. The layer height (520 layers) variations were verified within 3 mm.

Fig. 58 Case 6: a complex geometry including the overhang. They examined the effectiveness of the strategy for humping avoidance by demonstrating a thin-wall workpiece with overhanging characteristics. The deposition of sub-volumes was the main step in the deposition of the workpiece. A contour path for the sub-volume of the overhang was chosen. They demonstrated a humping free surface, which shows the effectiveness of the strategy.

Fig. 59 Case 7: propeller bracket. The marine propeller bracket is an important part of large ships and has high demands for dimensional precision and mechanical characteristics. Currently, casting and welding are integrated into its manufacturing cycle. Because the propeller bracket is manufactured using ZG230-450 steel, which has poor fluidity, and the thickness of the hub generally larger than 200 mm, shrinkage and porosity are easy to occur in the casting process. The grain structures of the heat-affected zone and the mechanical properties decrease and cannot comply with requirements for welding joints between the hub, support arm, cross arm. Hence, an ideal demonstrator part for WAAM. The cylindrical hub, cross-arm, and support arm were deposited sequentially by the block-forming strategy. Central deviations of the layer of deposition were obtained by a surface-structured light 3D scanner and a point cloud processing in real-time. The dimension deviation of the WAAM propeller bracket was 1.6 mm.

Fig. 60 Case 8: multi-directional pipe joint [247]. Due to the fact that the intersecting areas of a multi-directional pipe joint are space surfaces, the conventional slicing method is difficult to form a space surface with

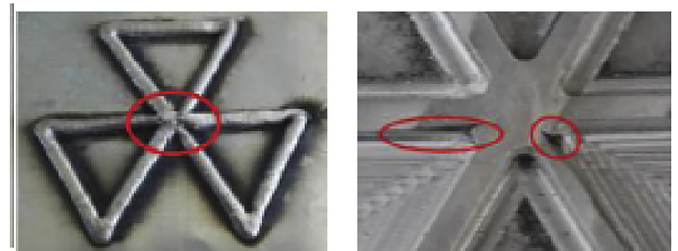
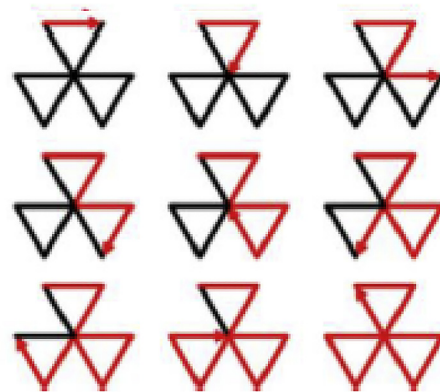


Fig. 35. A clover unit of Isogrid structure with 200 mm long and a 12 mm bead, a fine appearance; created two gaps in the center [66].

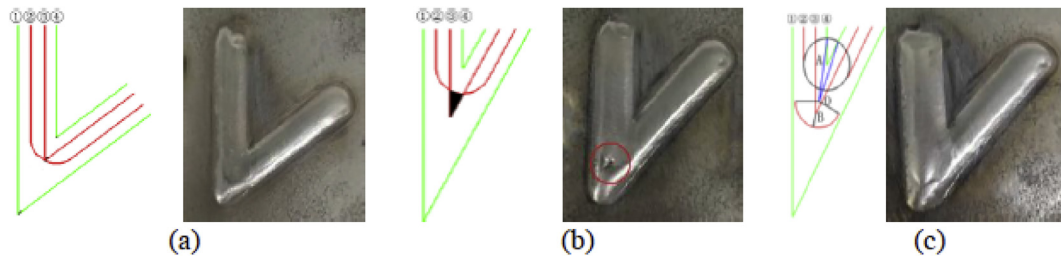


Fig. 36. Sharp corner reported by [249]: (a) lap angle of 56.85°, the adjacent bead was well-formed with no pores, (b) lap angle of 28.56°, at the sharp corner, a pore was formed, and (c) a closed-angle correction path resulting in no pores at a sharp corner.

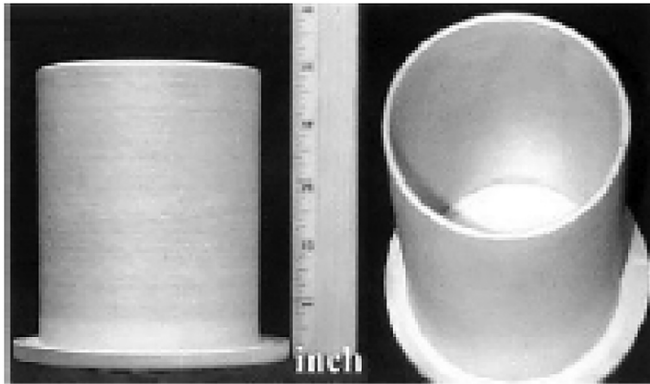


Fig. 37. A cylinder part of 5356-aluminum [124]

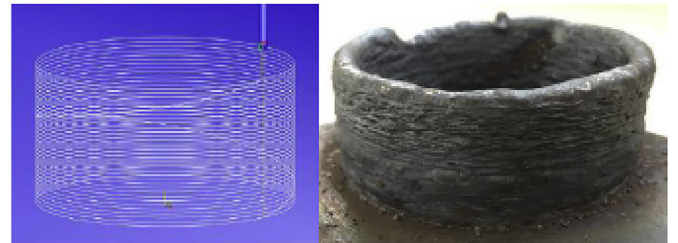


Fig. 39. Stager ramp strategy for closed path deposition [265]

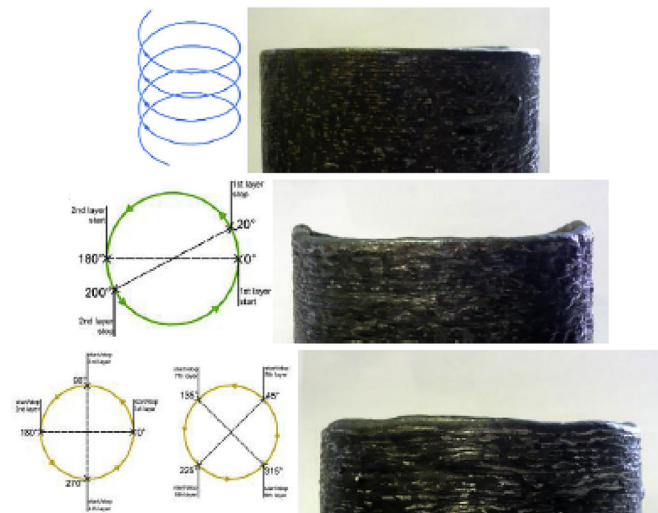


Fig. 38. Top surfaces and deposition strategies to deposit cylindrical features: helical strategy (up), aligned start-stop strategy (center), scattered stop-start strategy (bottom) [311]

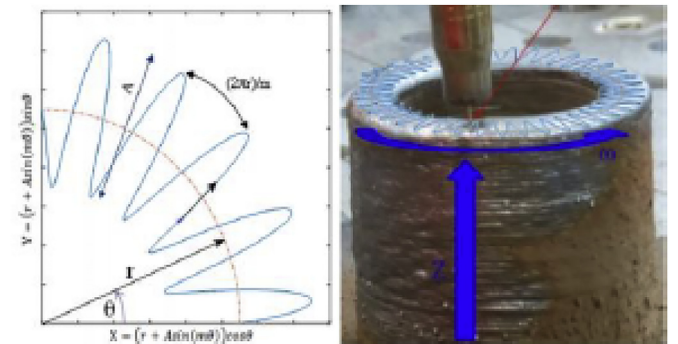


Fig. 40. Tool path for asymmetric parts and deposited cylinder [86]



Fig. 41. G4Si1 (steel) & AZ31 (magnesium) cylinder [318]

high precision. Space slicing and space path planning methods were therefore employed. Around 2 mm were monitored for the dimensioning deviations of pipes and less than 1° for the angles of crossing pipes. Rare defects such as pores and cracks were reported.

Fig. 61 Case 9: an example of the high-strength low-alloy steel S700MC (Mn4Ni2CrMo) crane construction. They showed that geometry such as corners and steep walls can be created.

Fig. 62 Case 10: Ti-6Al-4V landing gear rib near-net-shape demonstrator part. Compared to conventional subtractive machining, the main benefits include significant time, material, and cost savings.

Fig. 63 Case 11: thin-walled part with overhang geometrical features composed of three parts [254]. Both the bottom and the middle wall thicknesses were 5.5 mm (designed), and the upper part 3 mm. The deposited widths of the bottom and middle parts were 8 mm, and the top part was 6 mm in consideration of subsequent finishing of the

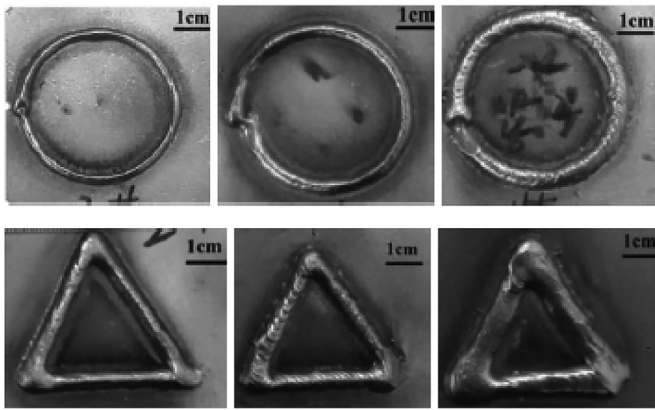


Fig. 42. Deposit shape of circle and triangle route using 100, 150 and 200 A (left-to-right) (V=18-20 V, TS=5 mm/s and WFS=30-65 mm/s) [319].

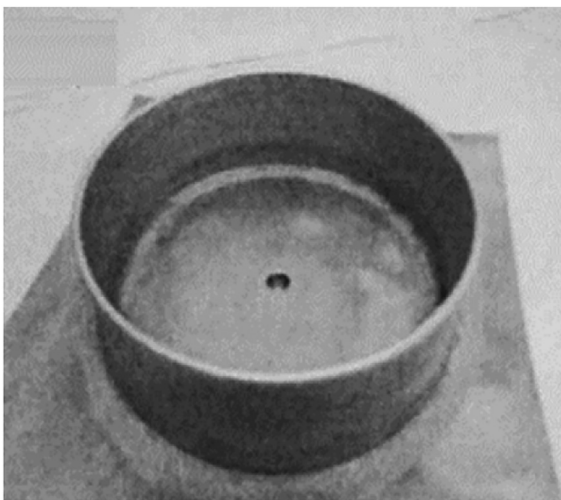


Fig. 43. A cylindrical 4043 Al-alloy parts (120-layer) [320]

component. It was observed a maximum of 1.4 mm geometrical deviation resulting in a rotating table's positioning accuracy, heat dissipation conditions in each layer, and stresses induced by phase transformations.

Fig. 64 Case 12 [285]: an inclined solid bulk part contains two main inclined components, the base component, and the upper component. The base part's length is 200 mm, and the upper part's length is 100 mm. The maximum deviation was found to be 4.4 mm. Except for the cover layer, a good agreement concerning the widths was observed. The absolute deviation was 1.8 mm.

Fig. 65 Case 13 [121]: airfoil. The goal of the case study was to show that the proposed technique allowed to avoid major part collapses without performing trial-and-error operations to select the idle time. The functional surfaces of the airfoil, namely the pressure and suction side, were scanned by the CMM and compared with the target surfaces. They showed that the average deviation from the target surface was 0.65 mm for the pressure side and 0.39 mm for the suction side. This result confirmed that no significant collapse occurred during the deposition process. However, it is worthwhile to highlight that despite the effectiveness of the proposed technique, an excessive inter-pass temperature could still collapse the workpiece. Therefore, it is important to refer to the literature that provides the inter-pass temperature values for various materials.

Fig. 66 Case 14 [332]: cone manufacture via 3-axis (vertical torch) and 5-axis (rotating torch) system. The cone was manufactured using 5-axis tool paths. The welding is continuous from the first point until the last one, removing the start/stop effect, which can create holes or hump. A comparative study between 3-axis and 5-axis manufacturing for a cone was shown that for a 3-axis path, from a 25° cone angle, the defect of the top of the part was approximately 1.7 mm compared to the real surface. For the 5-axis, defects were below 0.8 mm.

Fig. 67 Case 15: compression moulding mould. Moulds and dies are key features of high-quality products and WAAM can be used to increase the efficiency and reduce lead times and costs in this light. They addressed the advantages and limitations of WAAM for the manufacturing of a moulding mould. The mould was over-dimensioned by 3 mm, then machined to achieve the final geometry, tolerances, and surface quality required. The mould was successfully implemented to fabricate composite parts.

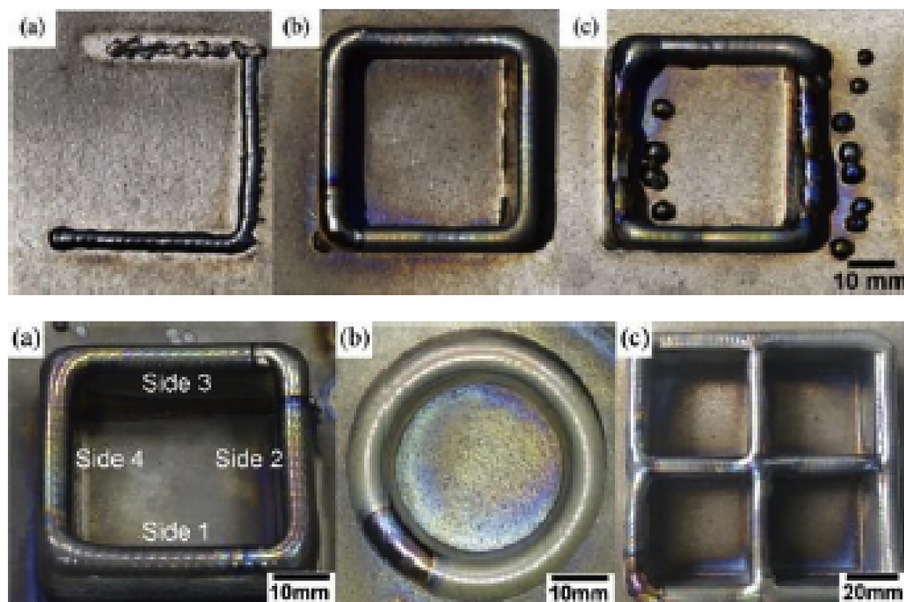


Fig. 44. a) A square feature, (b) a circular feature and (c) window-style feature [252]

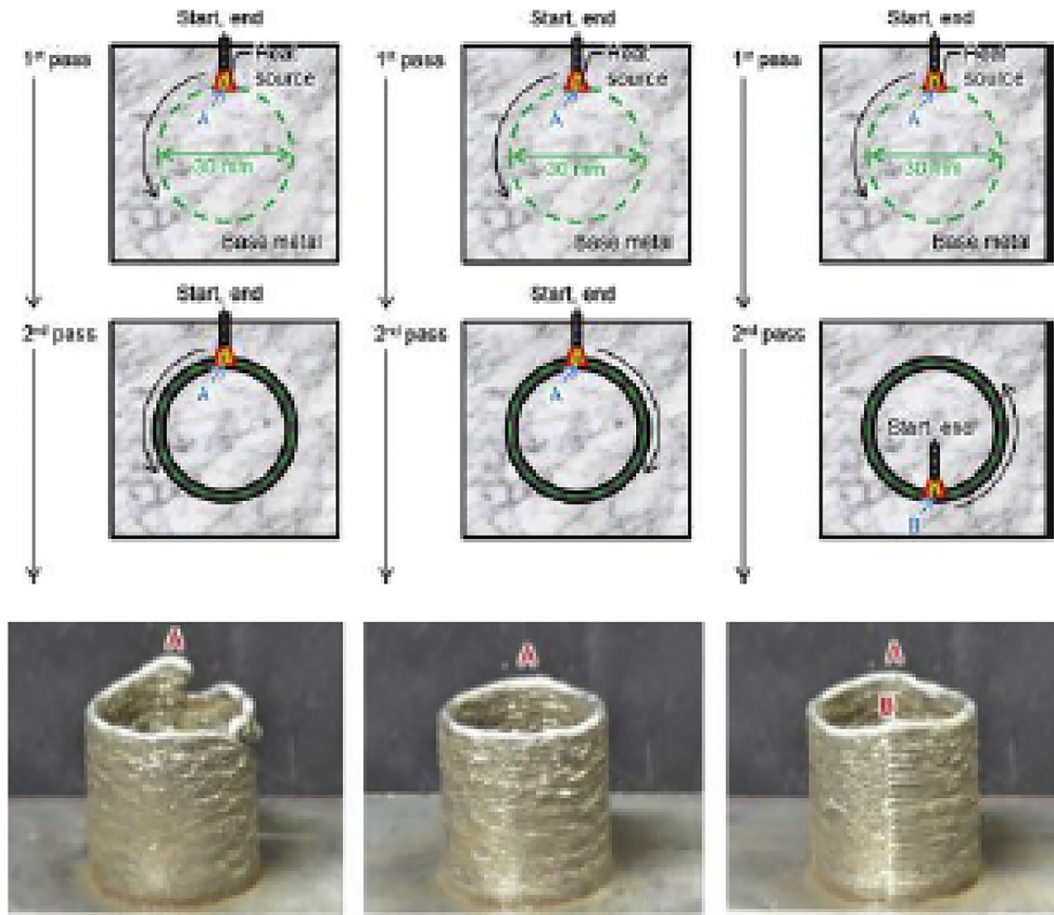


Fig. 45. Schematic images of torch motion and experimental results for cylindrical features; left to right: the starting position was the same and the torch movement direction was the same, the starting position was the same, but the torch motion direction for each layer was reversed, and the torch motion direction was the same but the beginning position was layer-by-layer changed [321].

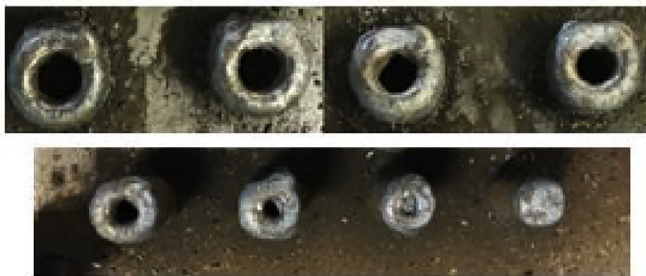


Fig. 46. 20.2 to 14 mm designed tube diameters while deposited as 12.46 to 4.8 mm (the 10 mm and 12 mm tubes failed), stainless steel 410 [322]

5. Discussion and summary

In summary, WAAM techniques have various possible applications across many industries. However, several problems prevent the broad integration of WAAM. In addition to the accuracy and assurance of quality, this includes the lack of process robustness, stability and repeatability. Improved process reliability, elimination or decreased deposition defects and high quality and mechanical-performing components have become significant research aimed at making the WAAM process more competitive with other AM methods. A detailed understanding of different materials, an ideal setup of processes, control of processes and postprocessing parameters are important to achieve this goal.

After a systematic review, this section summarizes and analyzes two main aspects: [Subsection 5.1](#) describes the part quality and accuracy challenges related the WAAM process and planning, and to explore potential solutions to the geometrical accuracy; [Subsection 5.2](#) presents some collected design rules from the literature.

5.1. WAAM processes – critical analysis

From a system identification perspective, the WAAM system consists of several variables, which influence geometrically and mechanically characterized parts deposited by the system. This includes wire material and diameter, WFS, TS, shielding gas characteristics, input power, deposition mode, part geometry, slicing path, slicing strategy, inter-pass temperature, and many others. The WFS, TS, interlayer temperature and input power related to arc voltage and current are the most influential parameters among the basic input parameters recorded in the literature. This Subsection discusses the set of significant WAAM parameters and their impact on the part performance.

Wire feed speed, travel speed, and heat input – To achieve stable welding and good weld quality, suitable WFS must be used for a given WAAM condition. [Fig. 68](#) shows the relationship between the WFS and arc current, providing a stable welding process. In this figure, the WFS equilibrium is stated under a given welding current for a feeding wire diameter of known size [116,118,258,270,294,334]. For example, a stable welding process for steel alloy can be established for the feeding wire with a diameter of 1.2 mm, under welding current of 100 A, within the WFS of approximately 2 mm/min. The equilibrium WFS is

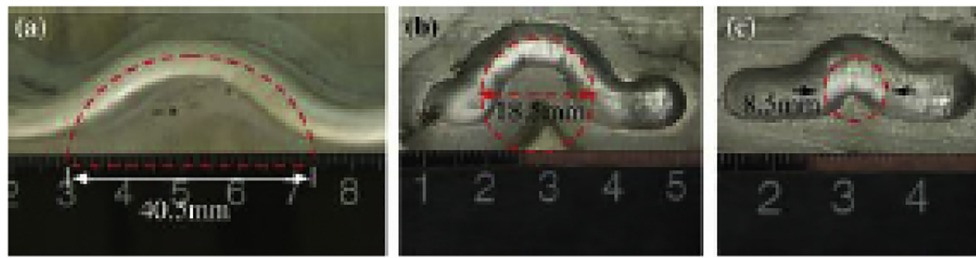


Fig. 47. The curved feature with large curvature 5, 10 and 20 mm. The actual curvature radius of 9.25, and 20.25 mm was observed. The interior was distortive by accumulating materials at the turning position of the welding gun for a designed radius of 10 mm and more obvious in the radius of 5 mm [315].

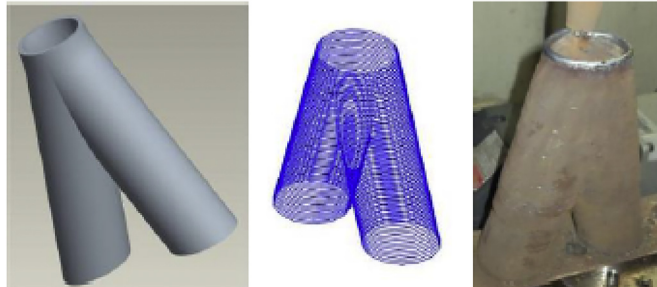


Fig. 48. CAD model and Deposited part (212 mm height, 60 mm diameter with 129 layers) [61]

demonstrated to depend on the diameter of the wire: a smaller diameter leads to a higher electrode-melting rate as electrode fusion requires less energy. Note that the arc pressure has a significant effect on the molten pool during WAAM deposition with a large current, and it can damage the previous layer [258]. The effect of arc pressure on the pool surface is minimal for small currents, so the distortions of the pool surface are small, and the molten pool surface is stable. However, consideration should be given to the necessary heat input to acquire a good forming weld bead.

The WFS and TS are two of the most important and easy to control variables in WAAM. The effects of WFS and TS on the geometry of a single track (the bead width and bead height) are shown in Fig. 70 and Fig. 69, respectively. From characteristic geometry parameters, it can be observed that:

- o With an increase in TS, bead width and bead height decrease. The effect of TS on the characteristic geometry parameters is opposite to that of WFS. In practice, both the filler material volume and the heat input per unit length ($P = \eta VI / TS$, where η is the efficiency of

the heat source, I is the current, V is the voltage) are reduced with the increase in TS when the WFS is constant. By increasing TS, the heat input decreases and therefore the weld bead size decreases [257,335].

- o With an increase in WFS, bead width and bead height increase. Single tracks with various geometries can be obtained using different WFSs and related TSs. The bead width increases significantly at lower WFSs, when keeping the TS constant. In practice, keeping the TS constant, the increase of WFS is associated with an increase in the welding current, and thereby a higher heat input.
- o Meanwhile, Fig. 69 shows W/H ratio (bead width/bead height), illustrating the variables between bead width and bead height when WFS changes. As evidenced, it increases and then decreases with increasing WFS, which means that bead height changes more significantly than that of the bead width at higher WFS. Song et al. showed that welding voltage and WFS contribute heavily to both spatter formation and bead width at lower WFSs [271]. Prado-Cerqueira et al. [150] concluded that the bead geometry is mainly a function of the welding current and therefore the WFS: a higher current increases the bead width by a larger margin than the bead height in a specific range of WFSs.

Note that a limited range of process parameter combinations results in a stable weld bead deposit. A constant WFS/TS ratio is one way to ensure adjustments of the process parameters. In particular, surface waviness has a great influence on the geometrical accuracy of fabricated parts. Fig. 71 shows the effects of the WFS/TS ratio on the surface waviness of different geometrical features. In general, the surface waviness shows an increasing trend with an increase in WFS/TS. Keeping WFS/TS constant, increasing WFS results in increasing the arc pressure on the molten pool, hence, the increase in deformation on the molten pool. This is not beneficial to the stability of the molten pool. Increasing the TS is associated with a decrease in arc stability, leading to decreased surface quality. Thus, a lower WFS combining with a lower TS can

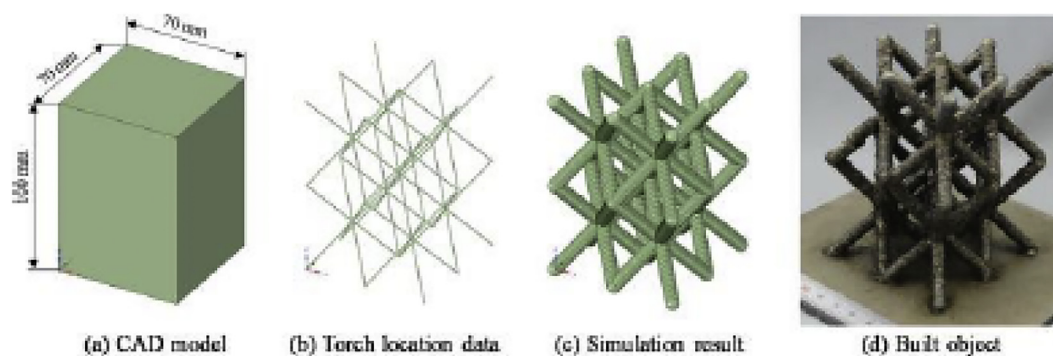


Fig. 49. A lattice structure built using WAAM [324]

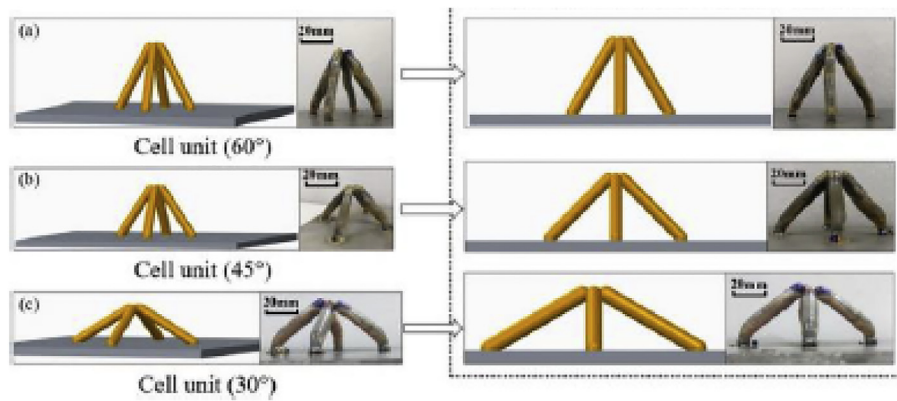


Fig. 50. The lattice truss cell units of different angles [327].

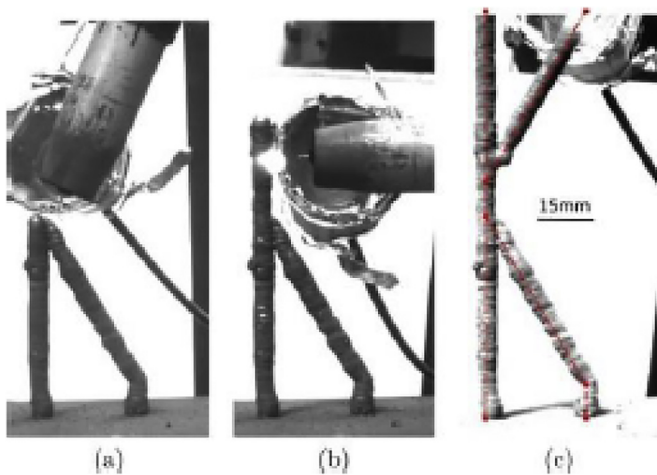


Fig. 51. Skeleton features manufactured via CMT [306]

improve the surface quality. The variation of surface waviness in an identical WFS/TS ratio can be explained by the variations in the interlayer dwell time, heat input, materials, geometrical features, and deposition path, among others [9,337]. In summary, macroscopic characteristics, including surface waviness as well as weld bead geometry are closely related to WFS and TS, and welding current.

One of the limiting factors for the bead geometry adjustment by TS and WFS is the heat input introduced in the part where the higher the heat can be inserted by the more higher the WFS. The relationship between the heat input and weld bead dimensions is shown in Fig. 72. It is evident that the weld dimensions depend on the heat input. As the heat input increases, the layer height and width are expected to be increased. However, decreasing the weld bead height can be explained by two scenarios:

1. Increasing the heat input is affected by the arc voltage. The layer width increases when a high heat input (high voltage) is used. Despite the increased width, the material deposition volume remained constant. Therefore, the layer height decreased under high-voltage conditions.
2. Increasing the heat input is affected by the arc current, and for a higher current, the wire feed volume increases. Unlike the voltage, the WFS increases, thus, the material deposition volume per layer also increases. The slightly decreasing of the layer height can be explained by the increasing penetration rate by increasing heat input.

Further studies on optimizing and formulating the above-mentioned process parameters for a wide range of materials and interlayer temperatures, including penetrating rate are needed for achieving better dimensional accuracy and surface quality of WAAM.

Interlayer temperature – In WAAM, a high heat input can lead to a progressive increase in the internal energy of the workpiece, known as heat accumulation, that could lead to excessive melting of the lower layers (see Subsection 3.2). This phenomenon results in an increase in the interlayer temperature, modification of the geometry of the layers [147,292] and the microstructure of the material [127,338], especially along the deposited height [150]. Fig. 73 shows the percent temperature changes at different layers of both thin wall and cylindrical features. According to the characteristics of the curve, a typical increasing temperature can be divided into three stages [116]:

- 1) A sharp temperature changes: at the beginning of the deposition process (first few layers), the interlayer temperature changes drastically increases. This is mainly due to the strong heat dissipation effect of the substrate plate.
- 2) Quasi-steady stage: in this stage, the mode of heat dissipation gradually changes from heat conduction to heat radiation. The change in the interlayer temperature is less sharp, which indicates that this stage is controllable.
- 3) Steady stage: in the last stage, the molten pool reaches the steady state, so that the heat flux of heat inflow and outflow from the molten pool remains unchanged. This stage is considered as the best case for WAAM because it enables the deposition of uniform layers without or with minimum changing the deposition variables.

The layer height must be controlled to achieve the desired final height. Fig. 74 shows the relationship between the percent layer height changes and layer number. A decreasing layer height with an increasing number of layers, likely due to heat accumulation, which leads to slump as reported by [339]. The accumulating heat causes slumping of beads due to a reduced solidification rate [114,115]. This gradual change in solidification rate and varying heating cycles can also lead to variations in the microstructure throughout the component [13]. It is also known that an excessive amount of heat while deposition leads to remelting of previously deposited layers, which further deteriorates the bead geometry. Therefore, it's better to decrease the heat input at upper layers to avoid excessive amount of heat. Typically, more heat input is needed for the first several layers in order to provide better wetting with the substrate. So, depending upon the material and features of part required consecutive reduction of heat input by 5%, 10%, or 20% between each layer is suggested [257]. According to the state of the art, several process parameters can be adjusted to correct layer height deviations as discussed in Section 4.

Table 21

The relation between geometric accuracy of different geometrical features and the WAAM processing parameters

Feature	Heat source/ Material	TS/WFS (m/min) Others	n./ width/ height of layers	Designed height/ width/ length or diameter (mm)	Deposited height/ width/ length or diameter (mm)	Error in height/ width/ length or diameter (mm or %)	Surface roughness (μm)
Cylinder [124]	GTAW/ 5356 Al	4.8/- 1 st -40 th : 140-100 A Rest; 100 A	300/4.4/0.4	120/4.4/101.6	116/4.3/102	3.3/2.3/1 (%)	2.45-2.77
Cross [250]	CMT-P/ ER 2319	0.6/6 Pre heat= 200°C	20/n.a./n.a.	n.a./10/80×80	n.a./n.a./n.a.	1-2.5/n.a./ n.a. (mm)	n.a.
Cross [85]	GMAW/ Ti-6Al-4V	n.a.	8/6/1.5	12/25/80×130	n.a./n.a./n.a.	n.a./n.a./ n.a.	n.a.
Cross [246]	CMT/ mild steel	n.a.	30/n.a./n.a.	n.a./4/200×200	n.a./n.a./n.a.	1.5-2/ n.a./ n.a. (mm)	n.a.
T crossing [12]	GMAW/ER70S6	0.3/4.6 50A/19V	16/-/1.5	n.a/n.a/n.a	n.a/n.a/n.a	0.5/n.a/ n.a. (mm)	2.07 (back surface)
Thick T-crossing [313]	GTAW/Ti-6Al-4V	1 st -3 rd : 0.2/2.2 200A 4 th -12 th :0.2/2.4 190A	12/11/1.65 Overlap: 50%	19.8/22/100	15/20/80	24/9/20 (%)	n.a.
Cylinder [86]	GMAW/ER-70S-6	0.14/6.1 210A/23.9V	n.a./n.a./2	120/15/110	130/10-11/108	8.3/30/n.a (%)	n.a.
Cylinder [318]	CMT/ G4Si1 (steel) & AZ31 (magnesium)	0.4/2.5-5	20/4-6/2	n.a/n.a./60	n.a/n.a/n.a	n.a/n.a/n.a	n.a.
Cylinder	GTAW/ Ti6Al4V	0.12/1	15/n.a./1	n.a/n.a/n.a	15.26/6.1/40	n.a/n.a/n.a	n.a.
Sharp corners [317]	CMT/Al (4.8-5.2% Mg)	0.6/3.4	16/5/1.5	n.a/n.a/n.a	26.5/5.2/n.a	0.23-0.76/0.66-0.75/n.a (mm)	n.a.
Cylinder [321]	CMT/mild steel	0.6/3 110A/15V	40/4.6/1.9	n.a./n.a./50	n.a/n.a/n.a	n.a/n.a/n.a	n.a.
Thin-wall [322]	GMAW/SS 410	n.a.	20/n.a./n.a.	64/9.22/n.a.	41.8/8.2/n.a.	35/156/n.a (%)	n.a.
Thick-wall [322]	GMAW/SS 410	n.a.	20/n.a./n.a.	64/6.4/n.a.	56.3/11.3/n.a.	12.5/76/ n.a (%)	n.a.
4-bead wall [322]	GMAW/SS 410	n.a.	20/n.a./n.a.	64/12.8/n.a.	70.1/18/n.a.	9.3/40/n.a (%)	n.a.
Cylinder [322]	GMAW/SS 410	n.a.	15/n.a./n.a.	n.a./n.a./ 14, 16, 18.2, 18.7, 19.2, 20.2	n.a./n.a./ 4.8, 6.8, 10.1, 10.5, 11.6, 12.5	n.a/n.a./ 65.7 57.5 44.5 43.8 39.6 38.1 (%)	n.a.
Sharp Curve [315] Fig. 47	GTAW/ 5A06 Al	0.25/2	1/7.2/1.3	n.a./n.a./ 20, 10, 5 (curvature radius)	1.3/7.2/ 20.25, 9.25, failed (curvature radius)	n.a/n.a./ 1.25, 7.5, Failed (%)	n.a.
Sharp angle [315]	GTAW/ 5A06 Al	0.25/2	1/7.2/1.3	n.a./n.a./ 20°, 15°, 10°	1.3/7.2/ 19°, 9°, failed	n.a/n.a./ 5, 40, Failed (%)	n.a.
Thin cylinder [61]	CMT/ ER70S-6	0.45/7	30/4.35/ 2.04	61.2/n.a./n.a.	51.5/n.a./n.a.	15.9/n.a./ n.a. (%)	n.a.
Thin triangular [61]	CMT/ ER70S-6	0.35/5.5	30/4.88/ 2.37	71.1/n.a./n.a.	52.7/n.a./n.a.	25.9/n.a./ n.a. (%)	n.a.
Thin squared [61]	CMT/ ER70S-6	0.5/8	30/5.38/ 2.73	81.9/n.a./n.a.	60.5/n.a./n.a.	26.2/n.a./ n.a. (%)	n.a.
Pipe joint	GMAW/ IYHJ507M	0.420-0.48/n.a. 120-150 A/ 20-22 V	n.a./6/n.a.	220-700/ 20/265 20/195 10/165 10/150 15/95 20/195 10/165	n.a./ 20.85/265.5 20.5/195.6 10.7/165.7 10.2/150.2 15.3/195.2 20.25/195.2 10.3/165.2	n.a./ varied	

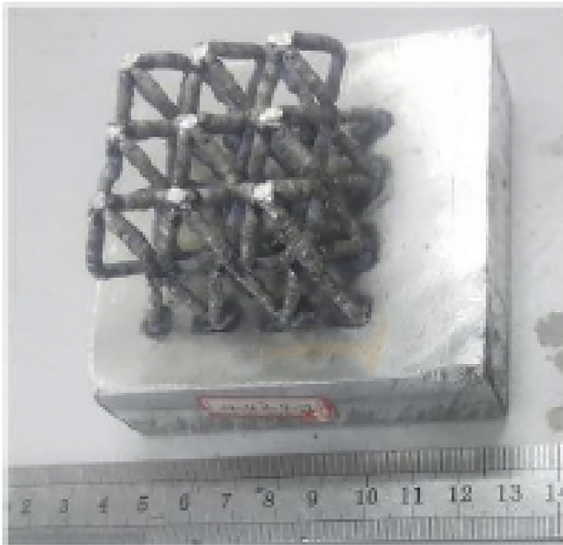


Fig. 52. Pyramid lattice structures [326]

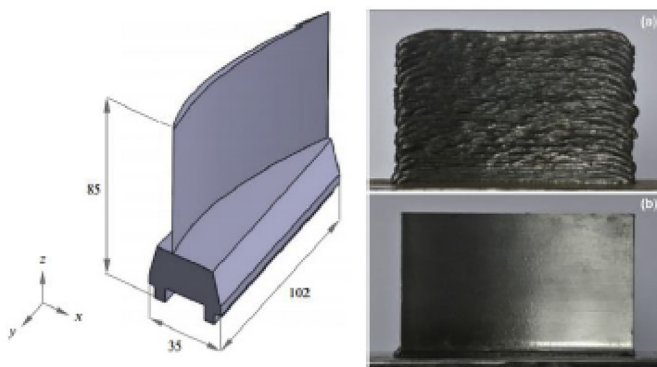


Fig. 53. Case 1 airfoil [328]

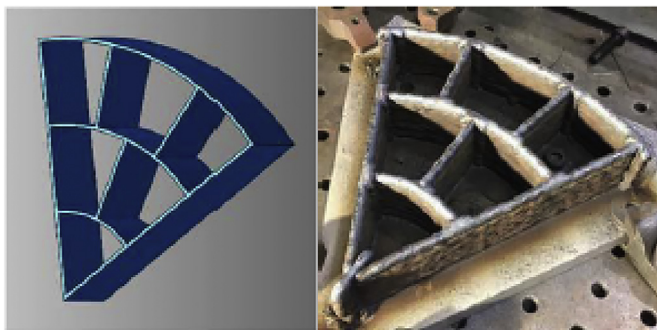


Fig. 54. Case 2 Complex T-crossing features [329]

In summary, a requirement to use WAAM technology is to identify system parameters and parameter envelopes within which the geometry and quality of the deposited bead can be influenced and optimized. This allows for the control of the geometry and geometric quality of 3D components [342]. In addition to part accuracy, the part quality

manufactured via WAAM is critical. The WAAM solidification characteristic comprises the thermal gradient and nucleation rate within the weld pool and determines the primary performance measures for a specific location and the quality. As outlined in Subsection 3, the heat dissipation factors influence on the part accuracy and various cooling systems as well as an introducing interlayer dwell period were reported to minimize heat accumulation resulting in high accuracy parts. However, the WAAM solidification characteristic obtained may be unsuitable for producing high quality WAAM parts efficiently. Further studies are required to balance the fabrication quality and the fabrication accuracy as well as production efficiency.

5.2. A need for design rules

Although AM has enormous design potential, geometrical freedom is not unlimited [343,344]. The technical method itself, the manufactured material, or even the system establishes new restrictions. Design engineers must be aware of the design rules to ensure production efficiency. As with standard processes, rules for different AM technologies have been established, ranging from general quality guidelines, such as manufacturing orientation, to precise quantitative limits, such as minimum wall thickness. In particular, for powder bed-based systems such as SLM, SLS or fused deposition modelling (FDM) design rules can be found in the literature [21]. The research primarily focuses on geometric constraints, minimum characteristic sizes and structural orientation [345–348] to include either general high-quality recommendations, depending on the build orientation [345] or design guidelines for the conditions on the respective boundaries (i.e., the thickness of layer, system, material, set of parameters, etc.) [347].

However, design for WAAM requires an even more design approach to other AM processes, as WAAM introduces different manufacturing constraints and certain unique production capabilities that cannot be used with other AM technologies. WAAM, for example, offers a unique capability in the manufacturing of custom geometries through direct production from 3D data and hybrid production, functionally graded materials, and the production of integrated functionality parts. Part designers often lack an understanding of these issues and their effect on the final products. During WAAM, major challenges include, among other issues, the development of deposition processes, geometry characterization, robotic path integration and implementation, heat management, and appropriate slicing in response to the WAAM process requirements to achieve necessary interface tolerances. Future studies need to focus on design rules to (i) promote the use of the WAAM process, (ii) take advantage of high-value product design, and (iii) quantify WAAM's geometrical constraints. The following is an example of a few design guidelines.

Design freedom – One of AM's major advantages over traditional manufacturing is design freedom. Given the constraints of traditional production technology, it may be necessary to compromise the functional product in order to make it cost-effective. Designers may then have to compromise their concept so that the product loses its meaning, which reflects the vision of the designers. Complexity and geometry should no longer affect manufacturability with WAAM in the future.

In addition, the promise of superior/equivalent strength for a component with a lower mass is one of the key thrusts for WAAM use in production. The goal is to optimize topology in order to obtain complex forms, which can be generated reasonably easily by WAAM processes. However, few examples of such component types can be found via WAAM [80] and an additional effort is required.

Build orientation – The quality of the part (strength, material properties, surface quality, etc.) is directly linked to the orientation of the deposition in WAAM. The selection of part orientation is an important task when designing a part for WAAM. The direction of the anisotropic, which takes the direction to the Z-axis or the vertical direction of deposition is determined by the position orientation. Therefore, if anisotropic is a major factor, the component must be deposited to have the

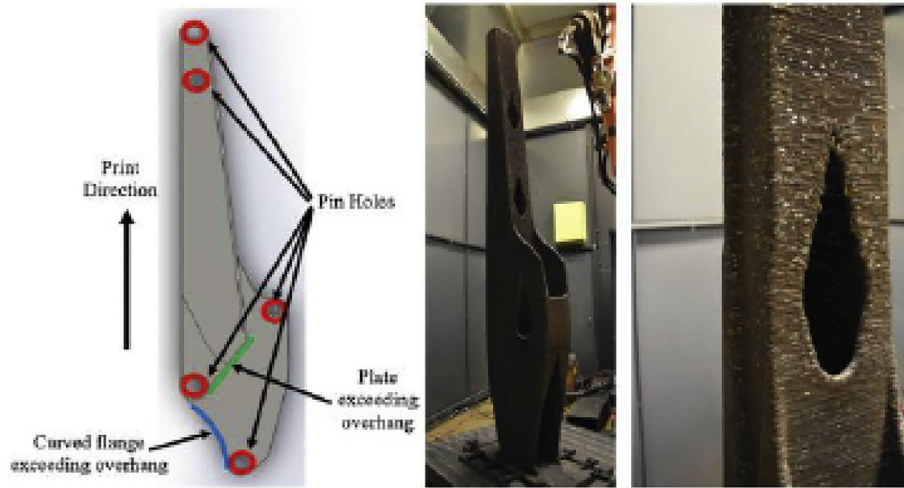


Fig. 55. Case 3 An excavator arm [80]

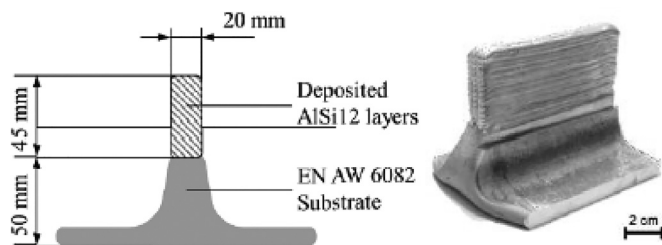


Fig. 56. Case 4 Rib [330]

characteristics that require maximum strength. For example, if the geometrical characteristic, for instance, the circularity of a cylindrical function, is critical, it should be deposited vertically. A horizontally deposited cylinder feature is affected by the step-stair effect and may become slightly elliptical.

The total build height defines how many material layers are required and, therefore, the deposition period affects the costs. If no other important criteria exist, generally, the best deposition orientation reduces the total building height to a minimum. However, as discussed in Subsection 4.1, the build temperature should be taken into account during deposition. In fact, larger thermal gradients from a cooler substrate induce thermal stresses that can exceed the material's yield strength, resulting in residual

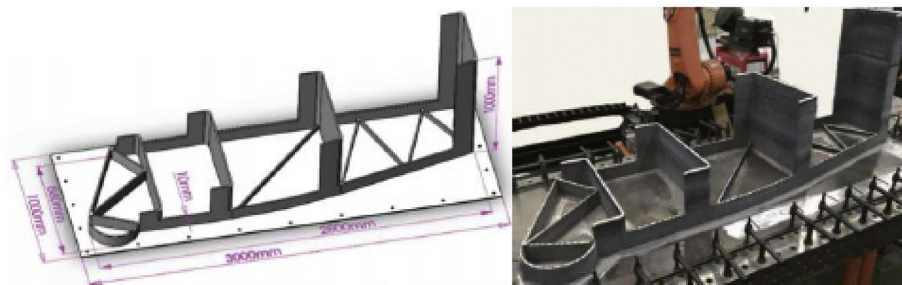


Fig. 57. Case 5 Complex large crossing features [263]

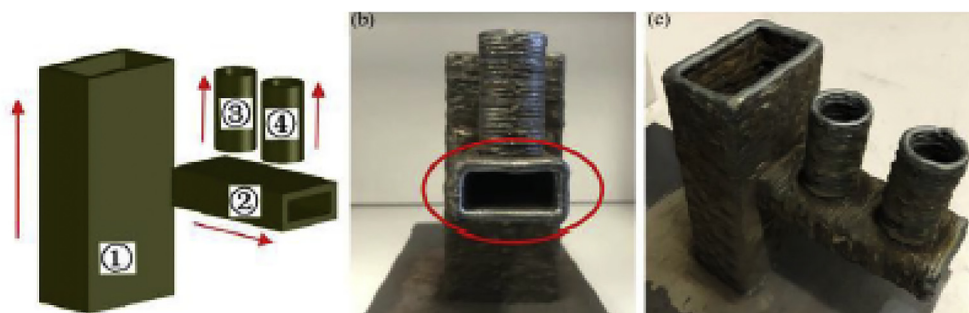


Fig. 58. Case 6 a complex geometry including overhang [201]

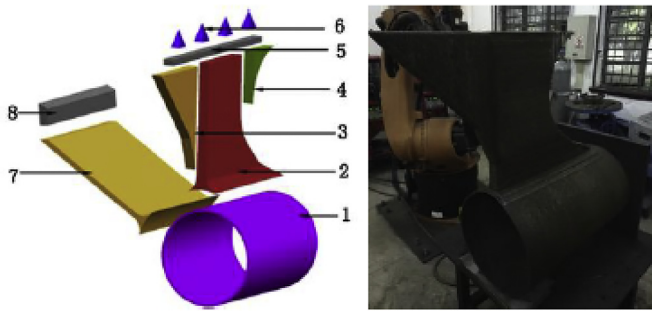


Fig. 59. Case 7 propeller bracket [331]

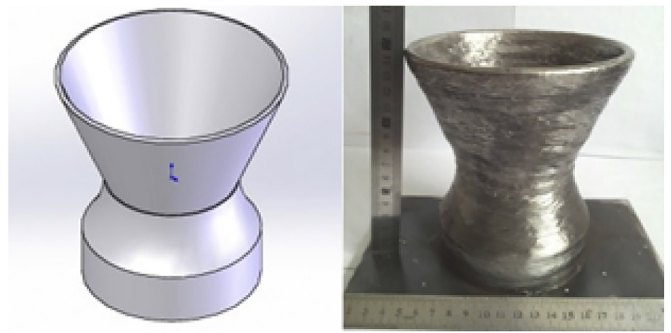


Fig. 63. Case 11 thin-walled part with overhang geometrical features [254]



Fig. 60. Case 8 Pipe joint [247]

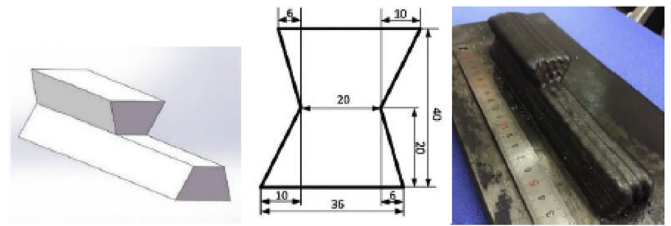


Fig. 64. Case 12 a bull overhang part [285]

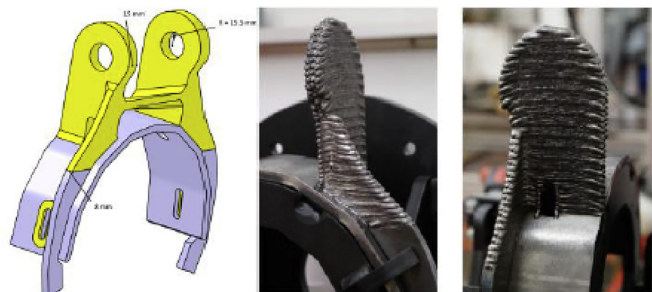


Fig. 61. Case 9 crane construction [269]

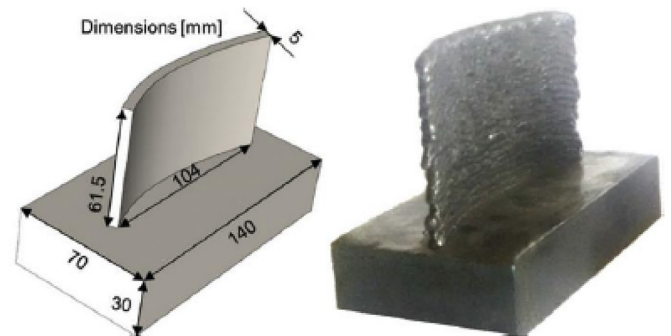


Fig. 65. Case 13 The airfoil design and deposited via GMAW [121]

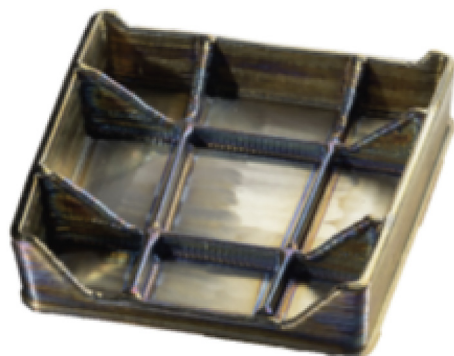


Fig. 62. Case 10 Bombardier Landing Gear [149]

stress in the component. The other issue is the warping of the build plate, which causes the first layers of the part to deform.

Overhang features – The overhang constraint in WAAM depends on the need to strike an electrical arc between the electrode and the work-piece and on the potential for the molten metal to flow across the sides of a wall. This overhang limit can be extended when changing the torch orientation, as a filler wire deposition in vertical positions is common in manual welding, but automatic tool orientation determination is not currently integrated with WAAM during tool path generation. In addition, the overhang limit does not allow the manufacturing of complex geometries.

For example, for overhang features, 45° is a safe default number for vertical torch deposition. For large components, it was confirmed that 15° overhang is a safe overhang angle that can be used without changing the torch orientation [80]. Steeper overhang angles are possible but are not reliable for the deposition time durations needed for large components [80]. On the other hand, horizontal or near horizontal overhangs can be deposited via using rotating torch [245,332], however, not all forming equipment can rotate the torch conveniently. Up to horizontal overhang is also possible using a rotating table. With the decline

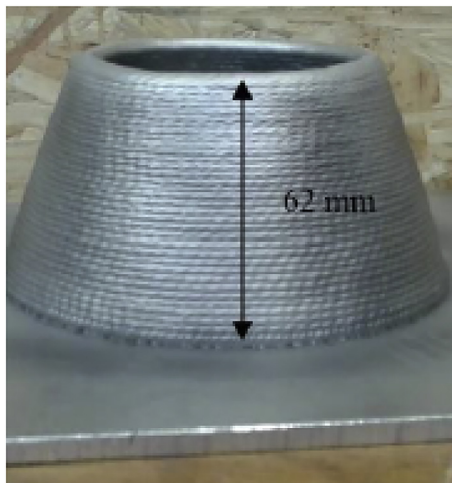


Fig. 66. Case 14 cone manufactured via GMAW [332]

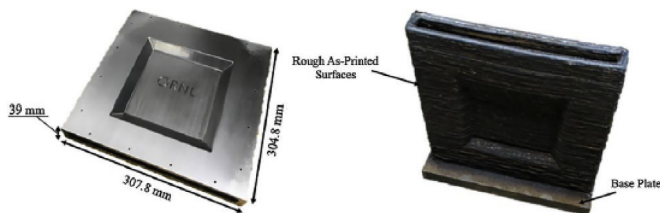


Fig. 67. Case 15 Compression moulding mould (female side) [333]

of heat input and increase in the cooling rate, the molten pool can be solidified rapidly, which may benefit the fabrication of overhang structure. A rotating table for large components is however a difficult task. Therefore, designers seek to design the component so that it is as similar as possible to vertical overhangs.

Internal and complex features - Another benefit of AM process is that many can produce internal functions easily. In certain cases, internal geometry can be practical, and in another case, geometry can simply reduce a component's material by generating internal material patterns. Internal functionality may be a 2D or 3D feature. The manufacturing of 2D features such as complex internal channels is not normally suggested by WAAM. WAAM can, however, be used to manufacture lattice and skeleton structures. Such features can traditionally be created with individual components that are joined to an assembly. With WAAM, these features can be manufactured in one part, saving time, materials, and costs.

Minimize large material mass - Large material mass in one-part costs a lot causes a great amount of residual stress and adds little technical value such as avoidance of porosity. Hence, unnecessary material that increases cost, causes more residual stress and therefore requires more post-processing should be avoided.

Omitted features from the deposited components - Some features must be omitted as the tolerances and surface finishes are too tight to reasonably be deposited. When the feature size is too small for WAAM, then the feature (e.g., pinhole) is omitted with over-manufactured geometry. The functionality is introduced in post-processing [80].

In summary, WAAM can manufacture various features and impose different restrictions than other AM technologies. Due to the manufacturing principles of WAAM, discussed in Section 3, important factors and effects on the geometrical accuracy must be taken into account. For example, the sharp angle and curve form usually cannot be formed

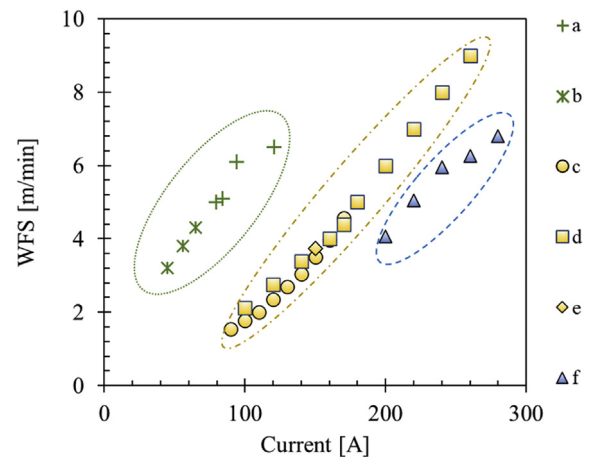


Fig. 68. Wire feed speed vs. deposition current: (a) [294] and (b) [116] aluminium alloys with a feeding wire diameter of 1.2 mm, (c) [334], (d) [258] and (e) [270] steel alloys with a wire diameter of 1.2 mm, and (f) [118] steel alloy with a feeding wire diameter of 1.6 mm.

accurately due to the large molten pool and surface tension in WAAM processes. More research needs to be performed with respect to the geometrical structure and properties of deposited parts using WAAM technology. This can be used to further determine how the deposited components can be used directly. WAAM should also establish related standards to facilitate industrial applications, similar to other manufacturing technologies. There is currently no industry standard for assessing the features and mechanical properties of WAAM parts. One of the main aims of future studies should be to clarify these limitations and provide basic data about WAAM for path planning and structure designers. Table 21 shows an overview of the relation between the precision of the various deposited features and the WAAM processing parameters including dimensional deviation, highlighting the future needs to focus on geometrical accuracy and part quality.

Not available, n.a.

6. Summary of future needs

Macroscopic features, quality of the part, and precision are closely linked to processing planning and parameters such as scanning speed, wire feeding rate, welding mode, cooling time, interlayer temperature, etc. The influences of main process parameters and deposition strategies on the macroscopic properties and geometrical accuracy of WAAM for different geometrical features and case studies are discussed in this paper. For better dimensional accuracy and surface quality of WAAM parts, further studies are needed to exploit the above-mentioned process parameters as discussed below.

- o Process planning in WAAM plays a key role in assessing the performance of manufactured parts, such as geometric accuracy and mechanical properties, which can be applied on various scales from track to part size. For example, the same component designs can be manufactured with different process configurations often results in components with distinct quality and geometric precision. In this light, the most methods of process planning in WAAM adjust process settings at the bead/track scale level. This leaves the design space in large undiscovered regions. There is however a considerable potential for improving product characteristics through part-scale process planning. Many concerns need therefore to be resolved on different scales, including features and the component scale level, in order to make WAAM processes viable, including (i) creating relationships between process variables and the resulting properties at the scale of interest, and (ii) tractable optimizing process parameters in size

- and solving in a rapid-manner.
- o Typical design practices for AM require the optimization of topology, shape, and scale, taking into account the impact of the resulting geometry on the component quality characteristics. Despite modelling and simulations of WAAM processes on the part scale, due to its high heat input and high cooling cycles, process parameters are difficult or impossible to optimize with current methodological capacities. For example, the finite-element modelling of the WAAM processes and induced residual stresses have been successfully studied, but most of these methods are computationally costly and cannot be implemented in an iterative design process. The inability to correctly predict the as-deposited geometry of the component and the surface finish is another challenge of the existing modelling techniques. In order to optimize the production process and ensure consistent quality materials, the aim should be to predict thermal dynamics, deformation, residual stress, and material properties at multi-scale levels. Note that WAAM has different energy characteristics, and high-speed simulation targeting makes it even more difficult. It is important to be able to simulate the process in a short time considering the system complexity, scale, and variety of geometrical features.
 - o The WAAM path planning is a complex task, as the evolution of residual stress and the relationship between the welding track and component structure have to be tackled. The study of residual stress evaluation concerning patterns and sequences can particularly guide

path planning. Dimension problems are another challenge to automated path planning for complex geometry components. A more robust, automatic, closed-loop control system would be the next generation WAAM system.

- o The feature scales reflect specific geometrical regions of components that have different process plans. Examples of these elements are thin/thick-walls, crossing features, overhang features, and lattice structures. Previous process planning efforts at this scale were driven by the need to enhance the properties of characteristics and were conducted individually or on a functional basis only for specific geometric features. A comprehensive approach is required to produce components with an overall optimal performance that can simultaneously optimize process planning for various features of a product. The potential for improving part performance through feature-scale process planning is also not fully explored and implemented. Many publications have addressed deposition techniques for crossing features, for example, and all techniques need to be deposited in a particular way. Therefore, it is only easy to implement these strategies when one crossing occurs. For a complex workpiece that involves several crossing features, these strategies can lead to significant complications in the implementation process. Furthermore, the restriction of the deposition sense might lead to an impossible alternative in combining several features. More studies for a deposition strategy for a complex component are therefore needed.

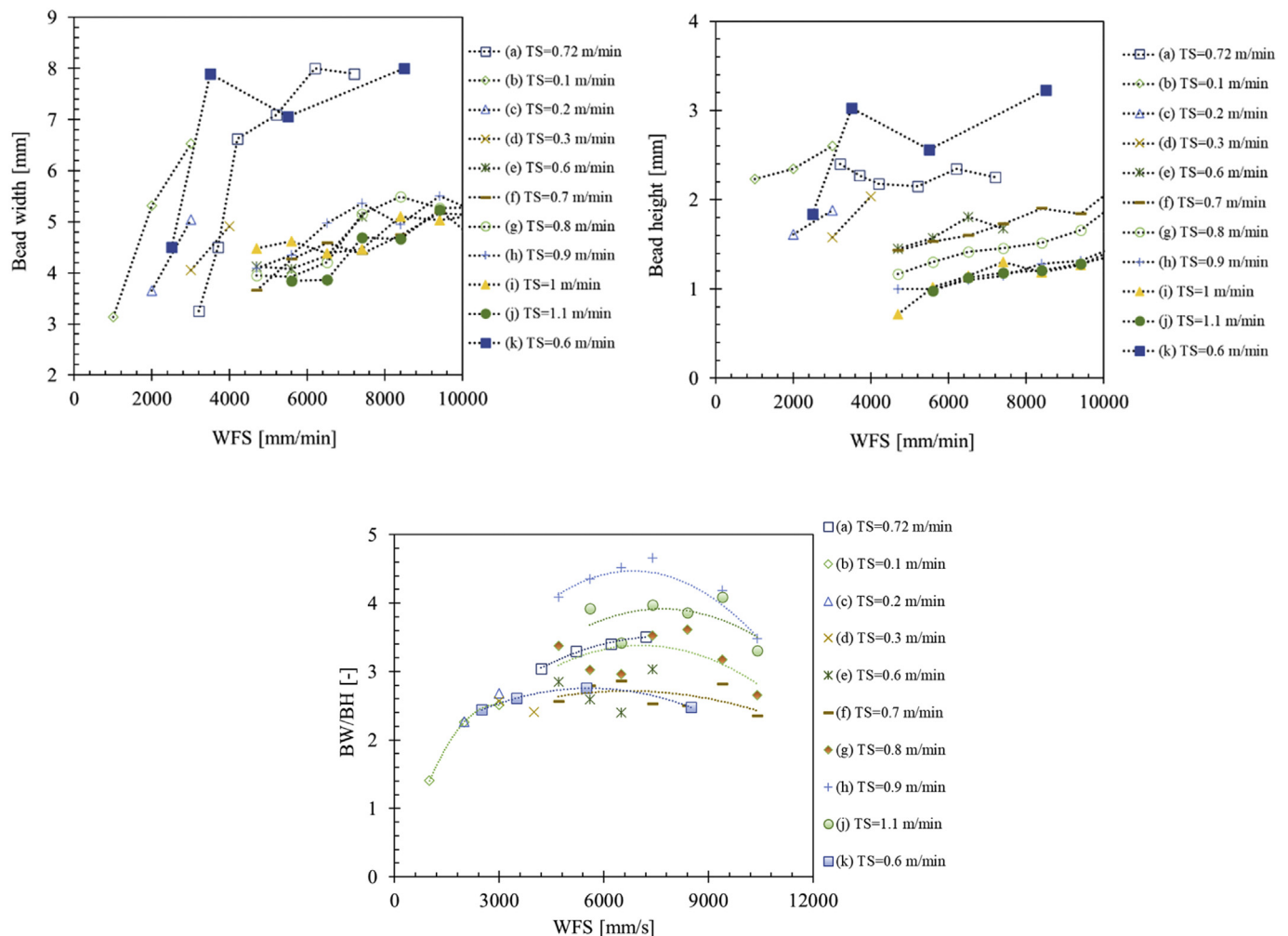


Fig. 69. The relationships between the wire feed speed (WFS) and the geometry of the single layers deposited via CMT process, the bead width (BW), bead height (BH) and BW/BH ratio. (a) Steel 2209, (b, c, d) ER70S-6 [336], (e-j) ER70S-6 [261], (k) ER70S-6 [269]

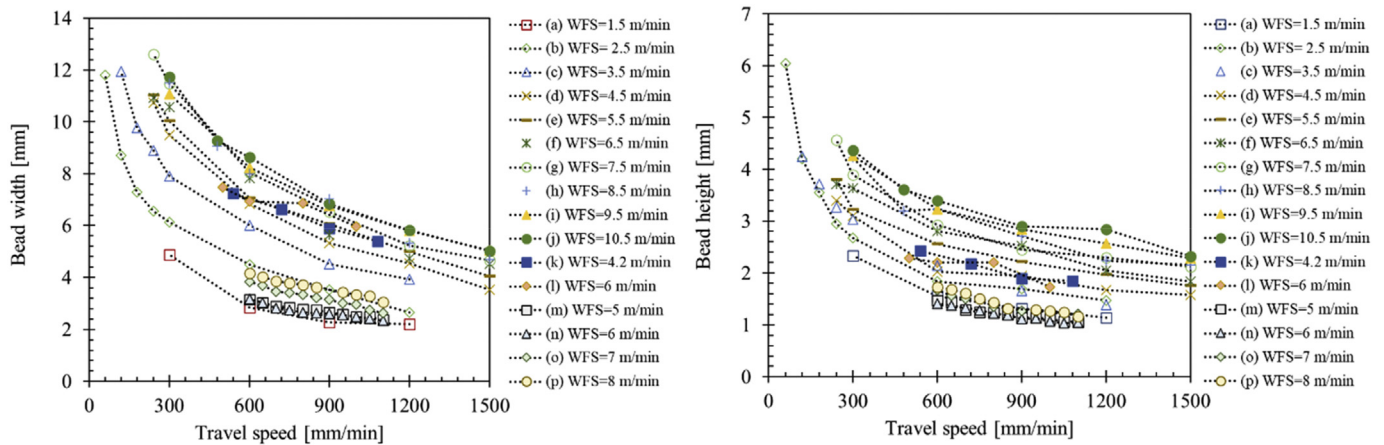
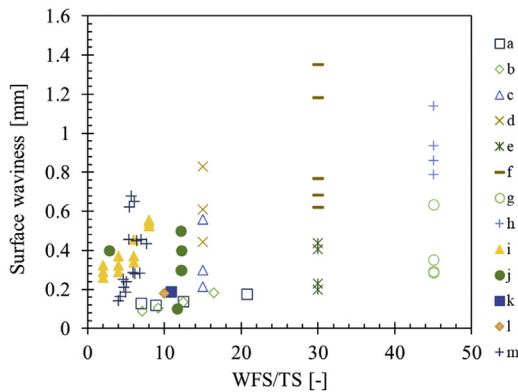


Fig. 70. The relationships between the wire feed speed (WFS) and the geometry of the single layers deposited via CMT process, the bead width (top) and bead height (bottom). (a–j) steel alloy [269], (j) Steel 2209, (k) aluminium alloy (2319) [176], (m–p) ER70S-6 [259]



	Heat source/Feature/material	WFS/TS (mm/min)
(a) [292]	GMAW/Thin Wall/ ER70S6	3730/180-540
(b) [292]	GMAW/Thin Wall/ ER70S6	2120-4930/300
(c) [245]	CMT/top surface/ ER70S6	1170-7500/ 78-500
(d) [245]	CMT/bottom surface/ER70S6	1170-7500/ 78-500
(e) [245]	CMT/top surface/ER70S6	2340-12000/ 78-400
(f) [245]	CMT/bottom surface/ER70S6	2340-12000/ 78-400
(g) [245]	CMT/top surface/ER70S6	3510-13500/ 78-300
(h) [245]	CMT/bottom surface/ER70S6	3510-13500/ 78-300
(i) [262]	GMAW/Thin wall/ R70S6	800-4800/ 400-600
(j) [294]	CMT/Thin wall/ER5356	4900-6500/ 410-535
(k) [293]	GMAW/Thin wall/ER5356	6500/600
(l) [278]	GMAW/Thin wall/ER70S6	4000/400
(m) [337]	CMT/Thin wall/ ER70S6	1520-2290/300-380

Fig. 71. The relationships between the surface waviness and WFS/TS ratio

- o In order to compete with traditional manufacturing technologies, and comply with the qualifying requirements for industrial applications, WAAM should have a good understanding of physical processes. The geometrical quality and precision of the WAAM-produced parts are highly variable, mainly as the standard of feature characteristics and process parameters are not known. The process instability and the lack of equipment in order to determine the structural effectiveness of the metals deposited are critical elements to accept WAAM in industrial applications. Improving surface consistency, higher accuracy in dimension, developing certification concepts, and quality assurance systems are also required to take into account the WAAM characteristics. For clarifying the requirements on geometrical precision and design guidelines, future efforts are required.
- o WAAM processes generally involve high residual stresses due to high deposition rates and heat inputs. The influences of process conditions (for example, energy input, wire-feed rate, welding speed and/or deposition pattern) on thermal history, microstructure and resultant mechanical and surface properties of parts need to be further analysed as there is not enough knowledge in the scientific community yet. For example, the dimensions and surface finish are generally large challenges in WAAM and many attempts have been reported to control of the temperature, idle time and heat sink to minimize the part distortion. However, it is unknown how to balance the fabrication quality and fabrication accuracy.

- o A more complete understanding of the governing process-structure-property relationships is required. The fabrication of even simple wall structures can be complicated by changes in the build path, leading to changes in geometrical performance, microstructural and mechanical properties at different locations and orientations, which cannot be easily predicted. One area, which has not been widely investigated, is the role of geometrical features in part accuracy in addition to the resulting mechanical properties within a component.
- o Appropriate benchmark parts for WAAM and process performance evaluation should be designed and manufactured to address the aforementioned needs. Besides the performance and the material, other factors such as specific process parameters may also affect the accuracy and surface finish of the part. In WAAM benchmarking, the design of the benchmark part, as well as production and measurement processes, must be standardized. Geometric features which are more required or expected WAAM technology must include the benchmark design. We believe that WAAM needs a standard test part design to achieve both geometric tolerance characterization and process development. Accordingly, all the capabilities and constraints of WAAM need to be addressed and defined for successful industrial applications. Manufacturing guidelines cannot simply be adopted for WAAM similar to other AM technologies such as powder bed fusion or fused deposition modelling. However, specific design guidelines for WAAM should be developed because

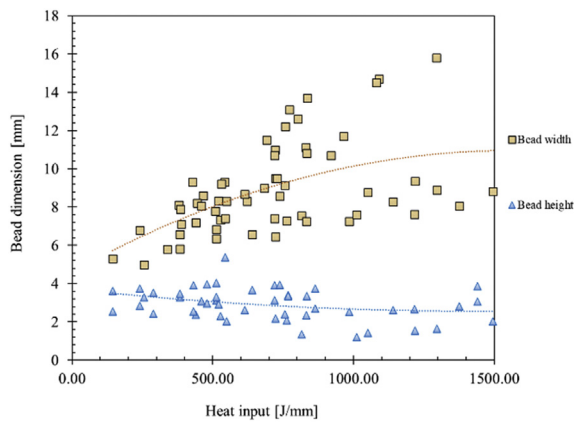


Fig. 72. The relationships between the heat input and single-track weld bead dimensions

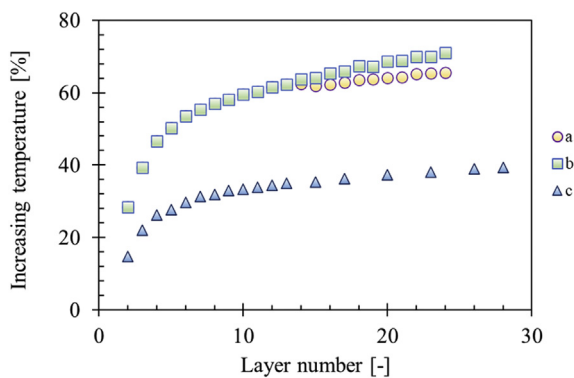


Fig. 73. The relationships between the percent interlayer temperature changes and layer number: (a and b) thin wall manufactured via the GMAW process under free convection cooling and airjet cooling, respectively [137] (c) cylindrical geometry manufactured via the CMT process [116].

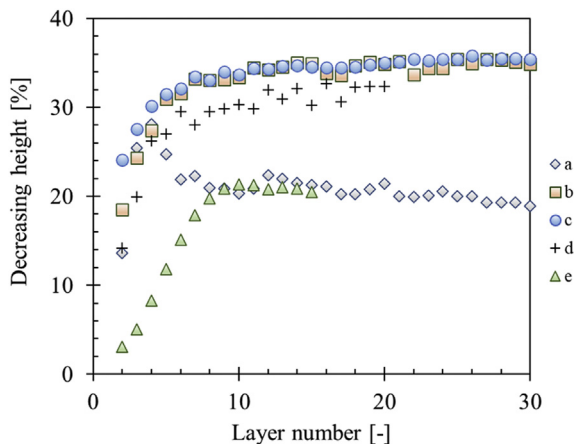


Fig. 74. The relationships between the percent layer height changes and layer number: (a, b, and c) ER70S-6 curved shapes manufactured via GMAW [61], (d) stainless steel thin wall manufactured via GMAW [340], and (e) ER4043 thin wall manufactured via GMAW [341].

of its complex process constraints.

- o While many works on parameter identification and optimization have been done, effects of thermal cycle and heat accumulation on the component geometry and part accuracy are limited.

Understanding the influence of the accumulated heat during fabrication of the benchmark components with varying process parameters is important to understand and correlated with the weld bead dimensions (e.g. weld bead height and width) in addition to correlating the microstructure and mechanical properties. In summary, the main contributions of future works are the identification of relevant deposition-related parameters and their optimization, metallurgical analyses of fabricated benchmark components, and the establishment of relationships between metallurgical variations, geometric quality and variations in heat accumulation during fabrication of the benchmark component. The provided studies and analyses will provide a detailed insight into the WAAM process and the factors that have a significant influence on the quality of a component fabricated through WAAM.

Declaration of Competing Interest

The authors declare that they have no known competing financial interests or personal relationships that could have appeared to influence the work reported in this paper.

Acknowledgement

This research was carried out under project number P16-46/S17024x, which is part of AiM2XL program framework of the Partnership Program of the Materials innovation institute M2i (www.m2i.nl) and the Netherlands Organization for Scientific Research (www.nwo.nl). The research was conducted in collaboration with industrial partners and supported by the Rotterdam Fieldlab Additive Manufacturing BV (RAMLAB) (www.ramlab.com).

References

- [1] D. Jafari, W.W. Wits, The utilization of selective laser melting technology on heat transfer devices for thermal energy conversion applications: A review, *Renew. Sustain. Energy Rev.* 91 (2018) 420–442.
- [2] I. Gibson, D. Rosen, B. Stucker, *Additive manufacturing technologies: Rapid prototyping to direct digital manufacturing*, Springer-Verlag, New York, 2010.
- [3] C.C. Ng, et al., Layer manufacturing of magnesium and its alloy structures for future applications, *Virtual Phys. Prototyping* 5 (1) (2010) 13–19.
- [4] D. Jafari, et al., Porous materials additively manufactured at low energy: Single-layer manufacturing and characterization, *Mater. Des.* (2020) 108654.
- [5] J.P. Oliveira, A.D. LaLonde, J. Ma, Processing parameters in laser powder bed fusion metal additive manufacturing, *Mater. Des.* 193 (2020) 108762.
- [6] W.E. Frazier, Metal Additive Manufacturing: A Review, *J. Mater. Eng. Perform.* 23 (6) (2014) 1917–1928.
- [7] A. Khorasani, et al., A review of technological improvements in laser-based powder bed fusion of metal printers, *Int. J. Adv. Manuf. Technol.* 108 (1) (2020) 191–209.
- [8] Y. Zhang, et al., Additive Manufacturing of Metallic Materials: A Review, *J. Mater. Eng. Perform.* 27 (1) (2018) 1–13.
- [9] S.W. Williams, et al., Wire + Arc Additive Manufacturing, *Mater. Sci. Technol.* 32 (7) (2016) 641–647.
- [10] C.V. Haden, et al., Wire and arc additive manufactured steel: Tensile and wear properties, *Additive Manuf.* 16 (2017) 115–123.
- [11] D. Ding, et al., Wire-feed additive manufacturing of metal components: technologies, developments and future interests, *Int. J. Adv. Manuf. Technol.* 81 (1) (2015) 465–481.
- [12] G. Venturini, et al., Optimization of WAAM Deposition Patterns for T-crossing Features, *Procedia CIRP* 55 (2016) 95–100.
- [13] M. Liberini, et al., Selection of Optimal Process Parameters for Wire Arc Additive Manufacturing, *Procedia CIRP* 62 (2017) 470–474.
- [14] C. Su, et al., Effect of heat input on microstructure and mechanical properties of Al-Mg alloys fabricated by WAAM, *Appl. Surf. Sci.* 486 (2019) 431–440.
- [15] P.C. Collins, et al., Microstructural control of additively manufactured metallic materials, *Annu. Rev. Mater. Res.* 46 (1) (2016) 63–91.
- [16] B. Wu, et al., Effects of heat accumulation on the arc characteristics and metal transfer behavior in Wire Arc Additive Manufacturing of Ti6Al4V, *J. Mater. Process. Technol.* 250 (2017) 304–312.
- [17] C.R. Cunningham, et al., Invited review article: Strategies and processes for high quality wire arc additive manufacturing, *Additive Manuf.* 22 (2018) 672–686.
- [18] T.A. Rodrigues, et al., In-situ strengthening of a high strength low alloy steel during Wire and Arc Additive Manufacturing (WAAM), *Additive Manuf.* 34 (2020) 101200.

- [19] D. Zhao, W. Guo, Shape and Performance Controlled Advanced Design for Additive Manufacturing: A Review of Slicing and Path Planning, *J. Manuf. Sci. Eng.* (2019) 142(1).
- [20] J. Plocher, A. Panesar, Review on design and structural optimisation in additive manufacturing: Towards next-generation lightweight structures, *Mater. Des.* 183 (2019) 108164.
- [21] M.K. Thompson, et al., Design for Additive Manufacturing: Trends, opportunities, considerations, and constraints, *CIRP Ann.* 65 (2) (2016) 737–760.
- [22] M. Kumke, H. Watschke, T. Vietor, A new methodological framework for design for additive manufacturing, *Virtual Phys. Prototyping* 11 (1) (2016) 3–19.
- [23] G.N. Levy, R. Schindel, J.P. Kruth, Rapid manufacturing and rapid tooling with layer manufacturing (lm) technologies, state of the art and future perspectives, *CIRP Ann.* 52 (2) (2003) 589–609.
- [24] D.D. Gu, et al., Laser additive manufacturing of metallic components: materials, processes and mechanisms, *Int. Mater. Rev.* 57 (3) (2012) 133–164.
- [25] K.P. Karunakaran, et al., Rapid manufacturing of metallic objects, *Rapid Prototyp. J.* 18 (4) (2012) 264–280.
- [26] W. Gao, et al., On-machine and in-process surface metrology for precision manufacturing, *CIRP Ann.* 68 (2) (2019) 843–866.
- [27] F. Xu, et al., Realisation of a multi-sensor framework for process monitoring of the wire arc additive manufacturing in producing Ti-6Al-4V parts, *Int. J. Comput. Integr. Manuf.* 31 (8) (2018) 785–798.
- [28] S. Singh, S. Ramakrishna, R. Singh, Material issues in additive manufacturing: A review, *J. Manuf. Process.* 25 (2017) 185–200.
- [29] N. Guo, M.C. Leu, Additive manufacturing: technology, applications and research needs, *Front. Mech. Eng.* 8 (3) (2013) 215–243.
- [30] R.K. Leach, et al., Geometrical metrology for metal additive manufacturing, *CIRP Ann.* 68 (2) (2019) 677–700.
- [31] A. Lopez, et al., Non-destructive testing application of radiography and ultrasound for wire and arc additive manufacturing, *Additive Manuf.* 21 (2018) 298–306.
- [32] Taminger, K. and R. Hafley, Electron beam freeform fabrication for cost effective near-net shape manufacturing. NATO AVT, 2006. 139: p. 16–1.
- [33] K.P. Karunakaran, et al., Low cost integration of additive and subtractive processes for hybrid layered manufacturing, *Robot. Comput. Integr. Manuf.* 26 (5) (2010) 490–499.
- [34] O. Yilmaz, A.A. Uglu, Shaped metal deposition technique in additive manufacturing: A review, *Proc. Inst. Mech. Eng. B J. Eng. Manuf.* 230 (10) (2016) 1781–1798.
- [35] A.G. Demir, Micro laser metal wire deposition for additive manufacturing of thin-walled structures, *Opt. Lasers Eng.* 100 (2018) 9–17.
- [36] Q. Miao, et al., Comparative study of microstructure evaluation and mechanical properties of 4043 aluminum alloy fabricated by wire-based additive manufacturing, *Mater. Des.* 186 (2020) 108205.
- [37] E. Brandl, et al., Mechanical properties of additive manufactured titanium (Ti-6Al-4V) blocks deposited by a solid-state laser and wire, *Mater. Des.* 32 (10) (2011) 4665–4675.
- [38] F. Moures, et al., Optimisation of refractory coatings realised with cored wire addition using a high-power diode laser, *Surf. Coat. Technol.* 200 (7) (2005) 2283–2292.
- [39] S.H. Mok, et al., Deposition of Ti-6Al-4V using a high power diode laser and wire, Part II: Investigation on the mechanical properties, *Surf. Coat. Technol.* 202 (19) (2008) 4613–4619.
- [40] B. Baufeld, E. Brandl, O. van der Biest, Wire based additive layer manufacturing: Comparison of microstructure and mechanical properties of Ti-6Al-4V components fabricated by laser-beam deposition and shaped metal deposition, *J. Mater. Process. Technol.* 211 (6) (2011) 1146–1158.
- [41] R. Xiao, et al., Influence of wire addition direction in CO₂ laser welding of aluminum, *Photonics Asia*, 4915, SPIE, 2002.
- [42] R.R. Unocic, J.N. DuPont, Process efficiency measurements in the laser engineered net shaping process, *Metall. Mater. Trans. B* 35 (1) (2004) 143–152.
- [43] K. Taminger, R. Hafley, Electron beam freeform fabrication: a rapid metal deposition process, *Proceedings of third annual automotive composites conference*, Society of Plastic Engineers, Troy, MI 2003, pp. 9–10.
- [44] P. Wanjara, M. Brochu, M. Jahazi, Electron beam freeforming of stainless steel using solid wire feed, *Mater. Des.* 28 (8) (2007) 2278–2286.
- [45] L. Rännar, et al., *Rapid Prototyp. J.* 13 (3) (2007) 128–135.
- [46] S.H. Oliari, D. Oliveira, M. Schulz, Additive manufacturing of H11 with wire-based laser metal deposition, *Soldagem & Inspeção* 22 (2017) 466–479.
- [47] Y.M. Zhang, et al., Automated system for welding-based rapid prototyping, *Mechatronics* 12 (1) (2002) 37–53.
- [48] G. Posch, K. Chladil, H. Chladil, Material properties of CMT–metal additive manufactured duplex stainless steel blade-like geometries, *Welding World* 61 (5) (2017) 873–882.
- [49] J.D. Spencer, P.M. Dickens, C.M. Wykes, Rapid prototyping of metal parts by three-dimensional welding, *Proc. Inst. Mech. Eng. B J. Eng. Manuf.* 212 (3) (1998) 175–182.
- [50] J. Ding, et al., Thermo-mechanical analysis of Wire and Arc Additive Layer Manufacturing process on large multi-layer parts, *Comput. Mater. Sci.* 50 (12) (2011) 3315–3322.
- [51] H.T. Zhang, et al., The arc characteristics and metal transfer behaviour of cold metal transfer and its use in joining aluminium to zinc-coated steel, *Mater. Sci. Eng. A* 499 (1) (2009) 111–113.
- [52] C.G. Pickin, S.W. Williams, M. Lunt, Characterisation of the cold metal transfer (CMT) process and its application for low dilution cladding, *J. Mater. Process. Technol.* 211 (3) (2011) 496–502.
- [53] W. Aiyiti, et al., Investigation of the overlapping parameters of MPAW-based rapid prototyping, *Rapid Prototyp. J.* 12 (3) (2006) 165–172.
- [54] B. Mannon, J. Heinzman, Plasma Arc Welding Brings Better Control, *Tooling Prod.* 5 (1999) 29–30.
- [55] N. Stenbacka, I. Choquet, K. Hurtig, Review of arc efficiency values for gas tungsten arc welding, IIV Commission IV-XII-SG212, Intermediate Meeting, BAM, Berlin, Germany, 18–20 April, 2012 2012, pp. 1–21.
- [56] B. Wu, et al., The anisotropic corrosion behaviour of wire arc additive manufactured Ti-6Al-4V alloy in 3.5% NaCl solution, *Corros. Sci.* 137 (2018) 176–183.
- [57] J. Gu, et al., The strengthening effect of inter-layer cold working and post-deposition heat treatment on the additively manufactured Al-6.3Cu alloy, *Mater. Sci. Eng. A* 651 (2016) 18–26.
- [58] C. Brice, et al., Precipitation behavior of aluminum alloy 2139 fabricated using additive manufacturing, *Mater. Sci. Eng. A* 648 (2015) 9–14.
- [59] W. Jin, et al., Wire arc additive manufacturing of stainless steels: a review, *Appl. Sci.* (2020) 10(5).
- [60] F. Xu, et al., Microstructural Evolution and Mechanical Properties of Inconel 625 Alloy during Pulsed Plasma Arc Deposition Process, *J. Mater. Sci. Technol.* 29 (5) (2013) 480–488.
- [61] J.S. Panchagnula, S. Simhambhatla, Manufacture of complex thin-walled metallic objects using weld-deposition based additive manufacturing, *Robot. Comput. Integr. Manuf.* 49 (2018) 194–203.
- [62] J. Shi, et al., Effect of in-process active cooling on forming quality and efficiency of tandem GMAW-based additive manufacturing, *Int. J. Adv. Manuf. Technol.* 101 (5) (2019) 1349–1356.
- [63] P. Almeida, Innovative process model of Ti-6Al-4V additive layer manufacturing using cold metal transfer (CMT), The 21st annual international solid freeform fabrication symposium, vol 2010, University of Texas at Austin, 2010.
- [64] M.A. Somashekara, et al., Investigations into effect of weld-deposition pattern on residual stress evolution for metallic additive manufacturing, *Int. J. Adv. Manuf. Technol.* 90 (5) (2017) 2009–2025.
- [65] G. Sproesser, et al., Environmental energy efficiency of single wire and tandem gas metal arc welding, *Welding World* 61 (4) (2017) 733–743.
- [66] J. Shi, et al., T-GMAW based novel Multi-node trajectory planning for fabricating grid stiffened panels: An efficient production technology, *J. Clean. Prod.* 238 (2019) 117919.
- [67] D. Yang, C. He, G. Zhang, Forming characteristics of thin-wall steel parts by double electrode GMAW based additive manufacturing, *J. Mater. Process. Technol.* 227 (2016) 153–160.
- [68] Y. Ma, et al., The effect of location on the microstructure and mechanical properties of titanium aluminides produced by additive layer manufacturing using in-situ alloying and gas tungsten arc welding, *Mater. Sci. Eng. A* 631 (2015) 230–240.
- [69] C. Shen, Z. Pan, D. Cuiuri, Fabrication of Fe-FeAl functionally graded material using the wire-arc additive manufacturing process, *Metall. Mater. Trans. A* 47 (2016) 763–772.
- [70] C. Shen, et al., Fabrication of iron-rich Fe-Al intermetallics using the wire-arc additive manufacturing process, *Additive Manuf.* 7 (2015) 20–26.
- [71] H. Geng, et al., Optimization of wire feed for GTAW based additive manufacturing, *J. Mater. Process. Technol.* 243 (2017) 40–47.
- [72] Y. Zhang, et al., Weld deposition-based rapid prototyping: a preliminary study, *J. Mater. Process. Technol.* 135 (2) (2003) 347–357.
- [73] H. Zhang, J. Xu, G. Wang, Fundamental study on plasma deposition manufacturing, *Surf. Coat. Technol.* 171 (1) (2003) 112–118.
- [74] F. Martina, et al., Investigation of the benefits of plasma deposition for the additive layer manufacture of Ti-6Al-4V, *J. Mater. Process. Technol.* 212 (6) (2012) 1377–1386.
- [75] A. Queguineur, et al., Evaluation of wire arc additive manufacturing for large-sized components in naval applications, *Welding World* 62 (2) (2018) 259–266.
- [76] E. Brandl, et al., Additive manufactured Ti-6Al-4V using welding wire: comparison of laser and arc beam deposition and evaluation with respect to aerospace material specifications, *Phys. Procedia* 5 (2010) 595–606.
- [77] A. Busachi, et al., Designing a WAAM based manufacturing system for defence applications, *Procedia CIRP* 37 (2015) 48–53.
- [78] T. Abe, H. Sasahara, Dissimilar metal deposition with a stainless steel and nickel-based alloy using wire and arc-based additive manufacturing, *Precis. Eng.* 45 (2016) 387–395.
- [79] W. Ya, K. Hamilton, *On-Demand Spare Parts for the Marine Industry with Directed Energy Deposition: Propeller Use Case*. in *Industrializing Additive Manufacturing - Proceedings of Additive Manufacturing in Products and Applications - AMPA2017*, Springer International Publishing, Cham, 2018.
- [80] C. Greer, et al., Introduction to the design rules for Metal Big Area Additive Manufacturing, *Additive Manufacturing* 27 (2019) 159–166.
- [81] D. Clark, M.R. Bache, M.T. Whittaker, Shaped metal deposition of a nickel alloy for aero engine applications, *J. Mater. Process. Technol.* 203 (1) (2008) 439–448.
- [82] Merlin, P., *Design and Development of the Blackbird: Challenges and Lessons Learned*, in *47th AIAA Aerospace Sciences Meeting including The New Horizons Forum and Aerospace Exposition*. 2009, Am. Inst. Aeronautics Astronautics.
- [83] Y. Nilsiam, P. Sanders, J.M. Pearce, Slicer and process improvements for open-source GMAW-based metal 3-D printing, *Additive Manuf.* 18 (2017) 110–120.
- [84] P. Colegrove, High deposition rate high quality metal additive manufacture using wire + arc technology, 2010.
- [85] F. Michel, et al., A modular path planning solution for Wire + Arc Additive Manufacturing, *Robot. Comput. Integr. Manuf.* 60 (2019) 1–11.
- [86] A. Shirizly, O. Dolev, From Wire to Seamless Flow-Formed Tube: Leveraging the Combination of Wire Arc Additive Manufacturing and Metal Forming, *JOM* 71 (2) (2019) 709–717.

- [87] T. He, et al., High-accuracy and high-performance WAAM propeller manufacture by cylindrical surface slicing method, *Int. J. Adv. Manuf. Technol.* 105 (11) (2019) 4773–4782.
- [88] W. Ou, et al., Fusion zone geometries, cooling rates and solidification parameters during wire arc additive manufacturing, *Int. J. Heat Mass Transf.* 127 (2018) 1084–1094.
- [89] T. Mukherjee, et al., Printability of alloys for additive manufacturing, *Sci. Rep.* 6 (2016) 19717.
- [90] S. Kumar, A.S. Shahi, Effect of heat input on the microstructure and mechanical properties of gas tungsten arc welded AISI 304 stainless steel joints, *Mater. Des.* 32 (6) (2011) 3617–3623.
- [91] R. Unnikrishnan, et al., Effect of heat input on the microstructure, residual stresses and corrosion resistance of 304L austenitic stainless steel weldments, *Mater. Charact.* 93 (2014) 10–23.
- [92] H. Zhao, et al., A 3D dynamic analysis of thermal behavior during single-pass multi-layer weld-based rapid prototyping, *J. Mater. Process. Technol.* 211 (3) (2011) 488–495.
- [93] S.M. Thompson, et al., An overview of Direct Laser Deposition for additive manufacturing; Part I: Transport phenomena, modeling and diagnostics, *Additive Manuf.* 8 (2015) 36–62.
- [94] S. Kou, in: J.W.S.I (Ed.), *Welding Metallurgy*, 2nd ed. Hoboken, 2002.
- [95] J.P. Oliveira, T.G. Santos, R.M. Miranda, Revisiting fundamental welding concepts to improve additive manufacturing: From theory to practice, *Prog. Mater. Sci.* 107 (2020) 100590.
- [96] J. Hu, H.L. Tsai, Heat and mass transfer in gas metal arc welding. Part I: The arc, *Int. J. Heat Mass Transf.* 50 (5) (2007) 833–846.
- [97] S. Cadiou, et al., 3D heat transfer, fluid flow and electromagnetic model for cold metal transfer wire arc additive manufacturing (Cmt-Waam), *Additive Manuf.* 36 (2020) 101541.
- [98] A. Li, et al., Thermal behaviors and fluid flow controlling the geometry of 7075 aluminum alloy single tracks during liquid metal flow rapid cooling additive manufacturing, *Int. Commun. Heat Mass Transfer* 116 (2020) 104664.
- [99] S.A. David, T. DeRoy, Current issues and problems in welding science, *Science* 257 (5069) (1992) 497.
- [100] A. Bandyopadhyay, K.D. Traxel, Invited review article: Metal-additive manufacturing—Modeling strategies for application-optimized designs, *Additive Manuf.* 22 (2018) 758–774.
- [101] Y. Zhao, et al., Effect of shielding gas on the metal transfer and weld morphology in pulsed current MAG welding of carbon steel, *J. Mater. Process. Technol.* 262 (2018) 382–391.
- [102] G. Costanza, A. Sili, M.E. Tata, Weldability of austenitic stainless steel by metal arc welding with different shielding gas, *Procedia Struct. Integrity* 2 (2016) 3508–3514.
- [103] J. Ding, et al., Development of a laminar flow local shielding device for wire+arc additive manufacture, *J. Mater. Process. Technol.* 226 (2015) 99–105.
- [104] X. Xu, et al., Oxide accumulation effects on wire+arc layer-by-layer additive manufacture process, *J. Mater. Process. Technol.* 252 (2018) 739–750.
- [105] A.B. Murphy, et al., A computational investigation of the effectiveness of different shielding gas mixtures for arc welding, *J. Phys. D. Appl. Phys.* 42 (11) (2009) 115205.
- [106] P. Almeida, S. Williams, Innovative process model of Ti-6Al-4V additive layer manufacturing using cold metal transfer (CMT), *Twenty-First Annual International Solid Freeform Fabrication Symposium*, Austin, America, 2010.
- [107] I. Pires, L. Quintino, R.M. Miranda, Analysis of the influence of shielding gas mixtures on the gas metal arc welding metal transfer modes and fume formation rate, *Mater. Des.* 28 (5) (2007) 1623–1631.
- [108] M. Guo, et al., Investigating the generation process of molten droplets and arc plasma in the confined space during compulsively constricted WAAM, *J. Mater. Process. Technol.* 275 (2020) 116355.
- [109] F. Lancaster, *Metallurgy of Welding*, fourth ed. Allen & Unwin, 1987.
- [110] J. Xiong, et al., Bead geometry prediction for robotic GMAW-based rapid manufacturing through a neural network and a second-order regression analysis, *J. Intell. Manuf.* 25 (1) (2014) 157–163.
- [111] P. Duranton, et al., 3D modelling of multipass welding of a 316L stainless steel pipe, *J. Mater. Process. Technol.* 153–154 (2004) 457–463.
- [112] F. Li, et al., Thermolectric cooling-aided bead geometry regulation in wire and arc-based additive manufacturing of thin-walled structures, *Appl. Sci.* (2018) 8(2).
- [113] X. Bai, H. Zhang, G. Wang, Improving prediction accuracy of thermal analysis for weld-based additive manufacturing by calibrating input parameters using IR imaging, *Int. J. Adv. Manuf. Technol.* 69 (5) (2013) 1087–1095.
- [114] D. Yang, G. Wang, G. Zhang, Thermal analysis for single-pass multi-layer GMAW based additive manufacturing using infrared thermography, *J. Mater. Process. Technol.* 244 (2017) 215–224.
- [115] X. Lu, et al., Open-source wire and arc additive manufacturing system: formability, microstructures, and mechanical properties, *Int. J. Adv. Manuf. Technol.* 93 (5) (2017) 2145–2154.
- [116] Y. Zhao, et al., Process planning strategy for wire-arc additive manufacturing: Thermal behavior considerations, *Additive Manuf.* 32 (2020) 100935.
- [117] Y. Ma, et al., Effect of interpass temperature on in-situ alloying and additive manufacturing of titanium aluminides using gas tungsten arc welding, *Additive Manuf.* 8 (2015) 71–77.
- [118] Z.H. Rao, J. Zhou, H.L. Tsai, Determination of equilibrium wire-feed-speeds for stable gas metal arc welding, *Int. J. Heat Mass Transf.* 55 (23) (2012) 6651–6664.
- [119] H. Geng, et al., Optimisation of interpass temperature and heat input for wire and arc additive manufacturing 5A06 aluminium alloy, *Sci. Technol. Weld. Join.* 22 (6) (2017) 472–483.
- [120] S. Ríos, et al., Analytical process model for wire + arc additive manufacturing, *Additive Manuf.* 21 (2018) 651–657.
- [121] F. Montevecchi, et al., Idle time selection for wire-arc additive manufacturing: A finite element-based technique, *Additive Manuf.* 21 (2018) 479–486.
- [122] M.P. Mughal, et al., Deformation modelling in layered manufacturing of metallic parts using gas metal arc welding: effect of process parameters, *Model. Simul. Mater. Sci. Eng.* 13 (7) (2005) 1187–1204.
- [123] J. Xiong, Y. Lei, R. Li, Finite element analysis and experimental validation of thermal behavior for thin-walled parts in GMAW-based additive manufacturing with various substrate preheating temperatures, *Appl. Therm. Eng.* 126 (2017) 43–52.
- [124] J.H. Ouyang, H. Wang, R. Kovacevic, Rapid prototyping of 5356-aluminum alloy based on variable polarity gas tungsten arc welding: process control and microstructure, *Mater. Manuf. Process.* 17 (1) (2002) 103–124.
- [125] E.A. Alberti, B.M.P. Bueno, A.S.C.M. D'Oliveira, Additive manufacturing using plasma transferred arc, *Int. J. Adv. Manuf. Technol.* 83 (9) (2016) 1861–1871.
- [126] Y. Lei, J. Xiong, R. Li, Effect of inter layer idle time on thermal behavior for multi-layer single-pass thin-walled parts in GMAW-based additive manufacturing, *Int. J. Adv. Manuf. Technol.* 96 (1) (2018) 1355–1365.
- [127] J.F. Wang, et al., Effect of location on microstructure and mechanical properties of additive layer manufactured Inconel 625 using gas tungsten arc welding, *Mater. Sci. Eng. A* 676 (2016) 395–405.
- [128] F. Montevecchi, et al., Finite Element Modelling of Wire-arc-additive-manufacturing Process, *Procedia CIRP* 55 (2016) 109–114.
- [129] F. Montevecchi, et al., Finite Element mesh coarsening for effective distortion prediction in Wire Arc Additive Manufacturing, *Additive Manuf.* 18 (2017) 145–155.
- [130] M.P. Mughal, H. Fawad, R.A. Mufti, Three-Dimensional Finite-Element Modelling of Deformation in Weld-Based Rapid Prototyping, *Proc. Inst. Mech. Eng. C J. Mech. Eng. Sci.* 220 (6) (2006) 875–885.
- [131] H. Zhao, et al., Effects of interpass idle time on thermal stresses in multipass multi-layer weld-based rapid prototyping, *J. Manuf. Sci. Eng.* (2013) 135(1).
- [132] C. Shen, et al., Influences of deposition current and interpass temperature to the Fe3Al-based iron aluminide fabricated using wire-arc additive manufacturing process, *Int. J. Adv. Manuf. Technol.* 88 (5) (2017) 2009–2018.
- [133] J. Ding, et al., A computationally efficient finite element model of wire and arc additive manufacture, *Int. J. Adv. Manuf. Technol.* 70 (1) (2014) 227–236.
- [134] D. Ding, et al., A multi-bead overlapping model for robotic wire and arc additive manufacturing (WAAM), *Robot. Comput. Integr. Manuf.* 31 (2015) 101–110.
- [135] F. Montevecchi, et al., Heat accumulation prevention in Wire-Arc-Additive-Manufacturing using air jet impingement, *Manuf. Lett.* 17 (2018) 14–18.
- [136] S. Reddy, et al., A new approach for attaining uniform properties in build direction in additive manufactured components through coupled thermal-hardness model, *J. Manuf. Process.* 40 (2019) 46–58.
- [137] W. Hackenhaar, et al., An experimental-numerical study of active cooling in wire arc additive manufacturing, *J. Manuf. Process.* 52 (2020) 58–65.
- [138] B. Wu, et al., The effects of forced interpass cooling on the material properties of wire arc additively manufactured Ti6Al4V alloy, *J. Mater. Process. Technol.* 258 (2018) 97–105.
- [139] E.M. van der Aa, *Local Cooling During Welding: Prediction and Control of Residual Stresses and Buckling Distortion*, Delft University of Technology, The Netherlands, 2007 2007.
- [140] S.R. Kala, N. Siva Prasad, G. Phanikumar, Studies on multipass welding with trailing heat sink considering phase transformation, *J. Mater. Process. Technol.* 214 (6) (2014) 1228–1235.
- [141] P. Henckell, et al., The Influence of Gas Cooling in Context of Wire Arc Additive Manufacturing—A Novel Strategy of Affecting Grain Structure and Size, in: T. TMS (Ed.), *TMS 2017 146th Annual Meeting & Exhibition Supplemental Proceedings. The Minerals, Metals & Materials Series*, Springer, Cham, 2017.
- [142] T.S. O'Donovan, D.B. Murray, Jet impingement heat transfer – Part I: The Mean and root-mean-square heat transfer and velocity distributions, *Int. J. Heat Mass Transf.* 50 (17) (2007) 3291–3301.
- [143] R. Li, J. Xiong, Y. Lei, Investigation on thermal stress evolution induced by wire and arc additive manufacturing for circular thin-walled parts, *J. Manuf. Process.* 40 (2019) 59–67.
- [144] X. Bai, H. Zhang, G. Wang, Modeling of the moving induction heating used as secondary heat source in weld-based additive manufacturing, *Int. J. Adv. Manuf. Technol.* 77 (1) (2015) 717–727.
- [145] B. Silwal, M. Santangelo, Effect of vibration and hot-wire gas tungsten arc (GTA) on the geometric shape, *J. Mater. Process. Technol.* 251 (2018) 138–145.
- [146] K. Hori, et al., Development of hot wire TIG welding methods using pulsed current to heat filler wire – research on pulse heated hot wire TIG welding processes, *Weld. Int.* 18 (6) (2004) 456–468.
- [147] B. Wu, et al., A review of the wire arc additive manufacturing of metals: properties, defects and quality improvement, *J. Manuf. Process.* 35 (2018) 127–139.
- [148] P.A. Colegrove, et al., Microstructure and residual stress improvement in wire and arc additively manufactured parts through high-pressure rolling, *J. Mater. Process. Technol.* 213 (10) (2013) 1782–1791.
- [149] J.R. Hönnige, et al., Residual Stress Characterization and Control in the Additive Manufacture of Large Scale Metal Structures, *Mater. Res. Proceedings* 2 (2017) 455–460.
- [150] J.L. Prado-Cerqueira, J.L. Diéguez, A.M. Camacho, Preliminary development of a Wire and Arc Additive Manufacturing system (WAAM), *Procedia Manuf.* 13 (2017) 895–902.
- [151] Q. Wu, et al., Residual stresses and distortion in the patterned printing of titanium and nickel alloys, *Additive Manuf.* 29 (2019) 100808.
- [152] T. Mukherjee, et al., Mitigation of thermal distortion during additive manufacturing, *Scr. Mater.* 127 (2017) 79–83.

- [153] W.J. Sames, et al., The metallurgy and processing science of metal additive manufacturing, *Int. Mater. Rev.* 61 (5) (2016) 315–360.
- [154] Y. Tian, et al., Microstructure evolution of Inconel 625 with 0.4 wt% boron modification during gas tungsten arc deposition, *J. Alloys Compd.* 694 (2017) 429–438.
- [155] M. Alimardani, et al., On the delamination and crack formation in a thin wall fabricated using laser solid freeform fabrication process: An experimental–numerical investigation, *Opt. Lasers Eng.* 47 (11) (2009) 1160–1168.
- [156] Y. Liu, Y. Yang, D. Wang, A study on the residual stress during selective laser melting (SLM) of metallic powder, *Int. J. Adv. Manuf. Technol.* 87 (1) (2016) 647–656.
- [157] J. Mathew, et al., Prediction of welding residual stresses using machine learning: Comparison between neural networks and neuro-fuzzy systems, *Appl. Soft Comput.* 70 (2018) 131–146.
- [158] Q. Wu, et al., Residual stresses in wire-arc additive manufacturing – Hierarchy of influential variables, *Additive Manuf.* 35 (2020) 101355.
- [159] J. Sun, C.S. Wu, Y. Feng, Modeling the transient heat transfer for the controlled pulse key-holing process in plasma arc welding, *Int. J. Therm. Sci.* 50 (9) (2011) 1664–1671.
- [160] X. Jian, C.S. Wu, Numerical analysis of the coupled arc–weld pool–keyhole behaviors in stationary plasma arc welding, *Int. J. Heat Mass Transf.* 84 (2015) 839–847.
- [161] X. Bai, et al., Numerical analysis of heat transfer and fluid flow in multilayer deposition of PAW-based wire and arc additive manufacturing, *Int. J. Heat Mass Transf.* 124 (2018) 504–516.
- [162] R. Cunningham, et al., Synchrotron-Based X-ray Microtomography Characterization of the Effect of Processing Variables on Porosity Formation in Laser Power-Bed Additive Manufacturing of Ti-6Al-4V, *JOM* 69 (3) (2017) 479–484.
- [163] T. Lu, et al., Hot-wire arc additive manufacturing Ti-6.5Al-2Zr-1Mo-1V titanium alloy: Pore characterization, microstructural evolution, and mechanical properties, *J. Alloys Compd.* 817 (2020) 153334.
- [164] W.W. Wits, et al., Porosity testing methods for the quality assessment of selective laser melted parts, *CIRP Ann.* 65 (1) (2016) 201–204.
- [165] I. Maskery, et al., Quantification and characterisation of porosity in selectively laser melted Al-Si10-Mg using X-ray computed tomography, *Mater. Charact.* 111 (2016) 193–204.
- [166] R. Cunningham, et al., Evaluating the Effect of Processing Parameters on Porosity in Electron Beam Melted Ti-6Al-4V via Synchrotron X-ray Microtomography, *JOM* 68 (3) (2016) 765–771.
- [167] Y. Kok, et al., Anisotropy and heterogeneity of microstructure and mechanical properties in metal additive manufacturing: A critical review, *Mater. Des.* 139 (2018) 565–586.
- [168] W. Xu, et al., Additive manufacturing of strong and ductile Ti-6Al-4V by selective laser melting via in situ martensite decomposition, *Acta Mater.* 85 (2015) 74–84.
- [169] A.P. Boeira, L.L. Ferreira, A. Garcia, Alloy composition and metal/mold heat transfer efficiency affecting inverse segregation and porosity of as-cast Al-Cu alloys, *Mater. Des.* 30 (6) (2009) 2090–2098.
- [170] F. Karimzadeh, et al., Effect of microplasma arc welding process parameters on grain growth and porosity distribution of thin sheet ti6al4v alloy weldment, *Mater. Manuf. Process.* 20 (2) (2005) 205–219.
- [171] Z. Yang, et al., Porosity elimination and heat treatment of diode laser-clad homogeneous coating on cast aluminum-copper alloy, *Surf. Coat. Technol.* 321 (2017) 26–35.
- [172] E.M. Ryan, et al., The influence of build parameters and wire batch on porosity of wire and arc additive manufactured aluminium alloy 2319, *J. Mater. Process. Technol.* 262 (2018) 577–584.
- [173] R. Biswal, et al., Criticality of porosity defects on the fatigue performance of wire + arc additive manufactured titanium alloy, *Int. J. Fatigue* 122 (2019) 208–217.
- [174] F. Wang, et al., Microstructure and Mechanical Properties of Wire and Arc Additive Manufactured Ti-6Al-4V, *Metall. Mater. Trans. A* 44 (2) (2013) 968–977.
- [175] K.F. Ayarkwa, S. Williams, J. Ding, Investigation of pulse advance cold metal transfer on aluminium wire arc additive manufacturing, *Int. J. Rapid Manuf.* 5 (1) (2015) 44–57.
- [176] B. Cong, J. Ding, S. Williams, Effect of arc mode in cold metal transfer process on porosity of additively manufactured Al-6.3%Cu alloy, *Int. J. Adv. Manuf. Technol.* 76 (9) (2015) 1593–1606.
- [177] J.L. Gu, et al., The Influence of Wire Properties on the Quality and Performance of Wire+Arc Additive Manufactured Aluminium Parts, *Adv. Mater. Res.* 1081 (2014) 210–214.
- [178] J. Ge, et al., Wire-arc additive manufacturing H13 part: 3D pore distribution, microstructural evolution, and mechanical performances, *J. Alloys Compd.* 783 (2019) 145–155.
- [179] J.V. Gordon, et al., Quantification of location-dependence in a large-scale additively manufactured build through experiments and micromechanical modeling, *Materialia* 7 (2019) 100397.
- [180] J. Gu, et al., The effect of inter-layer cold working and post-deposition heat treatment on porosity in additively manufactured aluminum alloys, *J. Mater. Process. Technol.* 230 (2016) 26–34.
- [181] E. Soderstrom, P. Mendez, Humping mechanisms present in high speed welding, *Sci. Technol. Weld. Join.* 11 (5) (2006) 572–579.
- [182] M. Motta, A.G. Demir, B. Previtali, High-speed imaging and process characterization of coaxial laser metal wire deposition, *Additive Manuf.* 22 (2018) 497–507.
- [183] H. Randhawa, Investigation into Positional Welding of Structural Steel Using Pulse Current GMAW Process, 1999.
- [184] D. Wu, et al., Understanding of humping formation and suppression mechanisms using the numerical simulation, *Int. J. Heat Mass Transf.* 104 (2017) 634–643.
- [185] U. Gratzke, et al., Theoretical approach to the humping phenomenon in welding processes, *J. Phys. D. Appl. Phys.* 25 (11) (1992) 1640–1647.
- [186] L. Yuan, et al., Fabrication of metallic parts with overhanging structures using the robotic wire arc additive manufacturing, *J. Manuf. Process.* (2020) <https://doi.org/10.1016/j.jmapro.2020.03.018>.
- [187] Y. Li, et al., Analysis of additional electromagnetic force for mitigating the humping bead in high-speed gas metal arc welding, *J. Mater. Process. Technol.* 229 (2016) 207–215.
- [188] C.S. Wu, F. Yang, J. Gao, Effect of external magnetic field on weld pool flow conditions in high-speed gas metal arc welding, *Proc. Inst. Mech. Eng. B J. Eng. Manuf.* 230 (1) (2014) 188–193.
- [189] M. Shoichi, et al., Study on the application for electromagnetic controlled molten pool welding process in overhead and flat position welding, *Sci. Technol. Weld. Join.* 18 (1) (2013) 38–44.
- [190] K. Nomura, Y. Ogino, Y. Hirata, Shape control of TIG arc plasma by cusp-type magnetic field with permanent magnet, *Weld. Int.* 26 (10) (2012) 759–764.
- [191] H.W. Hoi, D.F. Farson, M.H. Cho, Using a hybrid laser plus GMAW process for controlling the bead humping defect, *Weld. J.* 85 (8) (2006) (p. 174-17).
- [192] X. Meng, et al., High speed TIG-MAG hybrid arc welding of mild steel plate, *J. Mater. Process. Technol.* 214 (11) (2014) 2417–2424.
- [193] K.H. Li, J.S. Chen, Y.M. Zhang, in: J. Welding (Ed.), Double-electrode GMAW process and control, 86(8), 2007, pp. 2315–2375.
- [194] S. Kanemaru, et al., Study for TIG–MIG hybrid welding process, *Welding World* 58 (1) (2014) 11–18.
- [195] J. Zähr, et al., Numerical and Experimental Studies of the Influence of Process Gases in Tig Welding, *Welding World* 56 (3) (2012) 85–92.
- [196] L. Wang, et al., Backward flowing molten metal in weld pool and its influence on humping bead in high-speed GMAW, *J. Mater. Process. Technol.* 237 (2016) 342–350.
- [197] L. Wang, et al., Influence of the external magnetic field on fluid flow, temperature profile and humping bead in high speed gas metal arc welding, *Int. J. Heat Mass Transf.* 116 (2018) 1282–1291.
- [198] L. Wang, et al., Effects of malondialdehyde-induced protein modification on water functionality and physicochemical state of fish myofibrillar protein gel, *Food Res. Int.* 86 (2016) 131–139.
- [199] T. Nguyen, et al., The humping phenomenon during high speed gas metal arc welding, *Sci. Technol. Weld. Join.* 10 (2005) 447–459.
- [200] M.H. Cho, D.F. Farson, Understanding Bead Hump Formation in Gas Metal Arc Welding Using a Numerical Simulation, *Metall. Mater. Trans. B* 38 (2) (2007) 305–319.
- [201] L. Yuan, et al., Investigation of humping phenomenon for the multi-directional robotic wire and arc additive manufacturing, *Robot. Comput. Integr. Manuf.* 63 (2020) 101916.
- [202] D. Plakhotnik, et al., CAM planning for multi-axis laser additive manufacturing considering collisions, *CIRP Ann.* 68 (1) (2019) 447–450.
- [203] W. Gao, et al., The status, challenges, and future of additive manufacturing in engineering, *Comput. Aided Des.* 69 (2015) 65–89.
- [204] H. Lockett, et al., Design for Wire + Arc Additive Manufacture: design rules and build orientation selection, *J. Eng. Des.* 28 (7-9) (2017) 568–598.
- [205] A. Nycz, et al., *Challenges in Making Metal Large-scale Complex Parts for Additive Manufacturing: A Case Study Based on the Additive Manufacturing Excavator (AME), in Solid Freeform Fabrication - Austin, Texas, 2017.*
- [206] G. Zhao, et al., Nonplanar slicing and path generation methods for robotic additive manufacturing, *Int. J. Adv. Manuf. Technol.* 96 (9) (2018) 3149–3159.
- [207] C. Kirschman, C. Jara-Almonte, A parallel slicing algorithm for solid freeform fabrication processes, *Solid freeform fabrication proceedings, Austin, 1992.*
- [208] Z. Zhang, S. Joshi, An improved slicing algorithm with efficient contour construction using STL files, *Int. J. Adv. Manuf. Technol.* 80 (5) (2015) 1347–1362.
- [209] K. Tata, et al., Efficient slicing for layered manufacturing, *Rapid Prototyp. J.* 4 (4) (1998) 151–167.
- [210] S. Wang, et al., An adaptive slicing algorithm and data format for functionally graded material objects, *Int. J. Adv. Manuf. Technol.* 65 (1) (2013) 251–258.
- [211] M.Y. Zhou, Adaptive slicing of functionally graded material objects for rapid prototyping, *Int. J. Adv. Manuf. Technol.* 24 (5) (2004) 345–352.
- [212] K. Mani, P. Kulkarni, D. Dutta, Region-based adaptive slicing, *Comput. Aided Des.* 31 (5) (1999) 317–333.
- [213] E. Sabourin, A. Houser Scott, J. Helge Böhn, Adaptive slicing using stepwise uniform refinement, *Rapid Prototyp. J.* 2 (4) (1996) 20–26.
- [214] E. Sabourin, A. Houser Scott, J. Helge Böhn, Accurate exterior, fast interior layered manufacturing, *Rapid Prototyp. J.* 3 (2) (1997) 44–52.
- [215] Y.S. Liao, Y.Y. Chiu, A New Slicing Procedure for Rapid Prototyping Systems, *Int. J. Adv. Manuf. Technol.* 18 (8) (2001) 579–585.
- [216] S. Allen, D. Dutta, Wall thickness control in layered manufacturing for surfaces with closed slices, *Comput. Geom.* 10 (4) (1998) 223–238.
- [217] M. Kerschbaumer, G. Ernst, P. O’Leary, Tool path generation for 3D laser cladding using adaptive slicing technology, *Int. Congress Appl. Lasers Electro-Optics* 2005 (1) (2005) 604.
- [218] S. Singamneni, et al., Modeling and evaluation of curved layer fused deposition, *J. Mater. Process. Technol.* 212 (1) (2012) 27–35.
- [219] P. Singh, D. Dutta, Multi-Direction Slicing for Layered Manufacturing, *J. Comput. Inf. Sci. Eng.* 1 (2) (2001) 129–142.
- [220] I. Ilinkin, et al., A decomposition-based approach to layered manufacturing, *Comput. Geom.* 23 (2) (2002) 117–151.
- [221] X. Qian, D. Dutta, Feature Based Fabrication in Layered Manufacturing, *J. Mech. Des.* 123 (3) (1999) 337–345.
- [222] Y. Yang, et al., Feature extraction and volume decomposition for orthogonal layered manufacturing, *Comput. Aided Des.* 35 (12) (2003) 1119–1128.

- [223] Y. Yang, et al., Multi-orientational deposition to minimize support in the layered manufacturing process, *J. Manuf. Syst.* 22 (2) (2003) 116–129.
- [224] J. Zhang, F. Liou, Adaptive Slicing for a Multi-Axis Laser Aided Manufacturing Process, *J. Mech. Des.* 126 (2) (2004) 254–261.
- [225] J. Ruan, et al., Automated Slicing for a Multi-axis Metal Deposition System, *J. Manuf. Sci. Eng.* 129 (2) (2006) 303–310.
- [226] Singh, P. and D. Dutta, *Offset Slices for Multidirection Layered Deposition*, *J. Manuf. Sci. Eng.*, 2008, 130(1).
- [227] L. Ren, et al., Process planning strategies for solid freeform fabrication of metal parts, *J. Manuf. Syst.* 27 (4) (2008) 158–165.
- [228] D. Ding, et al., Automatic multi-direction slicing algorithms for wire based additive manufacturing, *Robot. Comput. Integr. Manuf.* 37 (2016) 139–150.
- [229] Y. Ding, R. Dwivedi, R. Kovacevic, Process planning for 8-axis robotized laser-based direct metal deposition system: A case on building revolved part, *Robot. Comput. Integr. Manuf.* 44 (2017) 67–76.
- [230] M.R. Dunlavey, Efficient polygon-filling algorithms for raster displays, *ACM Trans. Graph.* 2 (4) (1983) 264–273.
- [231] S.C. Park, B.K. Choi, Tool-path planning for direction-parallel area milling, *Comput. Aided Des.* 32 (1) (2000) 17–25.
- [232] V.T. Rajan, V. Srinivasan, A. Tarabanis Konstantinos, The optimal zigzag direction for filling a two-dimensional region, *Rapid Prototyp. J.* 7 (5) (2001) 231–241.
- [233] R.T. Farouki, et al., Path planning with offset curves for layered fabrication processes, *J. Manuf. Syst.* 14 (5) (1995) 355–368.
- [234] Y. Yang, et al., Equidistant path generation for improving scanning efficiency in layered manufacturing, *Rapid Prototyp. J.* 8 (1) (2002) 30–37.
- [235] H. Wang, P. Jang, J.A. Stori, A Metric-Based Approach to Two-Dimensional (2D) Tool-Path Optimization for High-Speed Machining, *J. Manuf. Sci. Eng.* 127 (1) (2005) 33–48.
- [236] F. Ren, Y. Sun, D. Guo, Combined reparameterization-based spiral toolpath generation for five-axis sculptured surface machining, *Int. J. Adv. Manuf. Technol.* 40 (7) (2009) 760–768.
- [237] W.K. Chiu, Y.C. Yeung, K.M. Yu, Toolpath generation for layer manufacturing of fractal objects, *Rapid Prototyp. J.* 12 (4) (2006) 214–221.
- [238] R. Dwivedi, R. Kovacevic, Automated torch path planning using polygon subdivision for solid freeform fabrication based on welding, *J. Manuf. Syst.* 23 (4) (2004) 278–291.
- [239] D. Ding, et al., A tool-path generation strategy for wire and arc additive manufacturing, *Int. J. Adv. Manuf. Technol.* 73 (1) (2014) 173–183.
- [240] J.-H. Kao, F.B. Prinz, Optimal motion planning for deposition in layered manufacturing, *Proceedings DETC* (1998) 13–16.
- [241] D. Ding, et al., A practical path planning methodology for wire and arc additive manufacturing of thin-walled structures, *Robot. Comput. Integr. Manuf.* 34 (2015) 8–19.
- [242] D. Ding, et al., Towards an automated robotic arc-welding-based additive manufacturing system from CAD to finished part, *Comput. Aided Des.* 73 (2016) 66–75.
- [243] D. Ding, et al., Adaptive path planning for wire-feed additive manufacturing using medial axis transformation, *J. Clean. Prod.* 133 (2016) 942–952.
- [244] X. Wang, A. Wang, Y. Li, A sequential path-planning methodology for wire and arc additive manufacturing based on a water-pouring rule, *Int. J. Adv. Manuf. Technol.* 103 (9) (2019) 3813–3830.
- [245] P. Kazanas, et al., Fabrication of geometrical features using wire and arc additive manufacture, *Proc. Inst. Mech. Eng. B J. Eng. Manuf.* 226 (6) (2012) 1042–1051.
- [246] J. Mehnen, et al., Design study for wire and arc additive manufacture, *Int. J. Prod. Dev.* 19 (2014) 2–20.
- [247] D. Yili, et al., Wire and arc additive manufacture of high-building multi-directional pipe joint, *Int. J. Adv. Manuf. Technol.* 96 (5) (2018) 2389–2396.
- [248] G.Q. Jin, W.D. Li, L. Gao, An adaptive process planning approach of rapid prototyping and manufacturing, *Robot. Comput. Integr. Manuf.* 29 (1) (2013) 23–38.
- [249] H.H. Liu, et al., A path planning and sharp corner correction strategy for wire and arc additive manufacturing of solid components with polygonal cross-sections, *Int. J. Adv. Manuf. Technol.* 106 (11) (2020) 4879–4889.
- [250] R. Li, et al., End lateral extension path strategy for intersection in wire and arc additive manufactured 2319 aluminum alloy, *Rapid Prototyp. J.* 26 (2) (2019) 360–369.
- [251] X. Zhang, et al., Fracture toughness and fatigue crack growth rate properties in wire + arc additive manufactured Ti-6Al-4V, *Fatigue Fract. Eng. Mater. Struct.* 40 (5) (2017) 790–803.
- [252] Q. Wu, et al., Obtaining uniform deposition with variable wire feeding direction during wire-feed additive manufacturing, *Mater. Manuf. Process.* 32 (16) (2017) 1881–1886.
- [253] T. Abe, H. Sasahara, Development of the shell structures fabrication CAM system for direct metal lamination using arc discharge-lamination height error compensation by torch feed speed control, *Int. J. Precis. Eng. Manuf.* 16 (1) (2015) 171–176.
- [254] J. Xiong, et al., Fabrication of inclined thin-walled parts in multi-layer single-pass GMAW-based additive manufacturing with flat position deposition, *J. Mater. Process. Technol.* 240 (2017) 397–403.
- [255] S. Jhavar, N.K. Jain, C.P. Paul, Development of micro-plasma transferred arc (μ -PTA) wire deposition process for additive layer manufacturing applications, *J. Mater. Process. Technol.* 214 (5) (2014) 1102–1110.
- [256] H. Wang, R. Kovacevic, Rapid prototyping based on variable polarity gas tungsten arc welding for a 5356 aluminium alloy, *Proc. Inst. Mech. Eng. B J. Eng. Manuf.* 215 (11) (2001) 1519–1527.
- [257] M. Dinovitzer, et al., Effect of wire and arc additive manufacturing (WAAM) process parameters on bead geometry and microstructure, *Additive Manuf.* 26 (2019) 138–146.
- [258] J. Xiong, G. Zhang, W. Zhang, Forming appearance analysis in multi-layer single-pass GMAW-based additive manufacturing, *Int. J. Adv. Manuf. Technol.* 80 (9) (2015) 1767–1776.
- [259] J.S. Panchagnula, S. Simhambhatla, Inclined slicing and weld-deposition for additive manufacturing of metallic objects with large overhangs using higher order kinematics, *Virtual Phys. Prototyping* 11 (2) (2016) 99–108.
- [260] H. Geng, et al., Formation and improvement of surface waviness for additive manufacturing 5A06 aluminium alloy component with GTAW system, *Rapid Prototyp. J.* 24 (2) (2018) 342–350.
- [261] S. Suryakumar, et al., Weld bead modeling and process optimization in Hybrid Layered Manufacturing, *Comput. Aided Des.* 43 (4) (2011) 331–344.
- [262] A. Adebayo, J. Mehnen, X. Tonnellier, Limiting travel speed in additive layer manufacturing, *Proceedings of the 9th International Conference on Trends in Welding Research*, Chicago, Illinois, USA, 2012.
- [263] G. Ma, et al., Optimization strategies for robotic additive and subtractive manufacturing of large and high thin-walled aluminum structures, *Int. J. Adv. Manuf. Technol.* 101 (5) (2019) 1275–1292.
- [264] J. Xiong, Z. Yin, W. Zhang, Forming appearance control of arc striking and extinguishing area in multi-layer single-pass GMAW-based additive manufacturing, *Int. J. Adv. Manuf. Technol.* 87 (1) (2016) 579–586.
- [265] Z. Hu, et al., Understanding and overcoming of abnormality at start and end of the weld bead in additive manufacturing with GMAW, *Int. J. Adv. Manuf. Technol.* 95 (5) (2018) 2357–2368.
- [266] P. Singh, D. Dutta, Multi-direction layered deposition—an overview of process planning methodologies, *Proc. Solid Freeform Fabrication Symp.* (2003) 279–288.
- [267] J. Xiong, et al., Modeling of bead section profile and overlapping beads with experimental validation for robotic GMAW-based rapid manufacturing, *Robot. Comput. Integr. Manuf.* 29 (2) (2013) 417–423.
- [268] Y. Cao, et al., Overlapping model of beads and curve fitting of bead section for rapid manufacturing by robotic MAG welding process, *Robot. Comput. Integr. Manuf.* 27 (3) (2011) 641–645.
- [269] J. Plangger, et al., CMT additive manufacturing of a high strength steel alloy for application in crane construction, *Metals* (2019) 9(6).
- [270] Y. Li, et al., Enhanced beads overlapping model for wire and arc additive manufacturing of multi-layer multi-bead metallic parts, 2018.
- [271] Y.-A. Song, S. Park, S.-W. Chae, 3D welding and milling: part II—optimization of the 3D welding process using an experimental design approach, *Int. J. Mach. Tools Manuf.* 45 (9) (2005) 1063–1069.
- [272] K.P. Karunakaran, et al., Retrofitment of a CNC machine for hybrid layered manufacturing, *Int. J. Adv. Manuf. Technol.* 45 (7) (2009) 690–703.
- [273] J.S. Panchagnula, S. Simhambhatla, *Additive Manufacturing of Complex Shapes Through Weld-Deposition and Feature Based Slicing*, 2015.
- [274] J. Xiong, G. Zhang, Adaptive control of deposited height in GMAW-based layer additive manufacturing, *J. Mater. Process. Technol.* 214 (4) (2014) 962–968.
- [275] Y. Chen, et al., Effect of weave frequency and amplitude on temperature field in weaving welding process, *Int. J. Adv. Manuf. Technol.* 75 (5) (2014) 803–813.
- [276] X. Zhan, et al., Microstructure and property characteristics of thick Invar alloy plate joints using weave bead welding, *J. Mater. Process. Technol.* 244 (2017) 97–105.
- [277] X. Xu, et al., Preliminary Investigation of Building Strategies of Maraging Steel Bulk Material Using Wire + Arc Additive Manufacture, *J. Mater. Eng. Perform.* 28 (2) (2019) 594–600.
- [278] P. Dirisu, et al., Wire plus arc additive manufactured functional steel surfaces enhanced by rolling, *Int. J. Fatigue* 130 (2020) 105237.
- [279] F. Martina, et al., Microstructure of Interpass Rolled Wire + Arc Additive Manufacturing Ti-6Al-4V Components, *Metall. Mater. Trans. A* 46 (12) (2015) 6103–6118.
- [280] J.R. Hönnige, et al., Control of residual stress and distortion in aluminium wire + arc additive manufacture with rolling, *Additive Manuf.* 22 (2018) 775–783.
- [281] S.W. Wen, et al., Rolling to control residual stress and distortion in friction stir welds, *Sci. Technol. Weld. Join.* 15 (6) (2010) 440–447.
- [282] P. Rangaswamy, et al., Residual stresses in LENS components using neutron diffraction and contour method, *Mater. Sci. Eng. A* 399 (1) (2005) 72–83.
- [283] J. Altenkirch, et al., Residual stress engineering in friction stir welds by roller tensioning, *Sci. Technol. Weld. Join.* 14 (2) (2009) 185–192.
- [284] C.R. Cunningham, et al., Cost Modelling and Sensitivity Analysis of Wire and Arc Additive Manufacturing, *Procedia Manuf.* 11 (2017) 650–657.
- [285] Y. Li, et al., GMAW-based additive manufacturing of inclined multi-layer multi-bead parts with flat-position deposition, *J. Mater. Process. Technol.* 262 (2018) 359–371.
- [286] C. Doumanidis, Y.-M. Kwak, Multivariable adaptive control of the bead profile geometry in gas metal arc welding with thermal scanning, *Int. J. Press. Vessel. Pip.* 79 (4) (2002) 251–262.
- [287] J. Xiong, Z. Yin, W. Zhang, Closed-loop control of variable layer width for thin-walled parts in wire and arc additive manufacturing, *J. Mater. Process. Technol.* 233 (2016) 100–106.
- [288] J. Xiong, et al., Vision-sensing and bead width control of a single-bead multi-layer part: material and energy savings in GMAW-based rapid manufacturing, *J. Clean. Prod.* 41 (2013) 82–88.
- [289] Y. Fu, et al., Investigation of mechanical properties for hybrid deposition and micro-rolling of bainite steel, *J. Mater. Process. Technol.* 250 (2017) 220–227.
- [290] N.P. Gokhale, P. Kala, V. Sharma, Thin-walled metal deposition with GTAW welding-based additive manufacturing process, *J. Braz. Soc. Mech. Sci. Eng.* 41 (12) (2019) 569.

- [291] Y. Li, J. Xiong, Z. Yin, Molten pool stability of thin-wall parts in robotic GMA-based additive manufacturing with various position depositions, *Robot. Comput. Integr. Manuf.* 56 (2019) 1–11.
- [292] J. Xiong, et al., Influences of process parameters on surface roughness of multi-layer single-pass thin-walled parts in GMAW-based additive manufacturing, *J. Mater. Process. Technol.* 252 (2018) 128–136.
- [293] Z. Zhang, et al., Surface quality and forming characteristics of thin-wall aluminium alloy parts manufactured by laser assisted MIG arc additive manufacturing, *Int. J. Lightweight Materials Manufacture* 1 (2) (2018) 89–95.
- [294] Y. Yehorov, J.L. da Silva, A. Scotti, Balancing WAAM production costs and wall surface quality through parameter selection: a case study of an Al-Mg5 alloy multilayer-non-oscillated single pass wall, *J. Manuf. Materials Processing* (2019) 3(2).
- [295] W. Wu, et al., Forming process, microstructure, and mechanical properties of thin-walled 316L stainless steel using speed-cold-welding additive manufacturing, *Metals* (2019) 9(1).
- [296] Y. Feng, et al., The double-wire feed and plasma arc additive manufacturing process for deposition in Cr-Ni stainless steel, *J. Mater. Process. Technol.* 259 (2018) 206–215.
- [297] G. Marinelli, et al., Microstructure, hardness and mechanical properties of two different unalloyed tantalum wires deposited via wire + arc additive manufacture, *Int. J. Refract. Met. Hard Mater.* 83 (2019) 104974.
- [298] L. Ji, et al., Research on mechanisms and controlling methods of macro defects in TC4 alloy fabricated by wire additive manufacturing, *Materials* (2018) 11(7).
- [299] M. Cheepu, C.I. Lee, S.M. Cho, Microstructural characteristics of wire arc additive manufacturing with inconel 625 by super-TIG welding, *Trans. Indian Inst. Metals* 73 (2020) 1475–1479.
- [300] Y. Li, et al., A layers-overlapping strategy for robotic wire and arc additive manufacturing of multi-layer multi-bead components with homogeneous layers, *Int. J. Adv. Manuf. Technol.* 96 (9) (2018) 3331–3344.
- [301] J. Jiang, et al., Investigation of printable threshold overhang angle in extrusion-based additive manufacturing for reducing support waste, *Int. J. Comput. Integr. Manuf.* 31 (10) (2018) 961–969.
- [302] J. Jiang, X. Xu, J. Stringer, Support structures for additive manufacturing: a review, *J. Manuf. Materials Processing* (2018) 2(4).
- [303] A.A. Shirali, K.C. Mills, The effect of welding parameters on penetration in GTA welds, *Welding J. N. York* (1993) 72(7).
- [304] H. Castner, J. Penoyer, Computer-aided programming for robotic welding, *Weld. J.* 96 (2017) 78–83.
- [305] L.A. Ferreira, et al., Offline CAD-based Robot Programming and Welding Parametrization of a Flexible and Adaptive Robotic Cell Using Enriched CAD/CAM System for Shipbuilding, *Procedia Manuf.* 11 (2017) 215–223.
- [306] S. Radel, et al., Skeleton arc additive manufacturing with closed loop control, *Additive Manuf.* 26 (2019) 106–116.
- [307] L. Yuan, et al., Application of Multidirectional Robotic Wire Arc Additive Manufacturing Process for the Fabrication of Complex Metallic Parts, *IEEE Trans. Industrial Informatics* 16 (1) (2020) 454–464.
- [308] Y.-A. Song, et al., 3D welding and milling: Part I—a direct approach for freeform fabrication of metallic prototypes, *Int. J. Mach. Tools Manuf.* 45 (9) (2005) 1057–1062.
- [309] Q. Wu, et al., Obtaining fine microstructure and unsupported overhangs by low heat input pulse arc additive manufacturing, *J. Manuf. Process.* 27 (2017) 198–206.
- [310] F. Montevecchi, et al., Cutting Forces Analysis in Additive Manufactured AISI H13 Alloy, *Procedia CIRP* 46 (2016) 476–479.
- [311] G. Venturini, et al., Feature based three axes computer aided manufacturing software for wire arc additive manufacturing dedicated to thin walled components, *Additive Manuf.* 22 (2018) 643–657.
- [312] A.A. Uгла, O. Yilmaz, Deposition-Path Generation of SS308 Components Manufactured by TIG Welding-Based Shaped Metal Deposition Process, *Arab. J. Sci. Eng.* 42 (11) (2017) 4701–4711.
- [313] A.R. McAndrew, et al., Interpass rolling of Ti-6Al-4V wire + arc additively manufactured features for microstructural refinement, *Additive Manuf.* 21 (2018) 340–349.
- [314] Z. Li, et al., Reducing arc heat input and obtaining equiaxed grains by hot-wire method during arc additive manufacturing titanium alloy, *Mater. Sci. Eng. A* 742 (2019) 287–294.
- [315] H. Geng, et al., Geometric limitation and tensile properties of wire and arc additive manufacturing 5A06 aluminum alloy parts, *J. Mater. Eng. Perform.* 26 (2) (2017) 621–629.
- [316] J.P. Morais, et al., Characterisation of a high-performance Al-Zn-Mg-Cu alloy designed for wire arc additive manufacturing, *Materials* (2020) 13(7).
- [317] F. Li, et al., Adaptive process control of wire and arc additive manufacturing for fabricating complex-shaped components, *Int. J. Adv. Manuf. Technol.* 96 (1) (2018) 871–879.
- [318] M. Graf, et al., Thermo-Mechanical Modelling of Wire-Arc Additive Manufacturing (WAAM) of Semi-Finished Products, *Metals* (2018) 8(12).
- [319] W. Ou, et al., Determination of the control points for circle and triangle route in wire arc additive manufacturing (WAAM), *J. Manuf. Process.* 53 (2020) 84–98.
- [320] H. Wang, et al., Rapid prototyping of 4043 Al-alloy parts by VP-GTAW, *J. Mater. Process. Technol.* 148 (1) (2004) 93–102.
- [321] Y. Ogino, S. Asai, Y. Hirata, Numerical simulation of WAAM process by a GMAW weld pool model, *Welding World* 62 (2) (2018) 393–401.
- [322] D. Vaughan, et al., *SS410 Process Development and Characterization*. Solid Freeform Fabrication Symposium (SFF 2019) - Austin, Texas, United States, 2019.
- [323] J. Kessler, et al., Basic research on lattice structures focused on the strut shape and welding beads, *Phys. Procedia* 83 (2016) 833–838.
- [324] T. Abe, H. Sasahara, Layer geometry control for the fabrication of lattice structures by wire and arc additive manufacturing, *Additive Manuf.* 28 (2019) 639–648.
- [325] Y. Luo, et al., Influence of pulsed arc on the metal droplet deposited by projected transfer mode in wire-arc additive manufacturing, *J. Mater. Process. Technol.* 259 (2018) 353–360.
- [326] Y. Li, et al., Wire and arc additive manufacturing of aluminum alloy lattice structure, *J. Manuf. Process.* 50 (2020) 510–519.
- [327] T. Xu, et al., Obtaining large-size pyramidal lattice cell structures by pulse wire arc additive manufacturing, *Mater. Des.* 187 (2020) 108401.
- [328] G. Campatelli, et al., Integrated WAAM-subtractive versus pure subtractive manufacturing approaches: an energy efficiency comparison, *Int. J. Precision Eng. Manuf. Green Technol.* 7 (1) (2020) 1–11.
- [329] T. Artaza, et al., Design and integration of WAAM technology and in situ monitoring system in a gantry machine, *Procedia Manuf.* 13 (2017) 778–785.
- [330] M. Hirtler, et al., Investigation of microstructure and hardness of a rib geometry produced by metal forming and wire-arc additive manufacturing, *MATEC Web Conf.* 190 (2018).
- [331] T. He, et al., Forming and mechanical properties of wire arc additive manufacture for marine propeller bracket, *J. Manuf. Process.* 52 (2020) 96–105.
- [332] J.-Y. Hascoët, V. Querard, M. Rauch, Interests of 5 axis toolpaths generation for wire arc additive manufacturing of aluminum alloys, *J. Machine Eng.* 17 (3) (2017) 51–65.
- [333] A.A. Hassen, et al., Scaling Up metal additive manufacturing process to fabricate molds for composite manufacturing, *Additive Manuf.* 32 (2020) 101093.
- [334] A. Waqas, et al., Optimization of process parameters to improve the effective area of deposition in GMAW-based additive manufacturing and its mechanical and microstructural analysis, *Metals* (2019) 9(7).
- [335] V. Gunaraj, N. Murugan, Prediction and optimization of weld bead volume for the submerged arc process - Part 1, *Weld. J.* (2000) 79(10).
- [336] L. Yuan, S. Ding, C. Wen, Additive manufacturing technology for porous metal implant applications and triple minimal surface structures: A review, *Bioactive Materials* 4 (1) (2019) 56–70.
- [337] T. Lehmann, et al., Concurrent geometry- and material-based process identification and optimization for robotic CMT-based wire arc additive manufacturing, *Mater. Des.* 194 (2020) 108841.
- [338] B. Wu, et al., Effects of heat accumulation on microstructure and mechanical properties of Ti6Al4V alloy deposited by wire arc additive manufacturing, *Additive Manuf.* 23 (2018) 151–160.
- [339] J. González, et al., Additive manufacturing with GMAW welding and CMT technology, *Procedia Manuf.* 13 (2017) 840–847.
- [340] A. Chabot, M. Rauch, J.Y. Hascoët, Towards a multi-sensor monitoring methodology for AM metallic processes, *Welding World* 63 (3) (2019) 759–769.
- [341] Y. Li, et al., Interlayer closed-loop control of forming geometries for wire and arc additive manufacturing based on fuzzy-logic inference, *J. Manuf. Process.* (2020) <https://doi.org/10.1016/j.jmapro.2020.04.009>.
- [342] E.R. Denlinger, et al., Effect of inter-layer dwell time on distortion and residual stress in additive manufacturing of titanium and nickel alloys, *J. Mater. Process. Technol.* 215 (2015) 123–131.
- [343] T.H.J. Vaneker, The Role of Design for Additive Manufacturing in the Successful Economical Introduction of AM, *Procedia CIRP* 60 (2017) 181–186.
- [344] J.M. Zheng, K.W. Chan, I. Gibson, Desktop virtual reality interface for computer aided conceptual design using geometric techniques, *J. Eng. Des.* 12 (4) (2001) 309–329.
- [345] D. Thomas, The development of design rules for selective laser melting, Thesis (PhD) University of Wales, 2009.
- [346] C. Seepersad, et al., A designer's guide for dimensioning and tolerancing SLS parts, *Solid Freeform Fabrication Symposium*. Austin, TX, 2014 921–931.
- [347] G.A.O. Adam, D. Zimmer, Design for Additive Manufacturing—Element transitions and aggregated structures, *CIRP J. Manuf. Sci. Technol.* 7 (1) (2014) 20–28.
- [348] J. Kranz, D. Herzog, C. Emmelmann, Design guidelines for laser additive manufacturing of lightweight structures in TiAl6V4, *J. Laser Appl.* 27 (S1) (2014), S14001.